Early-Warning Monitoring System for Masonry Structures

Dissertation

submitted to and approved by the

Faculty of Architecture, Civil Engineering and Environmental Sciences
University of Braunschweig – Institute of Technology

and the

Faculty of Engineering
University of Florence

in candidacy for the degree of a
Doktor-Ingenieur (Dr.-Ing.) /
Dottore di Ricerca in Risk Management on the Built Environment *)

by
Anna Bosi
Born 2nd September 1978
from Foligno, Italy

Submitted on	19th March 2008
Oral examination on	29th May 2008
Professorial advisors	Prof. Harald Budelmann
	Prof. Gianni Bartoli

2008

*) Either the German or the Italian form of the title may be used.

Tutors

Prof. Dott.-Eng. Gianni Bartoli *University of Florence*

Prof. Dott.-Eng. Harald Budelmann *Technical University of Braunschweig*

Coordinators of the Doctoral Course

Prof. Dott.-Eng. Claudio Borri *University of Florence*

Prof. Dott.-Eng. Udo Peil *Technical University of Braunschweig*

To my Mother, my Father, Ancilla
and my Uncle

ABSTRACT Collapse of historical buildings under static conditions has to been considered as a risk to deal with. Several events happened in the past as the collapse of the civic tower of Pavia, the bell tower of Venice (just to mention some of them) show that, even without a strong external event, structures can collapse.
Their collapse can produce enormous cultural, social and historical losses (intangible ones), if by chance human ones there are not. Therefore these structures present, on the same time, high vulnerability (that however is not possible to quantify) and high possible tangible and intangible losses.
The problem is complex above all because we refer to historical structure that very often had already suffered for a damaging process in their history. Monitoring, identifying the crack pattern is the first step to prevent an increase of the damage.
The present work try to deal with this problem, giving a tool able to indicate in real time if anomalous conditions are passing on the structure, giving an alarm that can help to prevent the final collapse or at least avoid human losses.
In our application we have referred to the Brunelleschi dome in Florence, a structure with an intangible value, economical, historical and cultural. A large monitoring system has been installed there in order to verify the stability of the structure that presents several cracks that cut completely the dome.
By means of a thermoelastic analysis of data logged by sensors and by the following use of mathematical tools, a signal that can check in real-time data that are far from the ones associated to a normal behavior of the structure, have been set up.
Also the stability of the crack in mechanical term has been studied, after making a simple model of the structure that is however able to reproduce the main features of the structural behavior.
The study gives also examples of an useful mathematical tool to detect singularities on a signal allowing also a spatial identification of the crack.
Crack identification, crack monitoring and crack stability has therefore been pursued in order to identify dangerous conditions for existing structures.

Acknowledgment

During these three years of study different persons contributed in many ways to this final manuscript. First, I want to thank the coordinators of the Doctoral Course Prof. Claudio Borri and Prof. Udo Peil and, of course, Prof. Gianni Bartoli and Prof. Harald Buldemm, my tutors, for their support during this period.

My gratitude goes to Prof. Paolo Maria Mariano for trusting in me since the beginning and for teaching me so much.

A special thanks is for Prof. Antonio Moro, who kindly gave me his scientific support expecially on the reduction of the thesis; to Prof. Giuseppe Modica, his competences apart, to hold me in esteem.

During my last period of the doctoral course I have been warmly welcomed to the Laboratoire des Mechanique des Solides of the Ecole Politechnique of Paris. All the staff and in particular Prof. Andrei Constantinescu and Prof. Lev Truskinovsky are gratefully acknowledged for all the scientific and not scientific discussions.

I have no way to thank Dr. Luca Salvatori, for being a friend who gave me his always sincere suggestions and Dr. Matteo Luca Facchinetti, who patiently proofread this work and supported me.

Finally, the most important thanks to all my family, always so close to me.

Contents

1
Introduction

"*It is perhaps trivial to remark of Greek, Roman, Byzantine, Romanesque and Gothic buildings that some of them still exist.[...] Moreover, the mere survival of ancient buildings implies an extreme stability of their structure. Minor failures have, of course, occurred, and there have been major catastrophes.*" [27].

In the introduction of '*The stone skeleton*' Heyman underlines the importance of an extreme stability of structure in the survival of ancient buildings; it is therefore not trivial to suppose their integrity although, when dealing with monumental buildings, we are more used to think that they could one day collapse only because of an extreme event as an earthquake.

We do not imagine that they could also collapse without '*an external good reason*' but only because of an internal weakness of the system. This internal weakness is often unknown or underestimated and the extreme stability of the structure is assumed *a priori* since 'these structures exist since a long time and, if no strong events in the past have already caused their collapse, they would survive forever'. In reality the risk of their collapse exists and, moreover, is difficult to deal with it. In fact, this '*lack of external cause'* is translated into the risk management vocabulary, in a lack of hazard or better an impossibility to quantify this hazard. Besides, monumental buildings are

complex structures characterized by several uncertainties and they can not be treated in statistical terms at all.

Thus, how it is possible to manage with the risk of collapse of a monumental building under its own weight? How can engineers deal with this risk? Is however possible to prevent the collapse, despite of all the problems?

After a short introduction on the risk management, an approach to the risk of collapse of monumental buildings under static conditions, in the general framework of the risk management, is here presented.

1.1 Risk management: a brief introduction

Risk management is the orderly process of dealing with natural or man induced hazards that can threaten life or property of a population [40]. The risk management process includes three sequential steps: the *risk identification*, the *risk assessment* and finally the *risk treatment* [48].

The identification of the risk consists in recognizing the potential sources of harm either natural events and human activities. This is not a trivial task since hazards are often unknown or underestimated[1] and in these cases nothing to prevent or to reduce the risk is done.

Once the identification has been done, one assesses this risk. This assessment consists of two general parts: the *risk analysis* in which the risk is calculated and the *risk evaluation*.

The risk analysis includes a *hazard analysis,* a *damage determination* and a *loss assessment* where:

- the hazard analysis consists *in identifying the hazard*, *determining the relevant intensity levels* and *the time dependent probability of occurrence*. The magnitude and frequency of occurrence of extreme events are determined such as the strength of an earthquake referred to the Richter scale (relevant intensity level) or the height of a flood level of a given return period

[1] Also smoking is a trivial exemple of an understimated risk; before it was discovered that the smoking is dangerous, to smoke was an unknown risk.

Building houses close to river or in not protected costal zones are other examples of understimated risks.

(time dependent probability of occurrence). These are calculated by means of an analysis of the available records of previous extreme values, when this is possible[2].

- The damage determination is directly related to the damage of the system under analysis and it describes the direct effect of the hazard on the system itself.

  The link between these two points (hazard and damage) is called *vulnerability* of the system i.e. the susceptibility of a structure towards the impact of an hazard[3].

- Finally the loss assessment is the sum of the direct and indirect consequences of the system damaging; they can be both tangible (human, economical) and intangible (cultural, social and historical).

The risk evaluation uses the results of the risk analysis to create classes of risk that will be used on the final step of the risk treatment. Here all the analyzed decisions on how to treat the risk are collected. These decisions are technical and non-technical ones in order to reduce the exposure to the hazard.

However, usually the risk of exposure to an extreme event can not be completely reduced; in this case steps of preparedness have to be taken as the planning for disaster relief or warning systems, which have the purpose of warning of threat of an imminent extreme event.

1.1.1 Early Warning

Within the risk management, the warning systems represent an important subsystem also included between the targets established by the Scientific and Technical Committee (STC-IDNDR) appointed by the UN Secretary General to provide guidelines for the UN International Decade for Natural Disaster Reduction (IDNDR) [40].

The elements of Early Warning can be illustrated very well by a famous Japanese anecdote [40].

---

[2] Take not that when the analysis of past data is not possible, the hazard analysis becomes difficult. This problem will be relevant in the following when the collapse of monumental buildings under static conditions is treated.

[3] A castle made by cards is more vulnerable than a castle made by Lego bricks to the impact of the same gust of wind.

> The people of a fishing village were celebrating a festival on the sea shore (*a vulnerable population*). An old man (*a forecaster*), living in a hut on a mound watched from a distance. He saw suddenly that the sea at the distant horizon was rising, and he recognized that a Tsunami wave (*an event that occurs in the future after a time* t_{crit}) was approaching the shore. Unable to reach the people by voice, he took his firebasket and threw it on the thatched roof of his house, which burst into flames (*a warning was generated and communicated*). The people on the shore could not see the Tsunami approaching, but they noticed the fire and ran to help (*they took action and heeded the warning*) and when the Tsunami wave arrived, they were on safe ground while extinguishing the fire.

The process has all the essentials of a successful early warning process: a forecast able to identify the danger, a critical time from the forecast to the occurrence of the disaster causing event, a means to communicate the warning, and a population at risk which responds to the warning and takes action, which saves lives [40].

It is evident that the recognition of the hazard to which the population is exposed is the basis for a warning system; if the hazard is not known, an effective warning system cannot be constructed. A discussion of warning systems must therefore start with an assessment of the hazard: to perform an early warning, it is first necessary to know *against what to warn*.

1.2 The risk management of monumental buildings

When dealing with existing buildings, the assessment of their reliability requires a number of assumptions that make the assessment an uncertain process [2]. In particular if one refers to historical or monumental buildings, the uncertainties increase: original designs are seldom available, there are uncertainties on the properties of the material (both at the original and at the present state), the structures suffered damaging process in their history that modified completely the original structural behavior, etc.

In order to deal with this problem, a classification between 'historical' and 'monumental' buildings has been introduced in the past [2].

The first ones are buildings of artistic and/or cultural value which are found in significant number as the historic centres of modern towns. For them the assessment of the vulnerability to a strong event is usually supported by statistical studies, based on analysis of the behavior of similar constructions during similar events occurred in the past.

Monumental buildings instead are unique, unlike any other; they are characterized by their own history, often resulting in a composite mixture of added or substituted structural elements, strongly interacting. In addition there are uncertainties on the mechanical properties of the materials and on the structural resistance due to the deterioration frequently accelerated by neglect or carelessness. Due to their uniqueness, Statistics can not be applied and subjective probabilities have been applied in evaluating risks [2].

A wide literature exists with reference to seismic vulnerability and risk (see for example [2], [1], [19], [48]). In particular in Urban's thesis a complete analysis of monumental buildings under earthquake actions has been performed; it starts from the determination of the probability of the events and arrives to define risk classes, by following all the intermediate steps of a risk management chain [48]. Although a monument is an unique building, it is however possible to estimate its vulnerability, even if in terms of a probabilistic relation between the predicted damage level[4] and the earthquake intensity expected.

Nevertheless systematic studies and data collection have been performed only with reference to seismic vulnerability and risk of monumental buildings. No analysis has been done with reference to the risk of collapse of monumental buildings under static conditions, that is the collapse induced by structural failure.

To deal with the risk of collapse of monumental buildings under static conditions is problematic since, as it will be clear later in this work, the subject presents uncertainties that do not allow to perform the *classical* risk management analysis.

The difficulties on dealing with this risk is first that the collapse of monumental building under static conditions is often not considered

[4] A probabilistic definition of the vulnerability is related to a probabilistic distribution of materials strenghts and of other relevant geometrical, mechanical and model paramenters; all these probabilities are essentially subjective (as previously said) due to the shortage of data.

at all between the potential sources of harm and thus this risk results underestimated or completely neglected.

In reality, just in reason of material decay, damaging processes, etc. several of these minor failures and major catastrophes have already occurred in the past. Some of the most famous collapses of monumental buildings under static conditions, happened in the past, are here collected, in order to show the relevance of the problem.

1.2.1 The most famous collapses of monumental buildings

Probably the most famous collapse in the history is the one of the cathedral of Beauvais in 1248. The enormous dimensions of the church were not much greater than those of other great churches of the period; nevertheless twelve years after the construction in which it stood without problems (a period ample enough to assure that equilibrium has been achieved between thrust and counterthrust), the cathedral suddenly collapsed. Several hypothesis have been done about the causes: some adverse geotechnical effects, creep effect..., but the real cause is not still clear probably because there were several acting in the meanwhile. After this event, the cathedral was rebuilt and in 1569 a tower of 153 m was also completed close to the church; two years after the construction, two of the four main crossing piers at the base of the tower presented already a dangerous out of plumb. The immediate works proposed as remedy to the problem were started only two year later and the tower fell down two weeks after the beginning of the works [27].

Most recently, in the 1902, the campanile of Venice collapsed; in this case the disaster was closely studied: not tilt of the tower was observed while several fissures were seen to wide. Notwithstanding this last monitoring of tower before the collapse, a main cause was not found. Examination of the foundations excluded the geotechnical failure. As often in this case, the reasons are several and they must been seen in the history of the monument. For example it was known the presence of vertical fissures in the fabric of the tower; the building underlaid thunderstorms and lightning that partially damaged it. It is not to undervalue the effects of these last two natural events: vertical fissures become wet in thunderstorms and become good conducting channels for a lightning stroke; the temperature rise and the virtual instantaneous production of steam generate a pressure that can damage severely the whole structure [27].

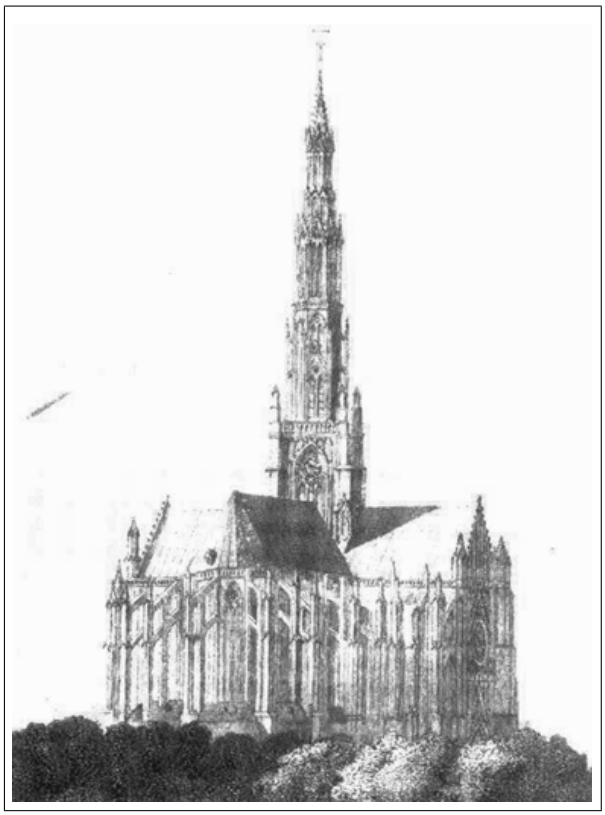

FIGURE 1.1. A sketch of the Beauvais Cathedral as it was after the reconstruction in 1569, just before the collapse.

The studies which followed the sudden collapse of the Civic Tower of Pavia in 1989 identified the cause on the time-dependent behavior of the masonry i.e. viscosity beyond the elastic range under heavy compressive loads. For the first time the phenomenon was deeply studied and it will be shown that it can be considered the basis of a large number of the partial or total collapses of the past. In fact such damage can evolve in a relatively long time determining a slow crack propagation that can lead to failure. This aspect suggests to carefully analyze the evolution of vertical cracks which might appear for example on the external walls of tower or on all the particularly slender or heavily loaded elements as columns or pillars. They can be overloaded by permanent compressive stress; concentration of stress in some points can also happen because of non homogeneous mater-

FIGURE 1.2. The rubble of the civic tower of Pavia after the collapse.

ial. Moreover one has to consider that this effect can also be coupled with the additional stress induced by cyclic wind action and temperature variations that may contribute to increase the damage [6].

Moreover, the effect of compressive load was probably the cause of the partial sudden collapse of Noto cathedral in 1996. The cathedral was damaged by the earthquake of 1990; it was closed for a certain time to build some provisional structures before the necessary repairs. Nevertheless these provisional structures were not sufficient since during the night on $13th$ March, the main dome, transept, complete roof and vault of the central nave, part of the drum and part of the small dome of the right nave fell down fortunately without any casualty. The studies confirm that the collapse certainly developed starting from one or more of the right piers of the central nave. After removing the plaster that covered the left piers, a series of vertical large cracks were found; they were clearly due to compressive stress. The damage would probably progress even without the last earthquake that only accelerated the process [6].

Previous examples show that collapse under static conditions is a potential source of harm for monumental buildings. Nevertheless performing a risk analysis (*risk identification*, *risk assessment* and finally *risk treatment*) presents several difficulties: besides all the uncertainties due to the fact that we are referring to monumental buildings, difficulties arise on the analysis of the hazard since it is

FIGURE 1.3. Noto Cathedral: immiditely after the collapse (the provisional system installed after the earthquake of the 1990 are still visible); during the recent reconstruction works; how now it appears.

characteristic of the structure itself and therefore to define an *intensity level* and the *time dependent probability of occurrence* (as for the seismic risk) is not possible. The collapse can be induced by a material decay, by an erroneous design (initial design or design of previous restorations works), etc. and often the causes are unknown; thus it is not possible to deal with this problem in probabilistic term of occurrence. Defining a vulnerability level is not possible due to the incapacity to evaluate the susceptibility of the structure towards the impact of the not assessable hazard.

Nevertheless it is evident that the collapse can produce enormous cultural, social and historical losses (intangible ones), if, by chance, there are not casualties or dead persons. Thus these structures present, at the same time, high vulnerability and high possible tangible and intangible losses.

In order to deal with it, we can not use Statistic or analysis of past data referred to similar structures but we have to perform an analysis strictly related to the monument itself. The process starts in identifying the hazard by determining if the structure has suffered a damaging process in the past, or if it has some internal weakness that could lead to a collapse. However, as the previous examples show, the correlation between effects and causes of damage is not often clear at first glance, and a deep investigation, both experimental and analytical, is necessary.

1.2.2 Monitoring: a tool for a risk analysis

Structural health monitoring has recently emerged as a reliable and efficient approach to control the system performance, to detect damage and to assess the structural serviceability. In Italy, Public Works Ministry explicitly required a diagnostic phase on support to the design or to the maintenance of existing buildings (*Legge Merloni*, 1994).

Therefore very often monitoring systems are in use; they consist of two major components: a network of sensors for collecting performance measurements and a data analysis algorithm/software for interpretation of the measurements as the physical condition of the structure.

A '*cognitive monitoring*' or a '*check-up monitoring*' is possible. '*Cognitive monitoring*' is based on the definition of some mechanical model of the structure under analysis that can help to interpret data logged by sensors. For a correct structural evaluation a deep knowledge of several parameters is required as:

- building history and evolution
- geometry
- structural details
- crack pattern and material decay map
- wall construction technique and materials
- material proprieties
- structure stability.

All these informations can be achieved trough on site and laboratory experimental investigations, structural analyses with *appropriate* models and final diagnosis.

Sometimes, as in case of the collapses of Pavia and Noto, the locations of the fractures can not be immediate since they can be hidden by the plaster or by some frescos which are not possible to be removed. In this case recent signal processing techniques based on *wavelet analysis* (see Chapter 2) have proven their ability to identify discontinuities which could represent cracks; a widespread set of instruments (deformometers, for example) must be placed on the

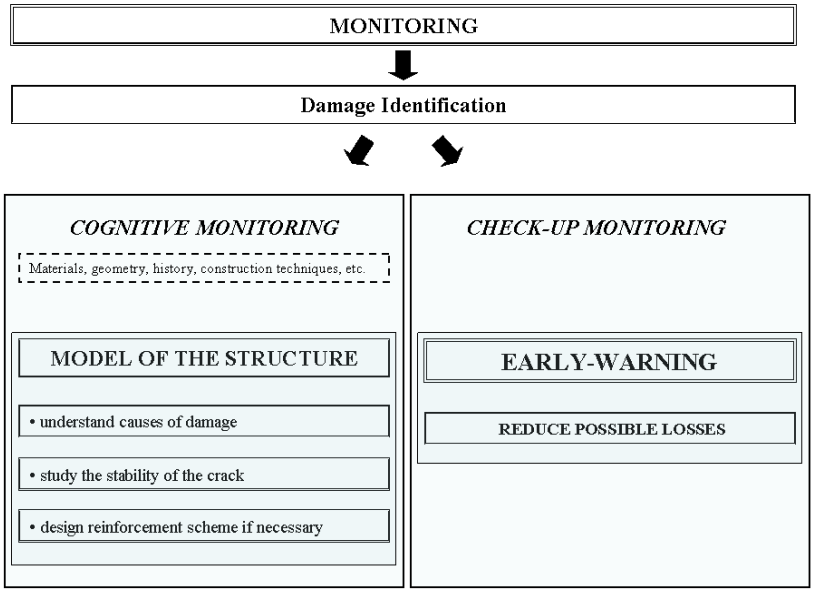

FIGURE 1.4. Monitoring process.

structure, in particular in the most critical points, and the analysis of data logged is necessary. It is important not to underestimate this phase of identification, since, as shown before, the presence of cracks could modify completely the global structural behavior and could be symptomatic of the overall safety of the building.

Once the set up model fits the data logged by the monitoring system, one may:

- try to understand if the cracks are stable or instable, identifying a possible scenario for the crack opening evolution;
- make hypothesis on the causes of the crack opening, design some reinforcement scheme (if necessary) and evaluate the effects of this one on the overall structural behavior (*risk prevention*);
- calibrate a numerical model in order to investigate the structural response under special loading conditions such as the ones induced by an earthquake (*vulnerability evaluation*).

Unfortunately, when dealing with historical buildings, a cognitive monitoring is particularly difficult because these structures are often irregular, construction phases and modalities are not known, there are uncertainties about the constitutive proprieties of the materials (the hypotheses of isotropy, homogeneity, elastic behavior of materials are not applicable) and often they have already suffered damaging processes that modified their structural behavior. Moreover, although several non destructive techniques have recently been implemented, the correlation between tests data and real masonry performance is still a difficult task.

In these cases it is however possible '*to control*' the structure or a part of it: a '*check-up monitoring*' can be performed. Data logged by the sensors are used to define a *normal* behavior of the structure (the one in which the structure behaves without increasing, in an irreversible way, damage) and therefore to identify possible *anomalous* conditions i.e. the ones that could lead to a severe increase of damage and in the worst case to the collapse.

A check-up monitoring results therefore a early warning system that gives alarm of a future risk of collapse.

1.2.3 Warning System

An efficient warning system starts from a risk recognition, therefore the initial cognitive monitoring that addresses to the identification of the damage in the structure is the first essential step. Once the risk has been identified, the warning system must be able to forecast the extreme event in real-time and to give a warn. In structural health monitoring, an early-warning must give warn if the structure is undergoing an *anomalous* behavior characterized for example, by *anomalous*[5] data of displacement.

Early-warning is only effective if the recipients have confidence in it and therefore the system must be as much as possible reliable, not giving false alarms.

By referring the example of the Japanese anecdote to the case of the collapse of structures, also in this case we must have a forecaster able to identify the danger (i.e. identify in real time the damage as for example a sudden crack opening); the forecaster must communicate

[5] *Anomalous* with respect to displacement data associated to the normal (already prooven safe) behavior of the structure.

the occurrence of the disaster (i.e. give an alarm before the possible complete collapse of the structure) within a critical time in order to reduce the final losses (critical time can be the time to perform some immediate restoration works to avoid the collapse, if the damage is not so relevant, or just the time to prevent casualties but not avoiding the partial or total collapse of the structure, if it is a severe damage).

The forecast of the event is the first step and it is usually performed by extrapolating of the value of a signal into the near future. By referring to an existing building embedded with some sensors (which log for example the displacements of some critical structural elements), if it has been possible to set up a model that reproduces in a satisfactory way the real structure, the future displacements can be forecasted in real-time by knowing loading conditions.

When dealing with monumental buildings this is seldom possible and thus forecasting systems are based on the analysis of the statistical properties of the past data and by comparing the resulted signal with the actual data: regression analysis, neural network, genetic algorithms are useful tools to forecast a datum at time t_{n+1} when data till time t_n are known.

It is important to note that these methods are not dependent on all the mechanical and structural uncertainties that one meets on trying to model the structural behavior of a monumental building.

In this work a check-up monitoring system set up to identify isolated events in real-time and to give an alarm of a possible imminent collapse has been developed.

To address the risk of collapse of monumental buildings under static conditions by means of early-warning system is, in fact, the most efficient way to overcome all the difficulties that characterizes the subject. In fact a warning system, able to forecast the risk of collapse in a reliable way, represents the most important way (if not the only one) to deal with this risk: leaving apart from the incapability of defining an intensity hazard, leaving apart the difficulties on defining the vulnerability of the structure, it could however prevent the risk of collapse or reduce at least the final losses.

1.3 Contribution of the present work

As we discussed till now, the application of the classical risk management theory meets several difficulties on dealing with the safety

of monumental buildings; the present work proposes an alternative approach.

The aim of this work is to give a contribution in the management of monumental buildings. We have seen that dealing with the risk of collapse under static conditions is a difficult task that requires some modifications from the *classical* path of the risk management.

Here, we have first to identify the risk and, since we are treating monumental buildings, we need to refer to a real one; we have seen that each of them is unique and not classifiable into schemes. The structure analyzed, S. Maria del Fiore Cathedral, is one of the most important monumental buildings in Florence and it has not only a religious value but also an artistic and historical one. It has already suffered during the past from a damaging process and its safety worried so much that a large monitoring system has been installed.

The cathedral and in particular the dome presents a complex crack pattern that completely modified the structural behavior. Analyses of the logged data show that the fractures change their amplitude by increasing in time. Is it possible that the structure will collapse one day due to the rising damage? What can be do to prevent the collapse or at least to reduce the final losses?

Here, in reason of all the uncertainties that arise when dealing with monumental buildings, we have first analyzed the problem by studying the logged data and by identifying the main features of the structural behavior.

To set up a finite element model meets always difficulties referring to monumental buildings: the model can not account of all the characteristics of the structure and thus it results in any case incomplete and not able to reproduce exactly the whole structural behavior.

Our aim was to give an operative tool that could help to prevent the risk of collapse. Thus, an early-warning system has been set up by introducing an *Effective Alarm Signal* that exceeds a fixed threshold only in case of risk. This system forecasts the possible risk only by means of the logged data (in particular deformations and temperature time-histories); it is completely independent on the materials uncertainties and on the unknowns about the structural behavior. In this way it overcomes all the difficulties that one can find in performing numerical analyses of the structure, or trying to reproduce it. In addition it is a reliable tool that gives an *Effective Alarm Signal* only for a possible structural problem as in case of a sudden increase

in crack opening and by neglecting the case of possible instrumental problems that can occur as in case of thunderstorms.

Once the alarm has been given to an appropriate decision maker, first it must be communicated to the population (the firebasket of the Japanese anecdote) in order to avoid casualties, then, in reason of the importance of the damage, if there is not an imminent collapse, one can decide for deeper investigation on the structure and restoration works.

In order to verify if S. Maria del Fiore cathedral is still safe (and how far a sudden increase of the crack opening could be), also an analysis of the stability of the main cracks has been performed. A basic finite element model has been set up; a model that, despite of all the uncertainties, is able to reproduce the most important local characteristics of the structure. The model has been used to evaluate in mechanical terms the tendency of the cracks to grow in an instable way.

The work is organized as follows: after this preliminary chapter on risk management of monumental building, chapter 2 presents an introduction on the use of wavelet analysis on isolated events detection in monitoring of structures. Isolated events are all the events that differ from the other ones, revealing the presence of a singularity. A singularity could represent the presence of a crack or could be an anomalous datum of displacement in a time-history. Therefore, their detection is a very important aim of monitoring a structure.

In chapter 3 the case of the Brunelleschi dome is presented: first a brief introduction on the structure, on the crack layout and on the monitoring system installed is given. The main results on the analysis of the logged data are also presented allowing to roughly define the structural behavior. Afterwards the early-warning system set up is presented. It is important to remark that this early-warning system, however performed on data of Brunelleschi dome, could however be useful for any structure that presents as well a thermoelastic behavior.

In chapter 4 finally the study of the stability of the cracks is analyzed. The analysis has been performed by means of a finite numerical model of the structure: a basic one has been done. Even if the finite element model can not reproduce the overall structural behavior, it is however able to simulate the most important characteristic

of the structure in the proximity of the crack, where it is important to study the stability.

The obtained results allow to state that the fracture is still stable, but a continuos monitoring is however necessary in order to control its growing, giving therefore a reason to the application of an early-warning system.

2

The use of wavelet analysis to detect isolated events

Structural health monitoring aims at a real-time characterization of structural performance to enhance structural safety and to significantly reduce lifetime operating costs by early detection for maintenance.

An increasing interest on damage localization[1] grew around *1970s* in mechanical and aerospace industry and arrived later also to civil engineering structures.

In this framework, most structural health monitoring systems developed in the past were performed by measuring structural dynamic characteristics and analyzing these data in the frequency domain by performing modal analysis. The premise of these vibration-based methods is that dynamic characteristics of a structure are a function of its mechanical properties: changes in mechanical properties as a result of localized structural damage, will result in changes in the characteristic dynamic vibrations of the structure due to a reduction in stiffness and an increase in damping. A comprehensive literature review on methods of damage detection and health monitoring using vibration signals was provided by Doebling *et al.* [18].

[1] Not always damage localization directly by visual inspection is possible or easy. Let us remind for exemple the case of Noto cathedral where cracks were covered by the plaster.

Nevertheless, there are some limitations to this methodology:

- first, the response of a structure before and after the damage must be provided. This is possible only in laboratory experiments: here small structures (scaled model of real ones), or parts of real structures are built up and their performances before and after introducing damaging are checked. A comparison between modal parameters of undamaged and damaged condition is thus possible. On the contrary, in real structures monitoring systems are installed only after damage has been discovered or an extreme event (that could have damaged the structure) has occurred. No information about undamaged structural behavior is available.

- Moreover, experimental verifications, performed in order to check modal analysis reliability, have shown that in large structures modal characteristics might be insensitive to localized damage and changes in the mode shapes due to damage might not be detected due to noise corruption of the signal.

- Finally, the traditional modal analysis is not applicable for a real-time detection. In fact it is performed in the frequency domain by implementing Fourier transform: a good frequency resolution, but not time resolution at all is then provided. A deep explanation of this remark will be given in the following (section 2.1).

To overcome these difficulties, alternative methods of damage detection have been proposed: wavelet analysis has recently gained a growing popularity as an efficient tool of signal processing in this field. Wavelet analysis may be viewed as an extension of Fourier transform with adjustable window location and size that allows to achieve at the same time frequency and time resolution.

In the next sections a brief summary of Fourier transform and wavelet analysis are first presented. A particular attention will be given to the differences between Fourier and wavelet analysis, underlying the main peculiarities of the second one comparing to the traditional one. An overview of wavelet application on damage detection will then follow.

2.1 A brief presentation of Fourier transform

The continuous formulation of Fourier transform is here reported, a discrete one is also possible.

For a given continuous function $f \in L^1(\mathbb{R})$, we define Fourier transform as the integral

$$\hat{f}(\omega) = \int_{-\infty}^{+\infty} f(t) e^{-i\omega t} dt, \tag{2.1}$$

where $\omega = 2\pi n$ is the angular frequency measured in radians per second and $e^{-i\omega t} = \cos(\omega t) + i \sin(\omega t)$ as usual.

Therefore, the function $\hat{f}$ allows to measure the frequency content of f: intuitively, for a given frequency ω, the Fourier transform measures 'how much' the function f matches sine and cosine functions with that frequency. A large value indicates that f has a major spectral component at that frequency.

If f is integrable, an inverse formula is also possible:

$$f(t) = \frac{1}{2\pi} \int_{-\infty}^{+\infty} \hat{f}(\omega) e^{i\omega t} d\omega. \tag{2.2}$$

Equation 2.2 decomposes f in a sum of sinusoidal waves $e^{i\omega t}$ of amplitude $\hat{f}(\omega)$.

A drawback of the Fourier transform is the result of an integration over the entire signal length: in this way it tells us which frequency components exist in the signal but not where in time the single components exist. As result, this global mix of informations makes difficult to analyze any local property of f directly from $\hat{f}$ and moreover it does not result useful in case of non stationary signals or for real-time applications.

In 1946 the physicists Dennis Gabor overcame this problem: he defined elementary time-frequency 'atoms' as waveforms that have a minimal spread in a time-frequency plane. To measure time-frequency 'information' content, he proposed to decompose the signal over these elementary atomic waveforms defined as[2]

$$g_{u,\xi}(t) = g(t-u) e^{-i\xi t}.$$

[2] The energy of $g_{u,\xi}$ is concentrated near u and in a time interval of σ_t (standard deviation of $|g|^2$). Its Fourier transform is a translation by ξ of the Fourier transform $\hat{g}$

The *windowed Fourier transform* defined by Gabor correlates a function f with each atom $g_{u,\xi}$:

$$Sf(u,\xi) = \int_{-\infty}^{+\infty} f(t)g(t-u)e^{-i\xi t}dt.$$

Therefore it represents a Fourier integral that is localized in the neighborhood of u by the window $g(t-u)$; the window can be shifted along the time axis allowing time resolution.

In a time-frequency plane (t,ω), the energy spread of the atom $g_{u,\xi}$ is symbolically represented by the Heisenberg rectangle illustrated in figure 2.1. The rectangle is centered in (u,ξ) and has a time width σ_t and a frequency width σ_ω. From the uncertainty principle[3], the area satisfies $\sigma_t\sigma_\omega \geq \frac{1}{2}$; when g is a Gaussian function, the equal holds [22].

Nevertheless since the support of the window function is constant with respect to the translation parameter u, also *windowed Fourier transform* is not optimal for non stationary signals.

The need for a transform that uses window functions of variable width (narrow for the analysis of high frequencies, wider for smaller frequencies), that is a transform with variable resolution, has led to the formalization of wavelet transform.

---

of g:

$$\hat{g}_{u,\xi}(\omega) = \hat{g}(\omega-\xi)e^{-iu(\omega-\xi)}.$$

The energy of $\hat{g}_{u,\xi}$ is therefore localized near the frequency ξ, over an interval size of σ_ω. A deeper description of Gabor's atoms can be found in [22].

[3]For the uncertainty principle the energy spread of a function and its Fourier transform cannot be simultaneously arbitrarily small.

For exemple the Dirac $\delta(t-u)$ has a support restricted to $t=u$ but its Fourier transform $e^{-iu\omega}$ has energy uniformly spread over all frequencies. One knows that $\left|\hat{f}(\omega)\right|$ dacays quikly at high frequencies only if f has regular variations in time. The energy of f must therefore be spread over a relatively large domain. To reduce the time spread of f, one can think to scale it by $s<1$, by maintaining constant its energy. Now, if $f_s(t) = \frac{1}{\sqrt{s}}f(\frac{t}{s})$, then $\|f_s\|^2 = \|f\|^2$ and the Fourier transform $\hat{f}(\omega) = \sqrt{s}\hat{f}(s\omega)$ is dilated by $1/s$, loosing in frequency localization what gained in time [33].

Exactly *Heisenberg uncertainty principle* states that the temporal variance and the frequency variance of $f \in L^2(\mathbb{R})$ satisfy $\sigma_t^2\sigma_\omega^2 \geq \frac{1}{4}$ [33].

This principle has a particularly important interpretation in quantum mechanics as an uncertainty of the position and momentum of a free particle [22].

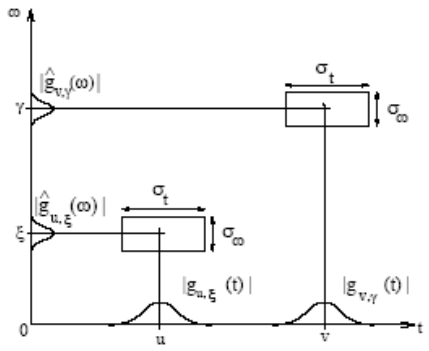

FIGURE 2.1. Time-frequency boxes: *Heisenberg rectangles* represent the energy spread of two Gabor atoms.

2.2 Essential summary of wavelets

2.2.1 Continuous Wavelet Transform

For every function $f \in L^2(\mathbb{R}, \mathbb{C})$, the continuous wavelet transform of f is defined as

$$(W_\psi f)(u,s) := \langle f, \psi_{u,s} \rangle = \int_{\mathbb{R}} f(t) \psi^*_{u,s}(t) dt \tag{2.3}$$

with $u, s \in \mathbb{R}$, with u the *translation* parameter and s the *scale* parameter. (ψ^* is the complex conjugate of ψ as usual). The functions $\{\psi_{u,s}\}_{s,u \in \mathbb{R}, s \neq 0}$ are obtained from translation and dilations of a basis function $\psi \in L^2(\mathbb{R}, \mathbb{C})$, defined as

$$\psi_{u,s}(t) = |s|^{-1/2} \psi\left(\frac{t-u}{s}\right). \tag{2.4}$$

This basis function is called *mother wavelet* and has to satisfy the *admissibility condition*

$$C_\psi := \int_{\mathbb{R}} \frac{\left|\widehat{\psi}(\omega)\right|^2}{\omega} d\omega < +\infty, \tag{2.5}$$

where $\widehat{\psi}(\omega)$ is the Fourier transform of ψ; t and ω are the time and the circular frequency. The condition (2.5) implies that:

(*i*) $\psi(t)$ has a zero average, that is $\int_{\mathbb{R}} \psi(t) dt = 0$ and $\widehat{\psi}(0) = 0$;

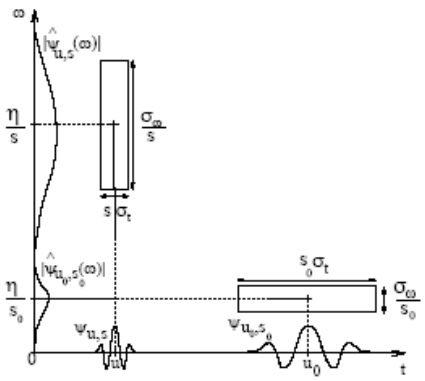

FIGURE 2.2. Time-frequency boxes of two wavelets $\psi_{u,s}$ and ψ_{u_0,s_0}. When the scale parameter s decreases, the time support is reduced but the frequency spread increases and covers an interval that is shifted towards high frequencies.

(*ii*) $\int_{\mathbb{R}} \left|\widehat{\psi}(\omega)\right|^2 dt < \infty$ i.e. the function has finite energy that implies that most of the energy in the basis function is confined to a finite duration.

The *continuous wavelet transform* is therefore a sort of windowed transform where the parameter of the scale allows to have windows of unequal lengths. If the scaling parameter s is $0 < s \ll 1$, the window is narrow and thus appropriate for high frequency components of the signal f. If $s \gg 1$ the window is wide and appropriate for low frequency components. In a time-frequency plane (t, ω), a wavelet atom $\psi_{u,s}$ is symbolically represented by a rectangle centered at $(u, \eta/s)$ The time and frequency spread are respectively proportional to s and $1/s$. When s varies, the height and width of the rectangle change but its area remains constant (figure 2.2) according to Heisenberg principle [33].

The condition (2.5) allows to define the inverse transform

$$f(t) = C_\psi^{-1} \int_{\mathbb{R}} \int_{\mathbb{R}} W_f(u,s) \psi_{u,s}(t) \frac{dsdu}{s^2}.$$

By the inverse formulation, the original signal $f(t)$ can be obtained starting from its wavelet decomposition.

2.2.2 Discrete Wavelet Transform

A *discrete* formulation follows by selecting s and u as powers of fixed numbers, namely s_0^j and $ku_0s_0^j$, with $j, k \in \mathbb{Z}$.

The discrete version of $W_\psi f\,(u,s)$ is then defined by

$$W_\psi(j,k) := \langle f, \psi_{j,k} \rangle = \int_{\mathbb{R}} f(t)\psi^*_{j,k}(t)dt \tag{2.6}$$

where now

$$\psi_{j,k}(t) = \frac{1}{s_0^{j/2}}\psi(s_0^{-j}t - ku_0s_0^j) \tag{2.7}$$

which decomposes the function f in the discrete set of coefficients $\{W_f(j,k) = \langle f, \psi_{j,k} \rangle\}_{j,k\in\mathbb{Z}}$.

Unlike the *continuous* version, the *discrete wavelet transform* is not always invertible; to ensure the reconstruction of a function from a set of wavelet coefficients is necessary to introduce the 'frames' [49]. A set of functions $\left\{\langle \psi_{j,k} \rangle\right\}_{j,k\in\mathbb{Z}}$ is a 'frame' for $L^2(\mathbb{R})$ if there exists the constants A and B with $0 < A \leq B < +\infty$ such that

$$A\,\|f\|^2 \leq \sum_{j,k} \left|\langle f, \psi_{u,s} \rangle\right|^2 \leq B\,\|f\|^2\,,\ \forall f \in L^2(\mathbb{R})\,.$$

The 'frame' is called 'exact' if $A = B = 1$. An exact frame forms an orthonormal basis in $L^2(\mathbb{R})$ that leads to the wavelet series expansion of f

$$f(t) = \sum_{j,k} \langle f, \psi_{j,k} \rangle\, \psi_{j,k}(t)$$

that is the formula of reconstruction.

By restricting to a dyadic scale (2^n) the values of s and assuming $u_0 = 1$

$$\left\{\psi_{j,n}(t) = 2^{-j/2}\psi\left(\frac{t - 2^j n}{2^j}\right)\right\}_{(j,n)\in\mathbb{Z}^2}, \tag{2.8}$$

we introduce the *multiresolution analysis* in which the basic idea is to reconstruct a function f as a limit of successive approximations, each smoother than the previous one, corresponding to a different level of resolution. The family $\left\{\langle \psi_{j,n} \rangle\right\}_{j,n\in\mathbb{Z}}$ is an orthonormal basis in $L^2(\mathbb{R})$.

In other words, starting from a function f, it is possible to neglect some details and still obtain a function f_1, smooter than the original

f, but that still preserves the main features. The procedure can be performed once again, by starting now form f_1 and going on in the decomposition till to obtain a final version f_n of f that has only the essential features of the original signal.

To build a *multiresolution analysis*, some conditions must be consider. *Multiresolution* approximation, see [33], is a sequence of closed subspaces $\{V_j\}_{j\in\mathbb{Z}}$ of $L^2(\mathbb{R})$ such that

(i) $\forall (j,k) \in \mathbb{Z}^2, \quad f(t) \in V_j \Leftrightarrow f\left(t - 2^j k\right) \in V_j,$

(ii) $\forall j \in \mathbb{Z}, \quad V_{j+1} \subset V_j,$

(iii) $\forall j \in \mathbb{Z}, \quad f(t) \in V_j \Leftrightarrow f(\frac{t}{2}) \in V_{j+1},$

(iv) $\lim_{j\to+\infty} V_j = \bigcap_{j=-\infty}^{+\infty} V_j = \{0\},$

(v) $\lim_{j\to+\infty} V_j = \text{Closure}\left(\bigcup_{j=-\infty}^{+\infty} V_j\right) = L^2(\mathbb{R}),$

(vi) There exists a unique function $\phi \in V_0$ such that the family of functions $\{\phi(t-n)\}_{n\in\mathbb{Z}}$ is an orthonormal basis in V_0.

By defining the function

$$\phi_{j,n}(t) = 2^{-j/2}\phi\left(\frac{t - 2^j n}{2^j}\right),$$

from (i) and (vi), the family of function $\{\phi_{j,k}\}_{k\in\mathbb{Z}}$ is an orthonormal basis for V_j with constant of normalization $2^{-j/2}$. Property (ii) means that V_j is invariant by any translation proportional to the scale $2^j$and it ensures that an approximation at a resolution 2^{-j} contains all the informations to compute an approximation at a coarser resolution $2^{-(j+1)}$ that is the function f_i has all the informations to calculate the function $f_{(i+1)}$. Property (ii) imposes that $V_j \subset V_{j-1}$. In particular $2^{-1/2}\phi\left(\frac{t}{2}\right) \in V_1 \subset V_0$. Since ϕ is an orthonormal basis of V_0, we can decompose

$$\phi\left(\frac{t}{2}\right) = \sqrt{2}\sum_{n=-\infty}^{+\infty} h[n]\phi(t-n) \tag{2.9}$$

with $h[n]$ *filter coefficients* of the *dilation equation* (2.9) with the *scaling function* ϕ[4].

The factor 2^{-j}, allowing to move from V_0 to V_j is called *resolution.*

Therefore, an approximation of a given function $f \in L^2(\mathbb{R})$, at level j, is the orthogonal projection of f in V_j

$$P_{Vj} f = \sum_{n=-\infty}^{+\infty} \langle f, \phi_{j,n} \rangle \phi_{j,n}.$$

Property (v) ensures that $\lim_{j\to\infty} P_{Vj} f = f$ for every $f \in L^2(\mathbb{R})$ i.e. the signal can be obtained as a limit of successive approximations with resolution 2^{-j}. Since $V_{j+1} \subset V_j$, the approximation at the scale j contains all the features of f captured by scale $j+1$ and adds some 'details'. Such details can be modelled as the orthogonal complement W_j of V_j in V_{j-1} that is $V_{j-1} = V_j \oplus W_j$; hence $W_l \subset V_{l-1} \subset V_j$ for $j < l$, W_j and W_l are orthogonal, therefore $L^2(\mathbb{R}) = \oplus_{j=-\infty}^{+\infty} W_j$. Indeed $V_{j-1} = W_j \oplus V_j$ and by substitution $V_L = \oplus_{j=L-1}^{J} W_j \oplus V_J$, for $L > J$. Since $\{V_j\}_{j\in\mathbb{Z}}$ is a multiresolution approximation, V_L and V_J tend respectively to $L^2(\mathbb{R})$ and $\{0\}$ when L and J go respectively to $-\infty$ and $+\infty$. Also an union of orthonormal bases of all W_j is therefore an orthonormal basis of $L^2(\mathbb{R})$.

In an intuitive way, we can say that at each level of approximation, the function f_{i+1} is obtained as $f_i + d_i$, where d_i are the neglected details. These details are in the space W, while the function f_i is in the space V. W and V are orthogonal.

Let us now define the *mother wavelet as a function* $\psi \in W_0$: the family $\{\psi_{j,n}\}_{n\in\mathbb{Z}}$ with

$$\psi_{j,n}(t) = 2^{-j/2} \psi\left(\frac{t - 2^j n}{2^j}\right) \tag{2.10}$$

for any scale 2^j, is an orthonormal basis of W_j and for all scales $\{\psi_{j,n}\}_{j,n\in\mathbb{Z}}$ is an orthonormal basis of $L^2(\mathbb{R})$.

Since $W_1 \subset V_0$ the *mother wavelet* can be derived by the *scaling function* ϕ as

$$\psi\left(\frac{t}{2}\right) = \sqrt{2} \sum_{n=-\infty}^{+\infty} g[n] \phi(t-n).^5 \tag{2.11}$$

---

[4] $h[n] = \left\langle \frac{1}{\sqrt{2}} \phi\left(\frac{t}{2}\right), \phi(t-n) \right\rangle$.

[5] $g[n] = \left\langle \frac{1}{\sqrt{2}} \psi\left(\frac{t}{2}\right), \phi(t-n) \right\rangle$.

We can summarize: an orthogonal wavelet system is a collection of functions obtained as translation and dilations of the two functions: *scaling function* ϕ and *mother wavelet* ψ

$$\begin{aligned}\phi_{j,n}(t) &= 2^{-j/2}\phi\left(\frac{t-2^j n}{2^j}\right),\\ \psi_{j,n}(t) &= 2^{-j/2}\psi\left(\frac{t-2^j n}{2^j}\right)\end{aligned}$$

such that the family $\{\psi_{j,n}\}_{n\in\mathbb{Z}}$ is an orthonormal basis of $L^2(\mathbb{R})$. The importance of the *multiresolution analysis introduced* by Mallat [33] is given by the fact that any function $f \in L^2(\mathbb{R})$ can be expressed by wavelet series

$$f = \sum_{j,n=-\infty}^{+\infty} \langle f, \psi_{j,n}\rangle \psi_{j,n}. \tag{2.12}$$

Since $V_{j_0} = \oplus_{i=-\infty}^{j_0-1} W_i$, equation 2.12 is equivalent to

$$f(t) = \sum_{n\in\mathbb{Z}} a_{j_0,n}\phi_{j_0,n}(t) + \sum_{j=j_0}^{\infty}\sum_{n\in\mathbb{Z}} d_{j,n}\psi_{j,n}(t),$$

where the scaling and wavelet coefficients are defined

$$\begin{aligned}a_{j,n} &= \langle f, \phi_{j,n}\rangle = \int_{\mathbb{R}} f(t)\phi_{j,n}(t)dt, \qquad (2.13)\\ d_{j,n} &= \langle f, \psi_{j,n}\rangle = \int_{\mathbb{R}} f(t)\psi_{j,n}(t)dt.\end{aligned}$$

Therefore each function f can be decomposed in a series of approximation and detail functions; at each approximation each function neglects some details d_i. The procedure is schematically represented in figure 2.3.

It is important to remark that not all wavelet functions have scaling functions; only orthogonal wavelets have their scaling functions. When scaling and mother functions exist together, they act as a low-pass and high-pass filters, respectively, i.e. scaling function captures low frequency components of the signal, mother function, high ones.

2.2.3 Wavelet families

There are many wavelet families in the literature, each characterized by different regularity criteria such as symmetry (useful in avoiding

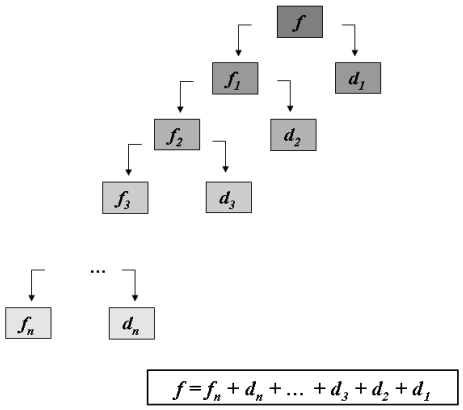

FIGURE 2.3. Schematic sketch of wavelet decomposition process. The original function f can be obtained as a limit of smoother approximations.

dephasing, in particular for image processing), regularity (useful for the reconstruction of the signal), and orthogonality (allowing fast algorithm and space-saving coding), see [33]. Here, Haar wavelet, Daubechies family and the biorthogonal one (the ones used in the following applications) are shortly described.

- The *Haar family* is the simplest family of wavelets with compact support that ensures a good localization in time. The basis is obtained with a multiresolution of piecewise constant functions. The scaling function is

$$\phi(t) = \begin{cases} 1, & 0 \leq t \leq 1, \\ 0, & \text{otherwise.} \end{cases}$$

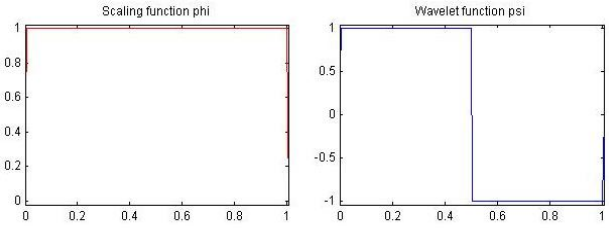

FIGURE 2.4. *Haar* family: *scaling* and *wavelet* functions.

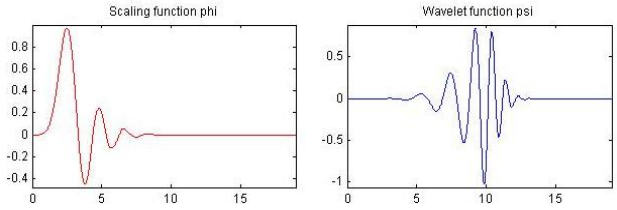

FIGURE 2.5. *10-th order Daubechies scaling* and *wavelet* functions.

The filter $h[n]$ of equation 2.9 has non-zero coefficients equal to $2^{-1/2}$ at $n = 0$ and $n = 1$. Hence

$$\begin{aligned} 2^{-1/2}\psi\left(\frac{t}{2}\right) &= \sum_{n=-\infty}^{+\infty} (-1)^{1-n}\, h[1-n]\phi(t-n) = \\ &= \frac{1}{\sqrt{2}}\left(\phi\left(t-1\right) - \phi(t)\right), \end{aligned}$$

so that the wavelet function obtained is

$$\psi(t) = \begin{cases} -1, & 0 \leq t \leq \frac{1}{2}, \\ 1, & \frac{1}{2} \leq t \leq 1, \\ 0, & \text{otherwise.} \end{cases}$$

- The mother wavelet of the *Daubechies family DaubN*, $N \in \mathbb{N}$, has compact support of length $2N - 1$ and N vanishing moments (i.e. ψ is orthogonal to polynomials with order $p \leq N$). The vanishing moments property ensures that coefficients at finer scales are larger in magnitude where the function has singularities.

  Except when $N = 1$, which corresponds to Haar wavelet, no analytical form of *Daubechies family* exists. Orthogonality and vanishing moments properties have been formulated in terms of the filter coefficients h.

Before presenting *biorthogonal wavelets*, it is necessary to introduce the fast orthogonal wavelet transform.

From Mallat theory, equation 2.13 can be written as

$$\begin{aligned} a_{j+1}[p] &= \sum_{n=-\infty}^{+\infty} h[n-2p]a_j[n] = a_j \star \overline{h}[2p], \\ d_{j+1}[p] &= \sum_{n=-\infty}^{+\infty} g[n-2p]d_j[n] = d_j \star \overline{g}[2p], \end{aligned}$$

where $\overline{h}[2p] = h[n-2p]$ and the operator $\star$ denotes a discrete convolution product. This means that the filter $\overline{h}$ removes the higher frequencies on the inner product sequence a_j while $\overline{g}$ is a high-pass filter which collects the remaining higher frequencies. Therefore an orthogonal wavelet representation of $a_L = \langle f, \phi_{j,n} \rangle$ is composed of the wavelet coefficients of f at scales $2^L < 2^j \leq 2^J$ plus the remaining approximation at the larger scale 2^J, that is

$$[\{d_j\}_{L<j\leq J}, a_J].$$

- *Biorthogonal wavelets* have an explicit expression only as splines defined piecewise. They are characterized by two wavelets and two scaling functions; a first one for the decomposition and a second one for the reconstruction of the signal,

$$\begin{aligned} \phi(t) &= \sqrt{2} \sum_{n=-\infty}^{\infty} h\,[n]\,\phi(2t-n), \quad \widetilde{\phi}(t) = \sqrt{2} \sum_{n=-\infty}^{\infty} \widetilde{h}\,[n]\,\widetilde{\phi}(2t-n), \\ \psi(t) &= \sqrt{2} \sum_{n=-\infty}^{\infty} g\,[n]\,\psi(2t-n), \quad \widetilde{\psi}(t) = \sqrt{2} \sum_{n=-\infty}^{\infty} \widetilde{g}\,[n]\,\widetilde{\psi}(2t-n). \end{aligned}$$

  Particular conditions have to be respected in order to have biorthogonal bases. By considering that

$$g\,[n] = (-1)^{1-n}\,h\,[n-1]\,, \quad \widetilde{g}\,[n] = (-1)^{1-n}\,\widetilde{h}\,[n-1]$$

  and choosing

$$\widehat{h}(\omega) = \sqrt{2} \exp\left(\frac{-i\epsilon\omega}{2}\right) \left(\cos\frac{\omega}{2}\right)^p$$

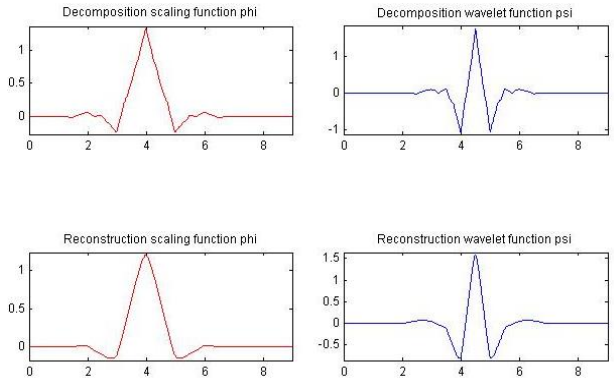

FIGURE 2.6. Scaling functions and biorthogonal wavelets when both $p, \tilde{p} = 4$.

with $\epsilon = 0$ for p even and $\epsilon = 1$ for p odd ($\epsilon = \frac{1-(-1)^p}{2}$), the Fourier transform of the scaling function used in the decomposition is

$$\widehat{\phi}(\omega) = \exp\left(\frac{-i\epsilon\omega}{2}\right)\left(\frac{\sin(\omega/2)}{\omega/2}\right)^p.$$

In this way, ψ is a compactly supported polynomial spline of same degree of ϕ and is obtained as a linear combination of box splines $\phi(2t-n)$.

By selecting $p = 4$ (both in the decomposition and reconstruction process), we obtain a family of wavelets that is often used in image analysis: it has symmetry, good numerical stability and produces small wavelet coefficients in regular domain.

2.3 Use of wavelet transform in structural monitoring

Due to the ability of wavelet transform on detecting and characterizing transients by using a zooming procedures across the scales, several applications in structural health monitoring are possible. In fact, by choosing for example a real ψ function, since it has a zero average, wavelet coefficients $Wf(u,s)$ measure the variations of f in the neighborhood of u whose size is proportional to s: sharp signal transitions create large amplitude wavelet coefficients.

Singularities are detected by following across scales the local maxima of wavelet coefficients. In image processing, high amplitude wavelet coefficients indicate the position of edges which are sharp variations of the image intensity.

These features can allow an identification of frequency components in time and a detection of singularities both in signals and images.

The identification of frequency components, as discussed, was already possible with Fourier transform. In this case it was moreover impossible to identify the instant in which each component appears. Thanks to time-frequency resolution of wavelet analysis, changes into modal parameters can be localized also in time allowing the use of this methodology for on-line application too.

Wavelet capability on detecting singularities has also been applied for a direct identification of damage from displacement and deformation signals. Let us for instance consider a structure (or a part of it) monitored in its displacements; a normal condition can be defined (i.e. the one associated to displacements when no damaging is occurring). When a rare event that damage the structure happens, this will produce an anomalous displacement datum. This datum is a singularity that wavelet analysis may allow to identify.

Wavelets are usually applied to analyze signals in the time domain. Spatial wavelets are also possible. The spatial wavelet formulation is obtained by substituting the parameters t with the the spatial coordinate x in the equations 2.3 and 2.4 for the continuous form and in equations 2.6 and 2.7 for the discrete one, obtaining respectively the continuous spatial wavelet

$$\left(W_\psi f\right)(u,s) := \left\langle f, \psi_{u,s} \right\rangle = \int_{\mathbb{R}} f(x)\psi^*_{u,s}(x)dx$$

$$\psi_{u,s}(x) = |s|^{-1/2}\,\psi\left(\frac{x-u}{s}\right)$$

and the discrete one

$$W_\psi(j,k) := \left\langle f, \psi_{j,k} \right\rangle = \int_{\mathbb{R}} f(x)\psi^*_{j,k}(x)dx$$

$$\psi_{j,k}(x) = \frac{1}{s_0^{j/2}}\psi(s_0^{-j}x - ku_0s_0^j).$$

In this case wavelet coefficients $c_{j,n}$ ($a_{j,n}$ and $d_{j,n}$) behave like a zoom that starts from a gross view of the signal and moves to finer and finer details of it. A sudden change in wavelet coefficients indicates now a local perturbation in the signal in the region spanned by the corresponding wavelet. The suitable scale of wavelet to use will depend on the perturbation present on the material (crack for instance); hence, detection can be poor if the scale does not commensurate with configuration of perturbation.

Spatial wavelet proved very useful for a spatial identification of damage. A spatially distributed set of instruments must be placed in critical regions to detect in the structure; analyses of characteristic data as displacements or deformations are then performed.

By extending in two-dimension wavelet theory (see [33]), applications also to images are possible; several experiments have already been done, in which images of beams or other structural elements have been passed through a wavelet decomposition allowing an identification of anomalies in the region under analysis, always by using wavelet capability to detect singularities.

In the next sections it will be presented two prominent examples of the use of wavelets on the detection of singularities; in the first one, spatial wavelets are used to detect the presence of a crack and to characterize the structural behavior of a notched beam. The second example, instead, presents wavelet capability on detecting anomalous data on time-histories as the ones that can be logged by instruments placed in a monitoring system.

The reported examples are both numerical simulations reproducing real situations that can be met on analyzing existing structures.

2.4 The spatial identification of cracks in a special case of complex body

In the following spatial wavelets are used to analyze the results of a numerical simulation over a notched specimen undergoing a four points bending test. The efficiency of spatial wavelets on detecting cracks has already been demonstrated in literature (see [51], [41]); the example here described presents a completely new application that shows other potentialities of this tool. In fact, the analysis is here performed on a beam made of a particular material, a quasicrystal.

Quasicrystals are metallic alloys that, due to their physical properties (above all high oxidation resistance and low friction coefficient), have gained a growing interest on both mechanical and civil applications (as for example on structures with problem of oxidation or structures that need low friction as trolleys).

These materials are characterized by the fact that the substructural changes can not be neglected (as is always done in studying simple bodies[6]) since they interplay with gross mechanical behavior. By using wavelet analysis it has been possible to characterize these substructural changes and in particular how they interact and influence the gross deformations, in particular around the crack.

2.4.1 A brief introduction on quasicrystals

Quasicrystals are aluminium based alloys with quasiperiodic arrangements of atoms. The break of the translational symmetry in the atomic lattice is determined by the presence of atomic clusters with symmetry different from the prevailing one: they are commonly called *worms*. The worms may be created and destroyed everywhere in the lattice as a consequence of atomic rearrangements: these atomic rearrangements (also called *phason activity*) have a prominent influence on the gross mechanical behavior. Therefore to describe these materials is necessary to introduce internal degrees of freedom, additional to the macroscopic ones, that account for the atomic activity. So, quasicrystals are prominent example of complex bodies; an introduction on the mechanics of complex bodies (in particular with reference to quasicrystals) is given in Appendix A. In order to focus here only on the use of wavelets in spatial detection, also informations on the set up of the numerical simulation are reported on the same Appendix.

2.4.2 The wavelet analysis

A standard four-point bending test of a notched beam (figure 2.7) has been considered; a characteristic dimension of the body $a = 1.0m$

[6] Therefore quasicrystals are a prominent example of *complex body* i.e. a body in which changes in the material substructure have prominent macroscopic effects due to the interactions generated by substructural changes.

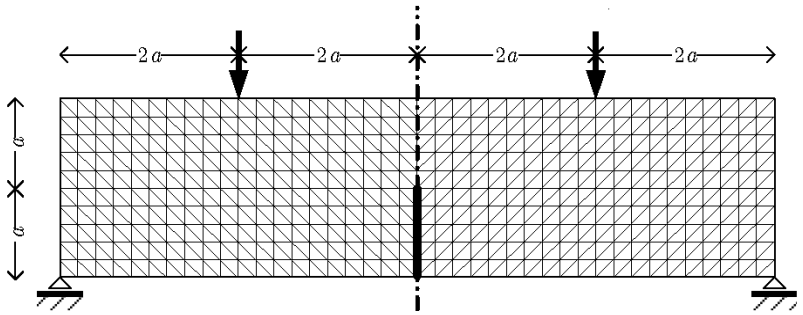

FIGURE 2.7. Four-point bending test of a beam made of quasicrystals and endowed by a notch.

and a unit thickness ($t = 1.0m$) are chosen. The reference value of the loading forces is $F = 1000N$ and no body force acts.

First, we consider a static setting. The 2-dimensional graphs (figure 2.8, figure 2.9 and figure 2.10) display the wavelet coefficients of the gross displacements and of the phason activity along the sections which present the most important results: horizontal sections at the top of the plate and a vertical section in the middle of the plate. Displacements and phason activity of the nodes placed along these sections have been analyzed by wavelet transform.

For this application, we used *biorthogonal wavelets family* since it produces small wavelet coefficients in regular domains; this means that if displacement field (for example) is quite uniform, wavelet coefficients will be all small; on the contrary the presence of a singularity on the displacement field will produce biggest wavelet coefficients in correspondence of the singularity. This feature makes biothogonal wavelets well suitable for singularity detection.

Wavelet analyses on the horizontal section at the top of the plate (figure 2.8) reveal differences between standard displacement (**a)**) and phason activity (**b)**). Standard displacements present perturbations in correspondence of the applied loads and also in the central section where the crack is located; on the contrary, phason activity have singularities only where the loads are applied, no influence of the crack is present. Therefore, it seems to be different the way in which the crack influences standard displacements and phason activity; this becomes even more evident by considering a vertical section on the middle of the plate. For this analysis *Haar wavelet* has also been used; *Haar wavelet* is usually applied in order to detect the

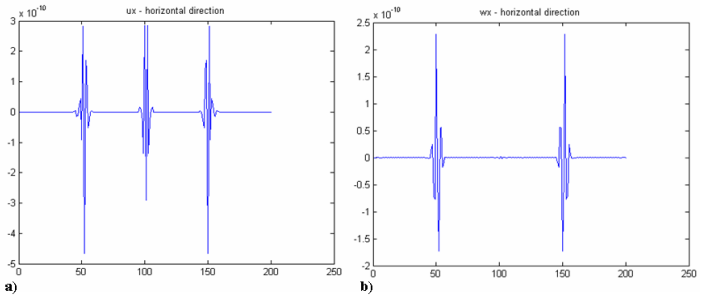

FIGURE 2.8. Wavelet coefficients along an horizontal section at the top of the plate. **a)** Standard displacements. **b)** Phason activity.

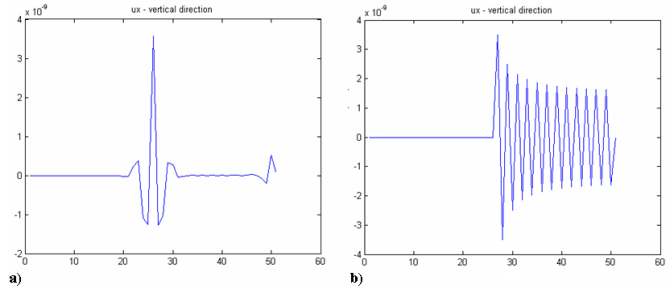

FIGURE 2.9. Wavelet coefficients of standard displacements along a vertical section at the middle of the specimen. **a)** biorthogonal wavelet captures crack tip; **b)** Haar wavelet captures all the span of the crack.

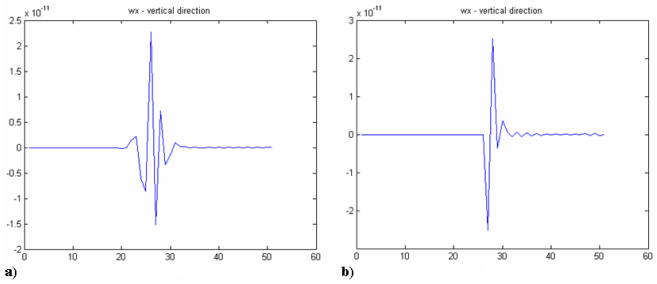

FIGURE 2.10. Wavelet coefficients of atomic activity along a vertical section at the middle of the specimen. **a)** biorthogonal wavelet; **b)** Haar wavelet. In both cases only the crack tip is identified.

spanning of a perturbation, while other wavelets (as the biorthogonal one) capture more exactly the beginning of it.

Figure 2.9 shows the analysis on standard displacements: biorthogonal wavelet captures exactly crack tip, Haar one all the span of the fissure. By performing the same analysis on phason activity instead (figure 2.10), one may note that both biorthogonal and Haar wavelet present not null coefficients only at the tip; since Haar wavelet coefficients too are almost null except on correspondence of the tip, this analysis allows to state that phason activity is perturbed only by the tip and not by all the following edges of the crack as in standard displacements.

Let us now consider a dynamic case in which an impulsive load of duration $t_{\text{imp}} = 0.125 \times 10^{-3} s$ is applied. The 3-dimensional graphs below display the evolution in time of the wavelet coefficients associated to the dynamic setting. In this case the same analyses as before have been performed for each instant of the simulation and reported in an unique plot that collects all time instants.

The analysis of the standard displacement (figure 2.11 **a)**) reveals that the perturbations induced by the presence of the loads and of the crack (the perturbations described before in figure 2.8 **a)**), do not remain localized and their effects tend to disappear in time. In fact the few big spikes initially present become several smaller spikes distributed along the section. On the contrary, in the phason activity, the effects of load application (shown before in figure 2.8 **b)**) do not propagate in time (figure 2.11 **a)**); they decrease in time but being always well localized.

The vertical section presents the same feature as regard as the standard displacement (figure 2.12 **a)**), while for the phason activity in this case the perturbation of the crack tip increases in time (figure 2.12 **b)**).

The analyses presented show that an application of wavelets allows to identify singularities in signals not evident at a first glance; crack influence, crack span, load application have been determined in standard displacement. In addition by means of wavelets, it has been possible to study also a behavior that is not possible to detect at a first glance i.e. the phason activity and in particular as cracks and loads influence it. This is important since as explained, *phason activity* interacts with gross deformations and influences them; in order to study the application of quasicrystals on engineering struc-

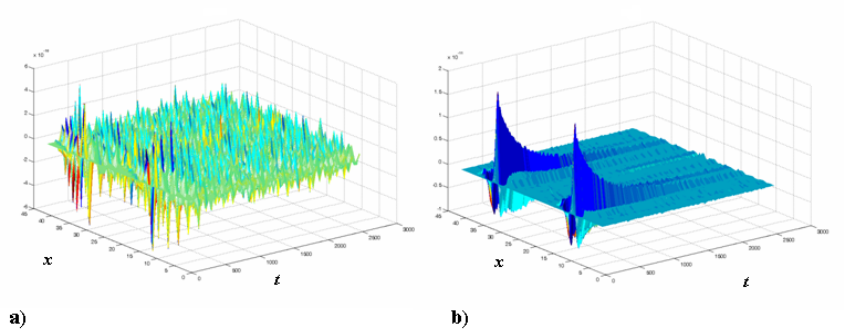

FIGURE 2.11. Time-histories of wavelet coefficients of standard displacements (**a)**) and atomic activity (**b)**) of the horizontal section at the top of the plate.

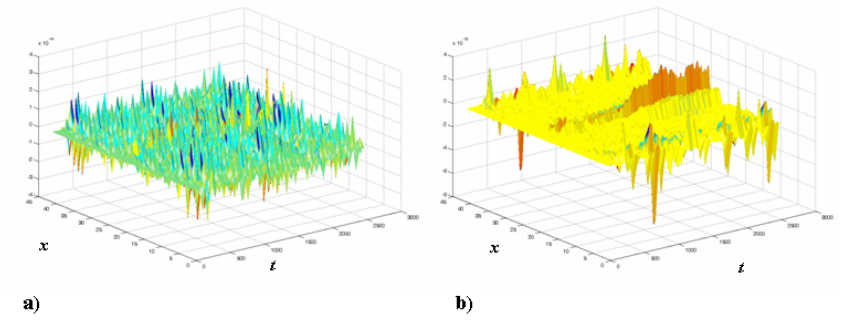

FIGURE 2.12. Time-histories of wavelet coefficients of standard displacements (**a)**) and atomic activity (**b)**) of the vertical section at the middle of the plate.

tures is therefore necessary to characterize substructural changes and wavelet application can result an useful tool.

2.5 Detection of isolated events in thermoelastic simple bodies: illustration of a methodology

Previous section presented a particular application of wavelet transform to detect singularities in space; singularities that influence the structural behavior (as crack or load application). However wavelets, as seen, can be expressed also in time variable and thus applied also for a temporal identification of singularities. In what follows a wavelet-based methodology for detecting critical events in displacement and temperature histories, obtained by monitoring in-situ thermoelastic structures, is proposed [8]. It is based on the wavelet analysis of thermoelastic potentials furnishing the possibility to detect cases in which sudden jumps occur in the displacement time-history.

This application results useful in particular in-situ measurements; in fact, in a static monitoring system in thermoelastic environment, measures of temperature variations and displacements are commonly acquired by sensors variously placed around the structure (thermometers) and on the structure itself (displacement trasducers often referred as 'deformometers'), in particular along cracks if they exist and are so large to be monitored. Previously the use of wavelet analysis to detect isolated events directly from displacement time-histories has been introduced. In case of high level of noise, direct identification can not be possible, even with wavelet analysis. Several studies have already been done on this field (see for example [3], [16]), but encountering always difficulties that do not allow to obtain good results. A deeper investigation that accounts on some mechanical parameters playing an important role in thermoelastic phenomena is necessary.

The attention has been focused on the internal energy and on the enthalpy (and, if possible, on other thermoelastic potentials) because they account for the cumulative effects of strain and temperature variations simultaneously, at least on the part of the structure under monitoring. In fact the coupling between temperature variations and deformations can play an important role in the structural response. The direct analysis of internal energy, enthalpy and even of other

thermoelastic potentials, may allow to account for the thermoelastic coupling.

In the sequel, analyses are developed in the framework of infinitesimal deformation setting in order to underline only the essential aspects of the proposed procedure.

Before presenting the methodology, a brief introduction on thermoelastic potentials is here reported.

2.5.1 Thermoelastic potentials in small deformation setting: a brief review

Basic equations (congruence relations, balance equations, constitutive relations and heat conduction equation) for a linear elastic heat conductor are deeply explained in [12] (see also [10], [46]).

Once the expression of thermoelastic potentials is known, by exploiting Clausius-Duhem inequality, constitutive restrictions on the stress and entropy follow as usual.

If strain and temperature histories are available at a point x, namely maps

$$t \mapsto \varepsilon_{ij}(t,x), \qquad t \mapsto T(t,x), \tag{2.14}$$

consequent histories of thermoelastic potentials follow and one obtains (at each x) maps

$$t \mapsto e(\varepsilon_{ij}(t,x),T(t,x)), \quad t \mapsto h(\varepsilon_{ij}(t,x),T(t,x)), \tag{2.15}$$

with e the internal energy and h the enthalpy. They are related by

$$h(\varepsilon_{ij},T) = e(\varepsilon_{ij},T) - \sigma_{ij}\varepsilon_{ij}, \tag{2.16}$$

where σ_{ij} is Cauchy stress tensor.

For example, for an isotropic thermoelastic body, the explicit expression of e is given by

$$e(\varepsilon_{ij},T) = \frac{1}{2}\lambda_T\varepsilon_{kk}^2 + \mu\varepsilon_{ij}\varepsilon_{ij} + k_T\alpha_0 T_0\varepsilon_{kk} + \frac{c_V^0}{2T_0}(T^2 - T_0^2), \tag{2.17}$$

where λ_T and μ are the isothermal Lamé elastic constants, $k_T = 3\lambda_T + 2\mu$ is the isothermal bulk modulus, α_0, and c_V^0 the coefficient of volumetric thermal expansion and the specific heat at constant strain, respectively. T_0 is the temperature of the reference state.

Cauchy stress σ_{ij} follows, namely

$$\sigma_{ij} = \left(\frac{\partial e}{\partial \varepsilon_{ij}} \right)_T . \tag{2.18}$$

In this way, one gets

$$h(\varepsilon_{ij}, T) = -\left(\frac{1}{2} \lambda_T \varepsilon_{kk}^2 + \mu \varepsilon_{ij} \varepsilon_{ij} \right) + k_T \alpha_0 T \varepsilon_{kk} + \frac{c_V^0}{2T_0} (T^2 - T_0^2). \tag{2.19}$$

The expressions of e and h above are now used to show explicitly how the methodology proposed here can be applied to real problems. It is assumed that only data about displacements and temperature variations from the in-situ sensors are available. If the reference value s_0 of the entropy is known for some reason, one can make use also of other thermoelastic potentials. For example, for an isotropic material, Helmholtz free energy and Gibbs potential are given respectively by

$$\begin{aligned} f(\varepsilon_{ij}, T) &= \frac{1}{2} \lambda_T \varepsilon_{kk}^2 + \mu \varepsilon_{ij} \varepsilon_{ij} - k_T \alpha_0 (T - T_0) \varepsilon_{kk} + \\ &\quad - \frac{c_V^0}{2T_0} (T - T_0)^2 - s_0 (T - T_0) + s_0 T, \end{aligned} \tag{2.20}$$

and

$$g(\varepsilon_{ij}, T) = -\left(\frac{1}{2} \lambda_T \varepsilon^2 + \mu \varepsilon_{ij} \varepsilon_{ij} \right) - \frac{c_V^0}{2T_0} (T - T_0)^2 - s_0 T. \tag{2.21}$$

Expressions of these potentials in terms of stress and entropy are also available [32].

Data are often obtained by disposing sensors along lines so that only one-dimensional displacement and/or temperature histories are recorded. Such a situation occurs for example in civil engineering structures in the case in which macroscopic cracks cut a wall (even partially). Sensors are placed along the width of the wall by crossing the lateral margins of the cracks themselves so that one has at disposal only data along one-dimensional sections.

In this case, the problem can be simplified: the internal energy and the enthalpy become respectively

$$e(\varepsilon, T) = \frac{1}{2} \left(\lambda_T + 2\mu \right) \varepsilon^2 + k_T \alpha_0 T_0 \varepsilon + \frac{c_V^0}{2T_0} (T^2 - T_0^2), \tag{2.22}$$

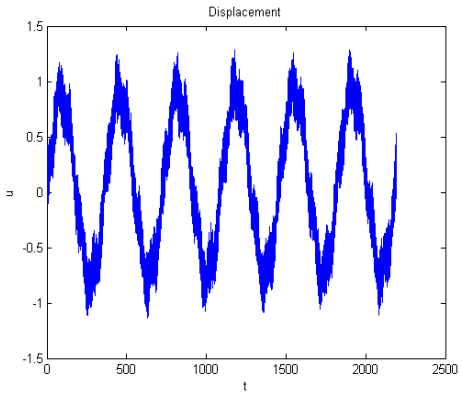

FIGURE 2.13. Displacement u versus time t.

$$h(\varepsilon, T) = -\frac{1}{2}\left(\lambda_T + 2\mu\right)\varepsilon^2 + k_T \alpha_0 T\varepsilon + \frac{c_V^0}{2T_0}(T^2 - T_0^2), \qquad (2.23)$$

where the strain ε is now

$$\varepsilon = u', \qquad (2.24)$$

i.e. the derivative of deformometer measure with respect to the spatial variable along the axis where sensors are placed. Along the same axis, it is also assumed to be able to detect variations of temperature. Let T be the thermometer measure at a given time t, T_0 the reference temperature and let also the material constant λ_T, μ, α_0, c_V^0 be assumed time-invariant (this last assumption implies that the variations of the temperature are not very large).

In this case a typical picture of data of displacement and temperature histories is collected in figure 2.13 and figure 2.14 respectively. A time interval of six years is simulated and data are sampled one time a day.

These data reproduce typical real data observed in thermoelastic structures but are not referred to a special case. They are similar to those obtained by monitoring on one-dimensional section cracks in historical buildings. They are a numerical simulation that accounts for features of temperature variations and temperature-induced displacements. Temperature signal is obtained as a superimposition of two sinusoids (with annual and daily periodicity respectively) to a linear trend that simulates the slow increment of temperature in time over years. Displacement signal is proportional to the temperature history and accounts also of a delay due to thermal inertia of

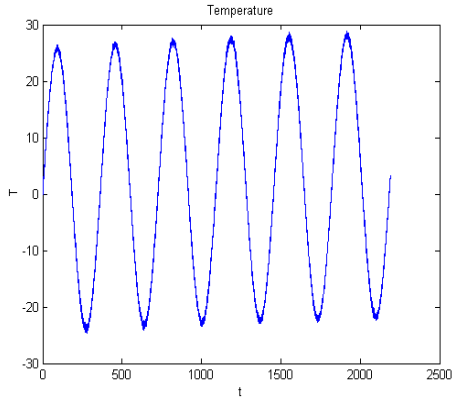

FIGURE 2.14. Temperature T versus time t.

masonry. In both temperature and displacement signals a Gaussian noise is also introduced in order to simulate instrumental noise.

2.5.2 Detection of singularities

Let us consider the case in which an isolated jump (a *spike*) occurs in the signal of displacement u versus time t (figure 2.15), a spike due to an unknown reason that could represent a dangerous event for the whole structure.

The monitoring system is not able to check data. A visual inspection of each of them is not possible, and even if it could be possible, it is necessary to be able to detect also anomalous data covered by the noise of the signal and therefore not remarkable by a visual inspection. In the figure 2.15 the spike is quite evident but often the presence of noise can cover spikes of various nature, not allowing a direct identification of them. It would be desirable to detect in real-time these spikes, even if a direct observation of the signal is not meaningful per se.

The wavelet analysis can be performed directly on the displacement signal. Here the wavelet function of 10-th order Daubechies is used due to its satisfactory resolution in both time and frequency.

Take note that in the analysis proposed below, reference is always made to detail coefficients at high levels of frequency, in particular to coefficients: $D1$ that cover the frequency range $[0.25 - 0.5]$ of day, $D2$ the frequency range $[0.125 - 0.25]$ and $D3$ the frequency

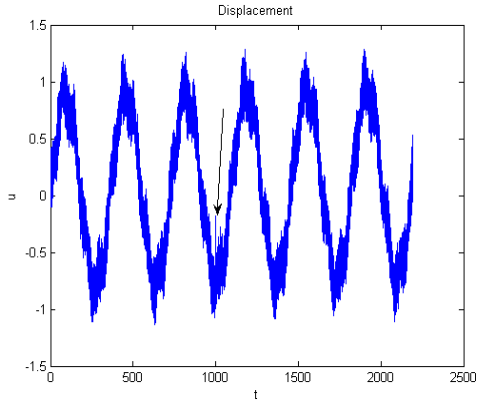

FIGURE 2.15. Displacement u with a spike (indicated by an arrow) versus time t.

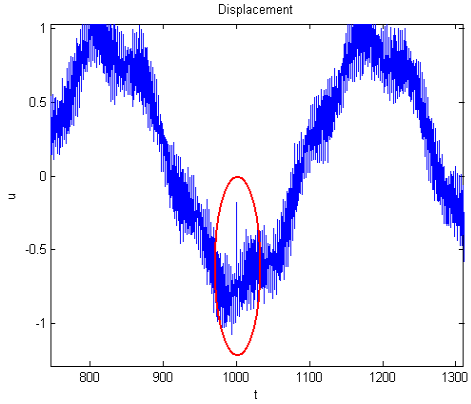

FIGURE 2.16. Zoom of Figure 2.15 around the spike.

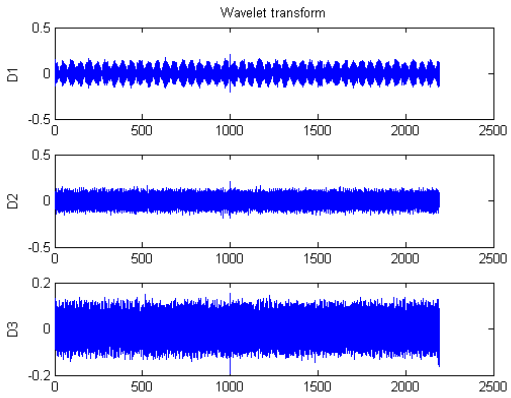

FIGURE 2.17. Wavelet transform of a displacement history that presents a spike the detection of which is covered by noise. Wavelet coefficients $D1$, $D2$ and $D3$ are not able to detect the singularity.

range $[0.0625 - 0.125]$ (frequency acquisition is a datum of every day activity of monitoring system). Since we are interested in sudden changes of the signal (that influence high frequencies, i.e. low levels of wavelet coefficients), lower levels of frequency (i.e. high levels of wavelet coefficients) are not able to identify these changes, resulting for this reason not meaningful.

However, in presence of noise, the singularity is covered by the noise itself and therefore the wavelet analysis is not useful. The typical situation is displayed in figure 2.17.

By evaluating thermoelastic potentials a more precise identification is possible. Notwithstanding the presence of noise, the histories of the internal energy and enthalpy reveal clearly a peak value in correspondence of the spike in the displacement, as shown in figure 2.18 and figure 2.19.

The wavelet analysis of internal energy (figure 2.20) and enthalpy histories (figure 2.21) emphasizes the singularity underlining its contributions at various frequencies. By this kind of analysis, local maxima of the potentials are levelled while the singularity, already noticeable in the plot of internal energy and enthalpy histories, appears as a peak value in different wavelet levels, avoiding cases of false positive alarms.

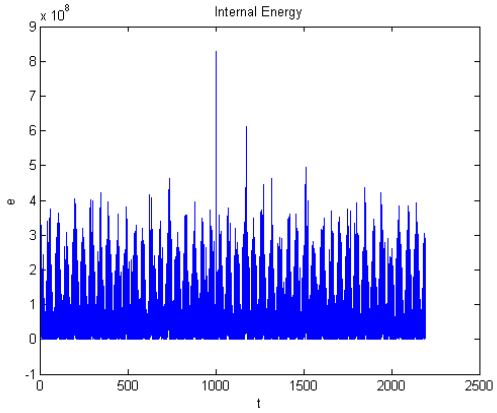

FIGURE 2.18. Internal energy e associated with the displacement of Figure 2.15.

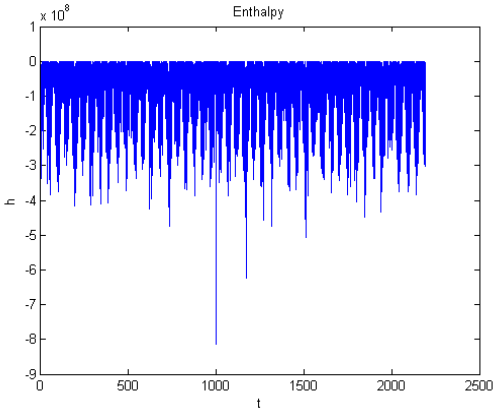

FIGURE 2.19. Enthalpy h associated with the displacement of Figure 2.15.

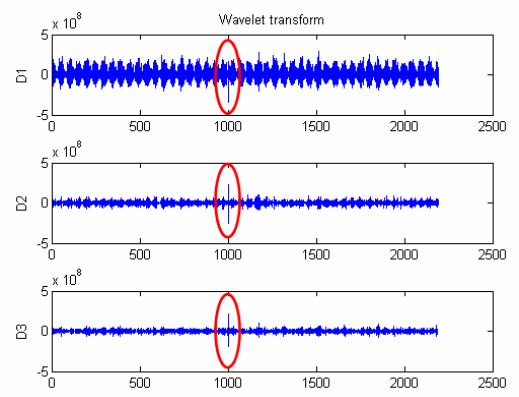

FIGURE 2.20. Wavelet transform of the internal energy e derived by signals of temperature and displacement with a spike covered by noise. An isolates spike appears on correspondence to the singulariry present on the displacement.

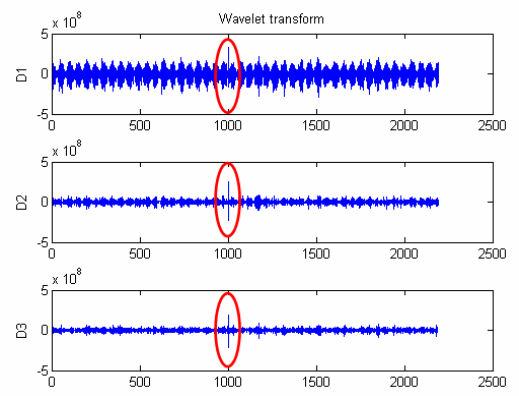

FIGURE 2.21. Wavelet transform of enthalpy h derived by signals of temperature and displacement with a spike covered by noise. Also here the singularity is detected by means of the wavelet analysis.

3
Early-warning monitoring

In this chapter an early-warning monitoring procedure based on a wavelet analysis of experimental data available on Brunelleschi dome of Florence will be presented. However this procedure could be applied to any structure that undergoes a temperature dependent variation of crack opening, allowing a real-time detection of anomalous deformations.

As a relevant example, we referred to Brunelleschi dome that is one of the most famous monuments of Italian Renaissance. It is a symbol for the city of Florence and it has also a relevant importance from an engineering point of view for its peculiar and complex building technique. Thus it can be argued that it has an intangible cultural, historical and economical value.

This structure during its history has suffered from a damaging process that has determined a complex crack pattern interesting the main structure: some of these cracks cut completely the dome from the intrados to the estrados. For this reason since 1988 a large monitoring system has been placed on it in order to verify structural safety and several studies have been done.

Analyses performed on the experimental data acquired by the sensors have established a temperature dependent behavior of displacement logged on the cracks. This behavior seems not to be dangerous for the structure itself. In addition, also a tendency to crack opening

increment is present; even if this process evolves quite slowly, it is an irreversible process: than it is necessary to monitor it because it could lead in the future to a sudden extreme deformation of the structure it-self.

The aim of this work is to identify in real-time if some anomalous structural deformation occurs, leading to an irreversible increment of crack opening. The early-warning procedure presented herein is based on a wavelet analysis of thermoelastic energy.

In most engineering applications in which temperature variations are involved, the analysis is simplified by uncoupled procedures that account for deformation and temperature histories separately. However, the coupling between temperature variations and deformations can play an important role in the structural response: a sudden change on the structural behavior is emphasized on the wavelet coefficients of internal power.

With this methodology, spikes on the deformation signal are analyzed by checking if they can be due to a real structural problem or to an anomalous acquisition of the monitoring system. Only the first case will produce the overcoming of a fixed threshold and therefore the warning signal.

Before to present the early-warning procedure a description of the Brunelleschi dome structure, the crack pattern and the monitoring system installed will be introduced.

3.1 Brunelleschi dome

3.1.1 The structure and the crack layout

S.Maria del Fiore cathedral construction took long time: it was started in 1295 and completed only in the XIX century. Even after 70 years of the beginning of the works the cathedral was almost completed, two centuries later the dome was not yet built: the drum (the structural element from which the dome starts) was too high to use scaffolding necessary for dome and nobody was able to build the dome without scaffolding. In 1407 Filippo Brunelleschi was not believed when he stated that he could construct a dome without scaffolding. He was still not believed in 1418, but was nevertheless entrusted with the work. Many books have been written about the technique used by Brunelleschi in the construction; the fact is that he overcame all

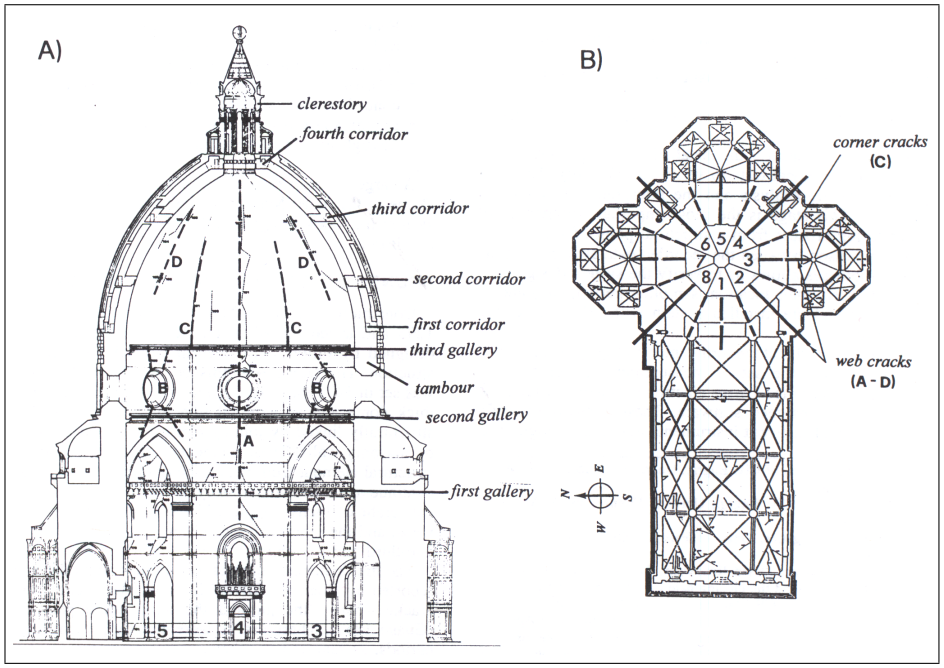

FIGURE 3.1. Static sketch of Brunelleschi dome.

the difficulties and in 1434 the dome was finished and in 1472 the clerestory was set (figure 3.1).

The dome realized by Brunelleschi is octangular at every horizontal section. It has, as San Pietro in Rome, two shells: the total thickness of $4,2\ m$ is composed of an outer dome of thickness from $0,7$ to $0,9\ m$, and an inner dome of $2,0$ to $2,2\ m$. Stairs in the void (of a meter to a meter and a half) give access to the clerestory. Joining elements, two for each web, constructed by masonry walls, link the two domes starting from the drum (see figure 3.1A)) and continuing as far as the clerestory.

In 1639 Gherardo Silvani reported the first historical informations about structural damage: he told about small cracks were "*the air and the wind could pass through*" [25]. In reality these cracks were already present in previous periods, as reported in other documents by Silvani himself and by Giovan Battista Nelli. A complete survey of the cracks was done later in 1757 by Leonardo Ximenes who described 13 different crack sets [52].

To present the crack pattern, the eight webs are numbered from 1 to 8, 1 being the web facing the nave and following the counter-clockwise direction (see figure 3.1B)). From an architectural point of view, even webs are located over the pillars, uneven numbered webs over the arches [3].

The two main cracks described by Ximenes were located in webs 4 and 6 (type A in figure 3.1). They start from the drum and continue as far as the higher part of the dome, passing through both the structural internal and external domes. Other small cracks near the edges between the webs were described.

Nevertheless he did not report the other two main cracks which are nowadays present in webs 2 and 8. These cracks are therefore formed after 1757 and are of the same type of those in webs 4 and 6.

Three additional types of cracks complete now the actual crack pattern; these include:

- several vertical cracks near the circular windows (called '*eyes*'), just above the keystones of the arches, in the uneven webs (type B);

- some minor vertical cracks, even if with less amplitude with respect to type A, and not passing through the width of the two domes, around the eight internal edges of the dome (type C);

- four cracks in the upper internal part of uneven webs that do not pass through the dome (type D).

The overall crack system is therefore quite symmetric about its center.

Figure 3.1B) shows as the main dome is buttressed to the north, south and east by dome apses, and on the west by the nave of the cathedral; the crack pattern seems to indicate that the north buttressing system has moved to the north, the east to the east and the south to the south, with perhaps the west side remaining firm. Heyman states the hypothesis that the dome has cracked through four of its shell (cracks type A) to accommodate these movements [27].

FIGURE 3.2. A crack of type A) and one of the displacement trasducers that logs its movements.

The cracks have always been of concern, so several control devices have been placed to measure their evolution. The largest one was installed in 1987 and has been working since 1988.

3.1.2 The monitoring system

An essential help for the design of the modern monitoring system placed on the dome were the studies and the experiences made by the Director of the *Osservatorio Ximeniano*, Padre Alfani in 1934 who first measured the 'breath' of the dome. Thanks to these informations it was decided to check in the same time variations of cracks width as well as movements of the overall structure. Temperature variations must also been provided since these were thought to be the main cause of crack width variations; therefore both air and masonry temperatures were logged.

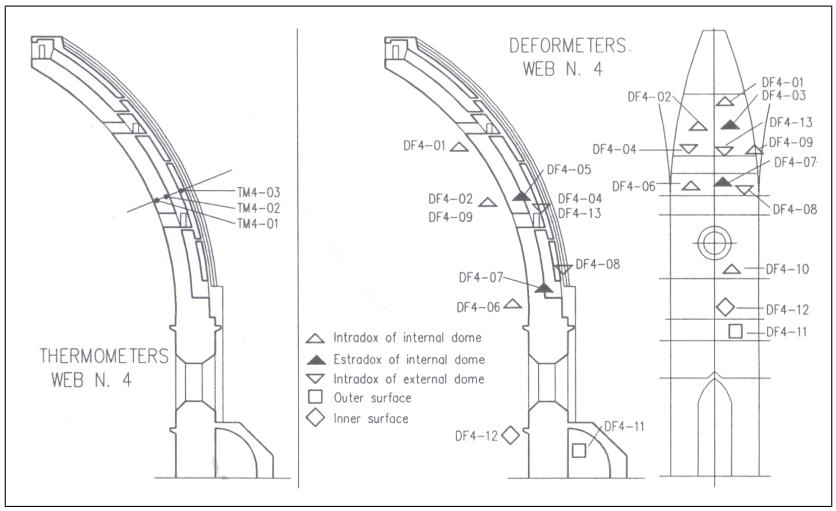

FIGURE 3.3. Position of instruments on web 4.

The monitoring system includes 166 instruments: displacement trasducers, telecoordinometers, livellometers, thermometers and piezometers:

- displacements trasducers have been placed mainly across full-depth cracks (figure 3.2) and near the wedges of the dome always in 'tangential direction'; in order to evaluate possible relative sinking between dome basement and superstructure, other instruments have been positioned near the lower edge of the circular openings (figure 3.3). They are marked *DFn-mm* where n indicates the web and mm the position. Their precision is of about $\pm 0.02\ mm$. Data are logged with respect to the reference at the day in which the instruments were placed: thus, only variations of crack width is given.

- In order to evaluate horizontal displacements telecoordinometers have been placed near the wedge of the dome. Vertical movements of the horizontal plane just below the edges of the circular openings are measured by means of livellometers.

- Thermometers were installed in each web at the second corridor level in such a way so as to measure the internal dome temperature in three different points and the external dome

temperature in two points (figure 3.3). *TM* indicates the thermometers on the masonry, *TA* the ones on the air.

- Piezometers placed externally of the dome, close to web 4 evaluate variation in the level of underground water.

The system was programmed to automatically log data every 6 hours for all instruments, starting at 6:0 a.m.

3.1.3 Analysis of experimental data

The logged data have been analyzed [3], [16] in order to investigate the structural behavior of the monument.

First it was noticed that in reason of this complex crack pattern, the dome does not behave as a circular shell, but like four drifting half-arches, linked just below the upper clerestory, the backs of which are constituted by pillars, the chapels and the nave of the church [16].

Chiarugi *et al.* [16] showed that the main cause of cracking must be looked for in the dome structure itself: its geometry, the combined effect of its self-weight and insufficient resistance of the drum. Vertical cracks are in fact already been observed in several historic masonry domes: they are due to the tensile stress along the parallel direction; this effect is amplified in Brunelleschi dome by the *"herringbone"* disposition of the bricks[1] that reduces the tensile resistance along the parallels.

Since the drum is supported by four pillars in correspondence of the even webs and by four arches in the uneven ones, this difference in support has probably caused the differences in cracking between even and uneven webs. In fact the tensile stress along the parallels is partially balanced in the uneven webs by compressive stress induced by the presence of arches, limiting cracks amplitude. Arches themselves, at the same time, determine an increment of tensile stress above the pillars, determining an increment in cracks amplitude in the even webs.

A particular attention has then been paid to the correlation between environmental actions and structural response. The following observations from experimental data have been done [3]:

[1] The *"harringbone"* disposition of the bricks was the technique used by Brunelleschi in order to build up the structure without falsework. (For deeper informations see [5], [27])

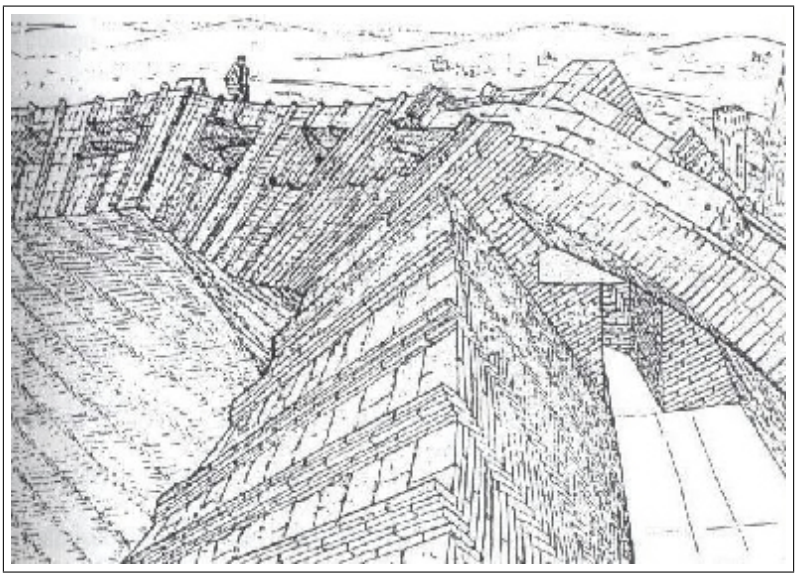

FIGURE 3.4. The *"harringbone"* disposition of the bricks: vertical bricks have been placed each 1.2 m.

- from a comparison between displacements and temperature time-histories, in both the same periodic phenomena have been observed: the first and main one is a long-term variation reproducing annual cycle; the second one is a daily variation (see figure 3.5).

- As regard temperature distribution, analyses of cross-correlation between data measured at the same level in different webs show good agreement and similarly to data for instruments placed at different levels in the same web and at the same distance from the center of the dome. Thus no particular influence has different sun exposition of the webs. This consideration implies that temperature distribution can be assumed constant along both the meridians and the parallels. In the radial direction instead, a gradient in temperature is present. This is a consequence of thermal diffusion between different layers of the dome and of the thermal inertia of the masonry itself.

- Along the main cracks (type A), a different behavior characterizes lower and higher part of the crack: while the inferior part is opening, the superior one is closing and vice versa. Where

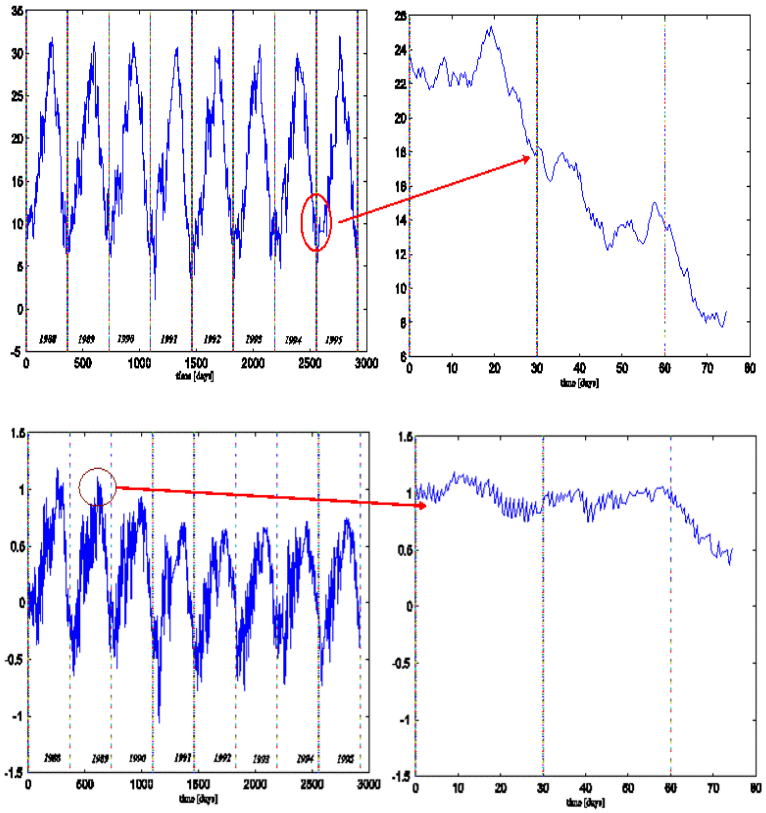

FIGURE 3.5. Annual (on the left) and daily (on the right) periodicity in temperature (top) and deformation (bottom) signals. (Temperatures in $°C$, displacements in mm).

the dome is more free to expand, an increase in temperature determines a great opening of the cracks, while where effective constrains are present (i.e. nave and chapels), the thermal dilatation causes crack closing. Crack behavior is therefore a complex phenomenon related to the complexity of the whole structure.

- In the radial direction too, opening and closing of the cracks between internal and external part of the dome are out phase.
- As regard the relationship between temperature and crack variations, the analyses have confirmed the strong correlation previously supposed concerning with the seasonal behavior of the structure. As mentioned before, temperature variations determine different crack movements depending on the site of the crack itself.
- The fact that the nave acts as a restrain for the dome has been confirmed by telecordinometers data that give information about the displacements of the pillars. Analyses of leveling instruments as well as of piezometers no additional informations have revealed.

The performed analyses on the recorded data show that both yearly and daily variations in width of the cracks are mainly temperature dependent. This one represents a reversible phenomenon. However, by removing these two periodicity in the deformation signal, also a trend is present that depicts an irreversible degree of cracking. Average annual increase of width cracks is about $0,06\ mm$. Even if this modest increase does not give rise to alert about an immediate structural stability, the pattern and magnitude of the cracks should be monitored and kept under control.

3.2 Early-warning procedure

In order to control in real-time structural behavior, a wavelet based analysis of early-warning monitoring has been implemented in this thesis. It is based on a general procedure for monitoring thermoelastic systems previously presented in 2.5, a procedure based on a

wavelet analysis of thermoelastic energy. In the procedure presented below it has been used the wavelet transform of the thermoelastic power and a wavelet analysis of the temperature history has also been performed to distinguish a spike due to instrumental error from one associated to a structural damage.

As discussed before, wavelet analysis is an efficient tool for damage detection, above all for its ability to examine data acting as a zoom that starts from a gross view of the signal and moves to finer and finer details of it, allowing an identification of local perturbations even invisible to a direct observation of the signal itself. A sudden variation of the original signal is therefore amplified in wavelet coefficients. Wavelet analysis is here performed on the internal power that accounts for the cumulative effects of strain and temperature variations simultaneously, at least on the part of the structure under monitoring.

As we have seen in Brunelleschi dome, displacement amplitudes as well as their time evolution are substantially regular, temperature dependent and not dangerous for the structure in the sense that they lie within a range that can be considered *normal*.

On the contrary, an irreversible degree of cracking would be represented by a sudden spike on the data displacement, followed by a rigid translation of the signal itself, a translation that indicates the beginning of a possible structural severe damage (see figure 3.6 A)). This is the event that a threshold monitoring system has to reveal in real-time. Take note that spikes on displacement values could also be due to problems in the acquisition system as in the case of a lightning: in this case spikes will appear also on temperature data (figure 3.6 B)).

With this methodology, spikes on the deformation signal are analyzed by checking if they can be due to a real structural problem or to an acquisition malfunction of the monitoring system. Only the first case will produce the overcoming of a fixed threshold and therefore the warning signal.

3.2.1 Wavelet application on displacement signal

Let us consider the case of the displacement signal recorded by deformometer *DF-406* (as introduced before, the number 4 indicates the web, 06 the position along the crack) placed on one of the main cracks of the dome (figure 3.7). Time t is expressed in day units.

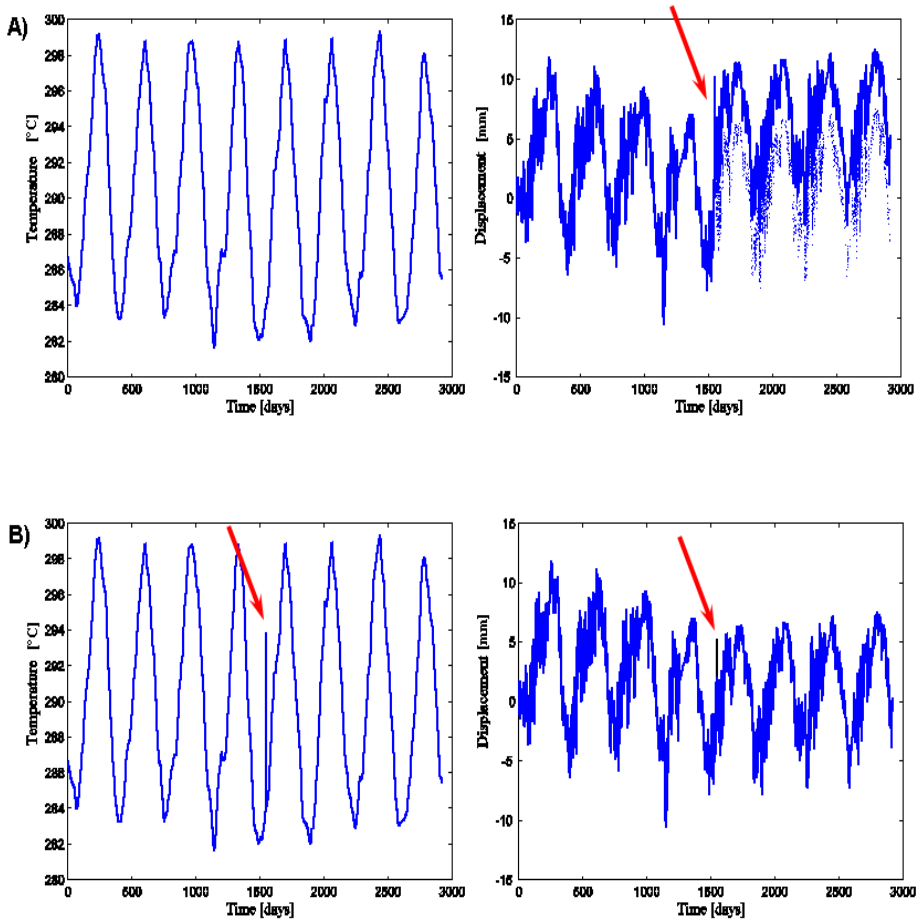

FIGURE 3.6. A) Temperature and displacement signals associated to a structural problem. (In displacement signal, original data are in dotted line, data representing the structural problem are in continuous line). B) Temperature and displacement signals in case of acquisition problems: an *irregular* datum appears at the same time in temperature and diaplacement signals.

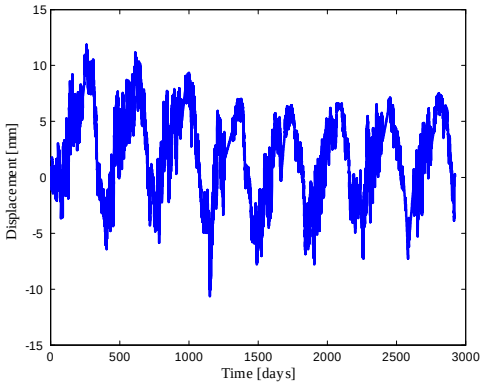

FIGURE 3.7. Displacement signal recorded by deformometer *DF-406*.

Since the aim of a threshold monitoring is to detect *in real-time* discontinuity, the signal has been modified by introducing a singularity represented by a spike on the last datum (Figure 3.8). (We have chosen the last datum since we suppose to operate in real-time and therefore *irregular* datum would be the last one logged by sensors).

This situation could happen at the beginning of a structural damaging.

It is important to note that Fourier analysis of the displacement signal (in figure 3.9) is not useful in this case, since it reveals only the frequency contents of the signal, but not when each spectral component appears in time. Moreover, it is also expected that Fourier transform is not sensitive to a spike in the last datum. Even if there is a difference (figure 3.9) between the Fourier spectrum associated with signal in figure 3.7 and the one associated with the signal in figure 3.8, no information about the instant in which these differences appears is given. Moreover it is not possible to know if these changes on the Fourier spectrum are associated with a real structural problem or simply to a malfunction on the acquisition system.

A wavelet analysis would be more relevant for this aim. Unfortunately, because of both the complexity of this signal and the noise level, also a direct application of wavelet transform on displacement of figure 3.8 is not able to identify clearly the singularity: only small spikes appear on the last datum of some wavelet coefficients (see figure 3.10 and 3.11) resulting not useful for a clear identification.

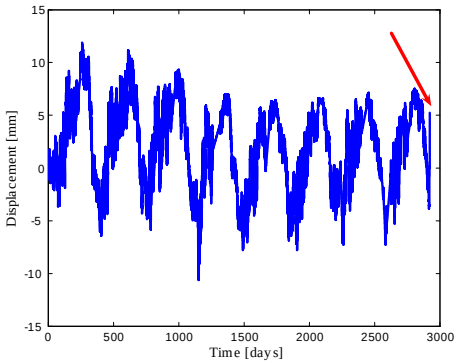

FIGURE 3.8. Displacement signal of the deformometer *DF-406* modified by introducing a singularity on the last datum logged.

Please note that, even if not evident at a first glance, displacement signals (in particular those logged by sensors placed on the external dome) have a high level of noise, probably due to wind effects, which corrupt the original data.

Many types of mother wavelet can be defined; here the wavelet function of *10-th* order Daubechies is used due to its satisfactory resolution in both time and frequency. Explicit form is not available for Daubechies wavelets; values of the filters used for the decomposition can be found in [10].

The represented wavelet coefficients spread frequency range respectively equal to: $D1$ frequency range $[0,5-1]$ day, $D2$ $[1-2]$, $D3$ $[2-4]$, $D4$ $[4-8]$, $D5$ $[8-16]$, $D6$ $[16-32]$, $D7$ $[32-64]$, $D8$ $[64-128]$, $D9$ $[128-256]$, $D10$ $[256-512]$, $D11$ $[512-1024]$, $D12$ $[1024-2048]$ days. It is important to note that coefficient $D10$ captures exactly the annual periodicity that characterized the signal. However the identification of the frequencies that characterize the signal is not our aim, it is not useful for a real-time monitoring and in any case could be done also by Fourier transform. In the identification of singularities instead the attention must be paid only on the low coefficients that represent the higher frequencies of the signal where singularities are detected. Low frequency components do not result useful and thus on the following they will be neglected.

Since in this case a simple application of wavelet analysis on the displacement signal is not useful for the sake of a damage monitoring, a more deep study on the mechanics of the structure is necessary.

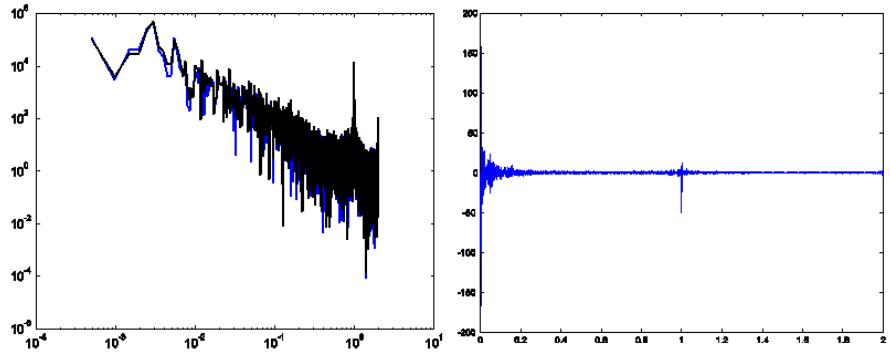

FIGURE 3.9. On the left the Fourier transform of displacement in figure 3.7 (blu line) and of displacement in figure 3.8 (black line). On the right difference between the two spectra. Note that here frequency equals to one correspond to one year period

3.2.2 Thermoelastic analysis

In order to analyze the coupled thermoelastic behavior of the dome, the evolution on time of the internal power associated with the crack width and the temperature variation has been studied. First it has been considered the case of a structural problem: temperature and displacement signals are those plotted in figure 3.12 where the displacement signal contains a spike while the temperature history does not.

Data of displacement refer to deformometer DF-406 placed along the crack on the intrados of the inner dome and data of the temperature refer to the thermometer TM-401, placed on the masonry close to the deformometer.

Note ε the deformation associated with the displacement history u of figure 3.12; the deformation history of a point x is given by a map $t \mapsto \varepsilon(t, x)$, where $\varepsilon = u'$ i.e. the derivative of trasducers measure with respect to the spatial variable along the axis where sensors are placed.

A map $t \mapsto T(t, x)$ represents also the temperature history. If one assumes that the material composing the dome can be considered homogeneous and isotropic at a first glance, the internal energy for one dimensional analysis results (see, e.g., [12], [32], [46])

$$e(\varepsilon, T) = (2\mu + \lambda)\,\varepsilon^2 - (2\mu + 3\lambda)\alpha_0 T\varepsilon + \frac{c_V^0}{T_0}(T^2 - T_0^2). \qquad (3.1)$$

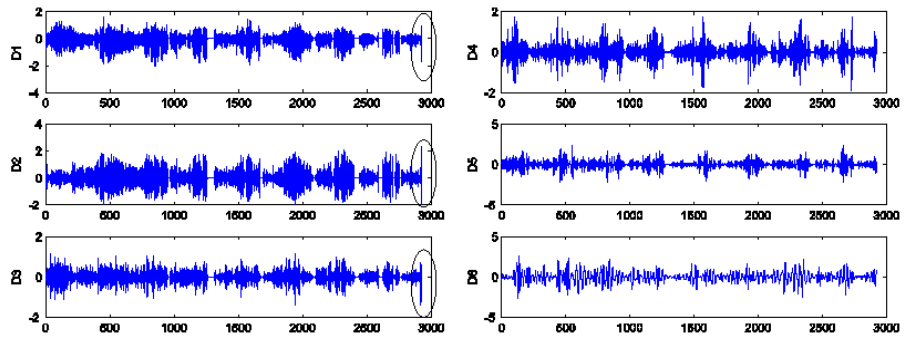

FIGURE 3.10. Wavelet transform of diaplacement signal in figure 3.8. Small spikes associated to the spike present on the displacement signal are reached only by the higher frequency coefficients. Coefficients from $D1$ to $D6$ correspond to a frequency range $[0,5-36]$ days.

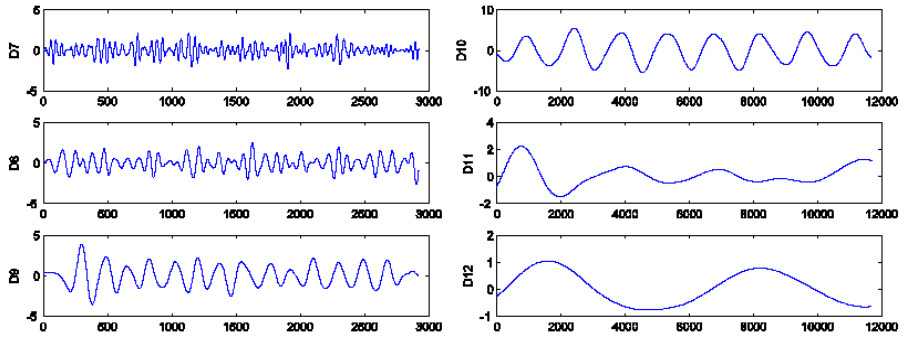

FIGURE 3.11. Coefficients from $D7$ to $D12$ correspond to a frequency range $[64-2048]$ days. No spike are reached at the last datum. Let us note that coefficient $D10$ exactly captures the annual periodicity.

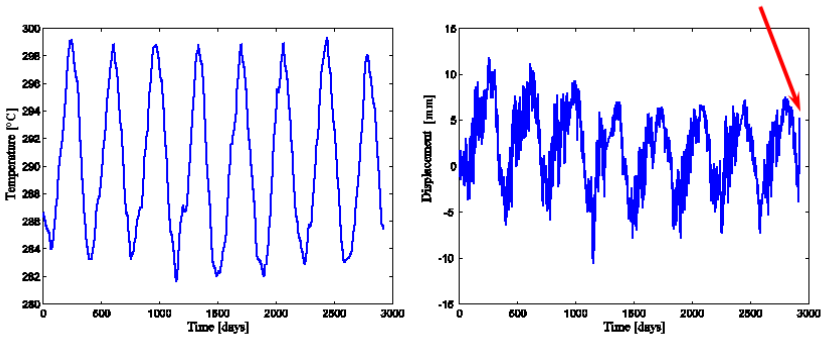

FIGURE 3.12. Temperature signal recorded by thermometer *TM-401* (on the left) and relative displacement (*DF-406*) with a spike on the last datum (on the right).

Values of λ (isothermal Lamé elastic constant), μ (shear modulus) and α_0 (coefficient of volumetric thermal expansion) are derived by the physical parameters obtained from experimental analyses [16] and are

Lamé constant	$\lambda = 0,57\ 10^{-9} N/mm^2$
shear modulus	$\mu = 2,27\ 10^{-9} N/mm^2$
coefficient of thermal dilatation	$\alpha = 0,8\ 10^{-5}\ °C.$

Moreover, since the interest is focused on 'rapid' changes on the deformation, i.e. rapid change of the energy, the internal power $p(\varepsilon, \dot{\varepsilon}, T)$ associated with the expression 3.1 has been considered,

$$p(\varepsilon, \dot{\varepsilon}, T) = (2\mu + \lambda)\, \varepsilon \cdot \dot{\varepsilon} - (2\mu + 3\lambda)\alpha_0 T \cdot \dot{\varepsilon}, \tag{3.2}$$

where $\dot{\varepsilon}$ is the rate of deformation, calculated as finite difference.

Particular attention has to be paid only on the coupling part of the total mechanical power, indicated by $\bar{p}$ and given by

$$\bar{p}(\varepsilon, \dot{\varepsilon}, T) = -(2\mu + 3\lambda)\alpha_0 T \cdot \dot{\varepsilon}. \tag{3.3}$$

Figures 3.13, 3.14, 3.15 represent respectively the internal energy e, the power p and the thermoelastic power $\bar{p}$ associated with displacement and temperature analyzed.

Despite of the presence of noise, a clear isolated peak value is located in the thermoelastic power time-history as the displacement spike occurs in the displacement time-history (figure 3.15).

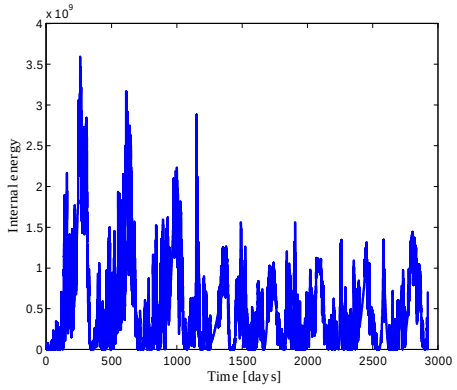

FIGURE 3.13. Internal energy associated with temperature and displacements of figure 3.12.

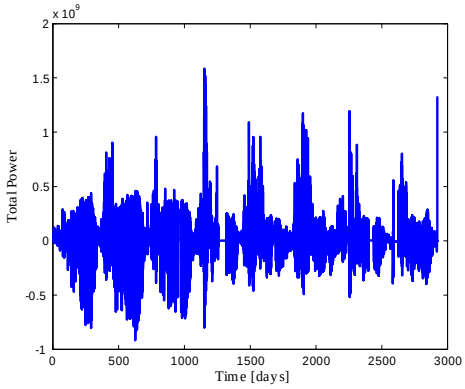

FIGURE 3.14. Total internal power associated with temparature and displacements of figure 3.12.

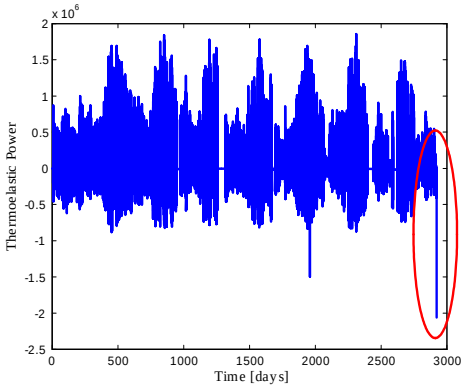

FIGURE 3.15. Thermoelastic power associated with temperature and displacements of figure 3.12.

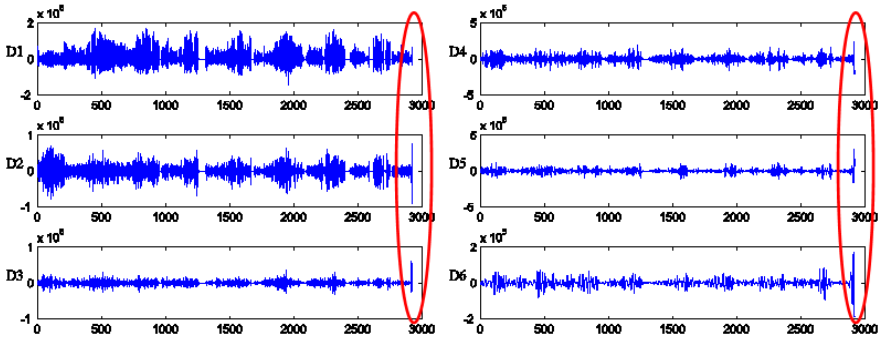

FIGURE 3.16. Wavelet analysis of thermoelastic power of Figure 3.15.

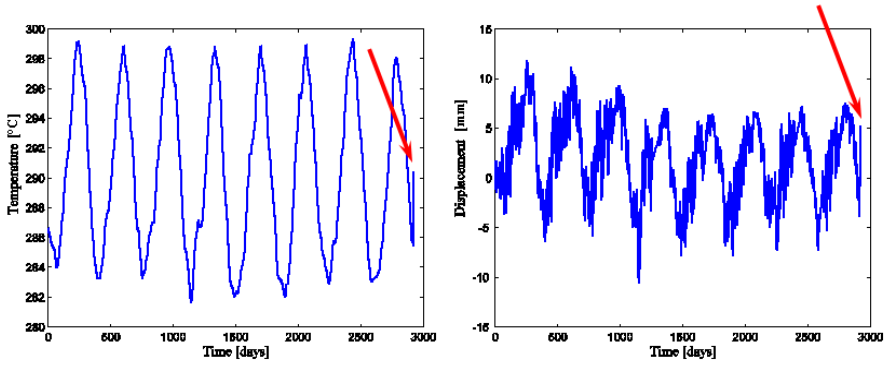

FIGURE 3.17. Temperature and displacement signals associated to a malfuction of acquisition system: a spike is present on the last datum of both the time-histories.

Let us now perform the wavelet analysis on the thermoelastic power (figure 3.16). While the simple analysis of displacement signal produces small wavelet coefficients corresponding to the singularity introduced (figure 3.10), with the same analysis performed now on the thermoelastic power, it is possible to emphasize the singularity underlining its contributions at various frequencies (see figure 3.16). Local maxima of the power are levelled while the singularity, already noticeable in the plot of power itself, appears as an isolated peak value in different wavelet levels, avoiding cases of false positive alarms.

Unfortunately this methodology is not able to distinguish this situation (that represents a possible dangerous event) from the case of an instrumental error, for instance due to a transient malfunction on the acquisition system.

Let us consider the case in which a spike is present also in the last datum of temperature (figure 3.17). These spikes are those typically caused by a transient problem on the acquisition system.

The associated internal energy (figure 3.18), total power (figure 3.19) and in particular thermoelastic power (figure 3.20) still presents a peak value corresponding to temperature and displacement spikes.

Wavelet analysis of the thermoelastic power (figure 3.21) presents isolated peak in correspondence with the spike as in the previous

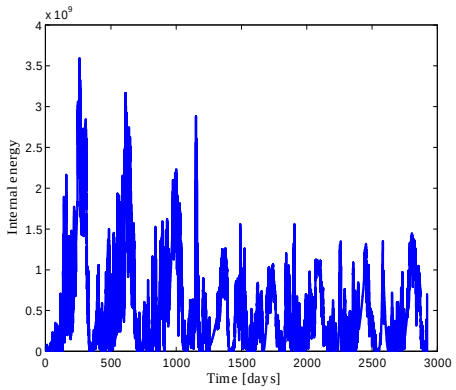

FIGURE 3.18. Internal energy associated with temperature and displacement of figure 3.17.

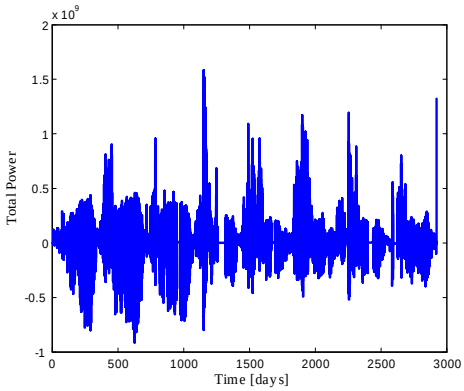

FIGURE 3.19. Total power associated with temperature and displacement of figure 3.17.

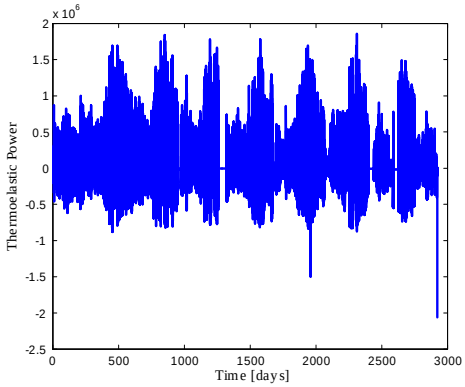

FIGURE 3.20. Thermoelastic power associated with temperature and displacement of figure 3.17.

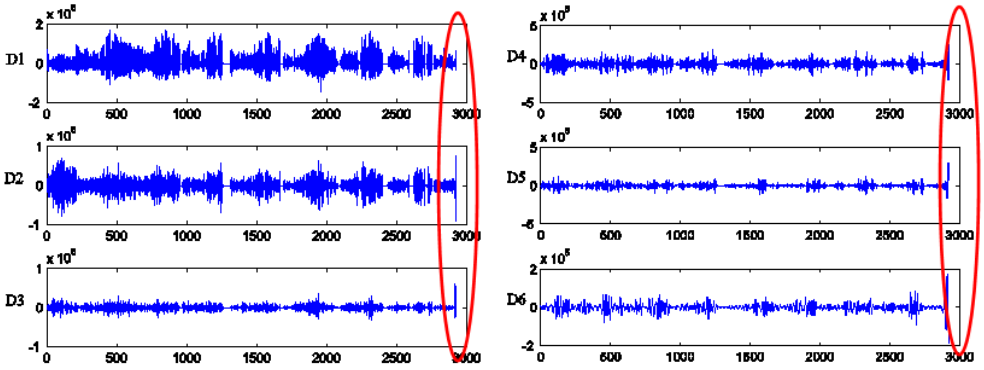

FIGURE 3.21. Wavelet analysis of thermoelastic power of figure 3.20.

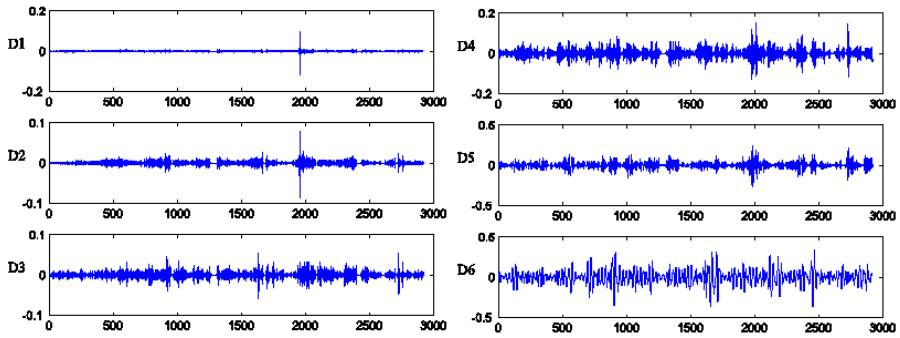

FIGURE 3.22. Wavelet analysis of temperature of figure 3.12.

case, not allowing a clear differentiation of the two situations proposed.

A way to separate these two situations can be obtained by considering also the wavelet analysis of the temperature.

Temperature signal presents a low level of noise (clearly wind can not influence on temperature registration and, due to thermal inertia of masonry, temperature fluctuations occur very slowly), therefore wavelet analysis is able to detect the presence of the spikes when there are some.

Figure 3.22 shows the wavelet analysis of the temperature signal in figure 3.12. Take note that the small spike present in the higher coefficients ($D1$) is probably due to a real instrumental problem that occurs on may 1990, while no spikes are present on the last datum.

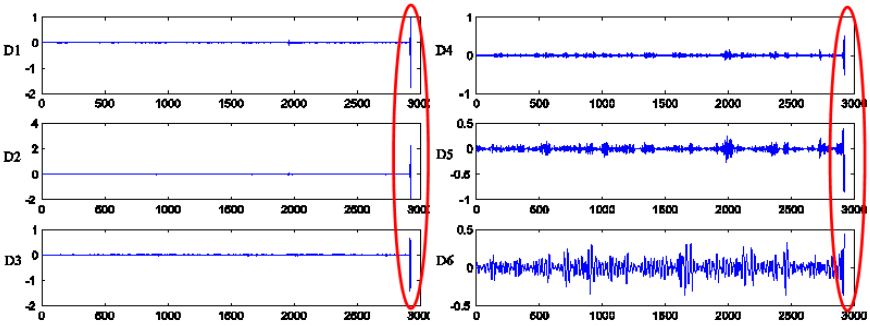

FIGURE 3.23. Wavelet analysis of temperature of figure 3.17.

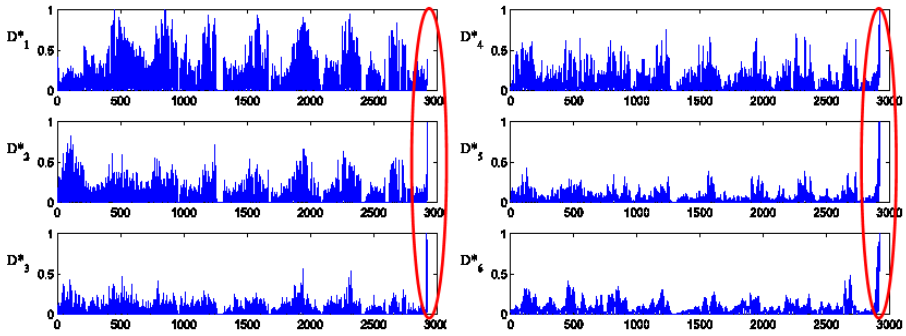

FIGURE 3.24. Absolute value of the normalized coefficients of figure 3.21.

Figure 3.23 instead shows the wavelet analysis of the temperature signal in figure 3.17: peak values are reached at all wavelet levels in correspondence with the last datum.

By combining the wavelet coefficients of the thermoelastic power with the coefficients of the temperature, one may obtain a signal that exceeds a fixed threshold only in case of a real structural problem, i.e. when the temperature signal does not present spikes.

Consider now that since temperature and displacement magnitude are different, also wavelet coefficients have different magnitude; in addition the range of wavelet coefficients could be different also at each level. Thus in order to make possible to combine them, here it is proposed first to normalize all the coefficients by dividing by their maximum value, and then by considering their absolute value, i.e. to take the quantity

$$D_j^* := \frac{|D_j|}{\max |D_j|}.$$

The coefficients D_j^* relative to the thermoelastic power of figure 3.15 (case of a real structural problem) are plotted in figure 3.24.

Our aim is to obtain from these normalized coefficients, an unique signal that accounts for all the features of the original signal (in particular that preserves spikes), by reducing noise contribute.

Therefore these coefficients have been combined in such a way to increase the weight of the lower levels of frequency of the signal and to reduce the contribution of the most noisy high coefficients:

$$DD := c_1 D_1^* + c_2 D_2^* + c_3\ D_3^* + c_4\ D_4^* + c_5\ D_5^* + c_6\ D_6^*, \qquad (3.4)$$

where c_i are weights to set up according to signal features. Here they have been assumed

$$\begin{aligned} c_1 &= c_2 = 1, \\ c_3 &= 3, \\ c_4 &= c_5 = c_6 = 2, \end{aligned}$$

by reducing the contribution of the most noisy levels (D_1 and D_2 associated to higher frequencies) and amplifying the contribution of the lower frequencies. It is important to remark that values of coefficients c_i must be chosen in each case according to the features of the signal under analysis (as for example the noise level).

The signal obtained is represented in figure 3.25: spikes that were present on the different levels of wavelet coefficients of figure 3.24 are combined and thus the resulting signal presents an amplified isolated peak in the last datum.

The same procedure is followed referring to the wavelet coefficients of temperature history in figure 3.12 (temperature without spikes since in case of a structural problem). Normalized wavelet coefficients (plotted in figure 3.26) are combined in a unique indicator:

$$DT := D_1^* + D_2^* + D_3^* + D_4^* + D_5^* + D_6^*. \tag{3.5}$$

This signal (in figure 3.27) has not isolated spikes as the temperature time-history from which it derives.

Now we have at disposal the signal of figure 3.25 that accounts for thermoelastic power and signal in figure 3.28 that accounts for temperature. Since the contemporary presence of spikes in thermoelastic power and in temperature is linked to an acquisition problem, case in which no alarm must be given, spikes present on the same time on the two signal before considered must be neglected. According to this consideration, the *Effective Alarm Signal* is obtained as difference between the wavelet transforms of thermoelastic power and temperature time-histories:

$$E.A.S. = DD - DT. \tag{3.6}$$

This signal, represented in figure 3.28, exceeds the fixed threshold only in correspondence with the spike in the original displacement signal, giving rise of a possible structural problem.

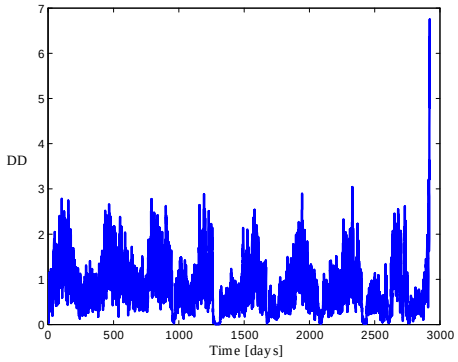

FIGURE 3.25. Signal obtained by combining as in eq. 3.4 coeffcients of figure 3.24.

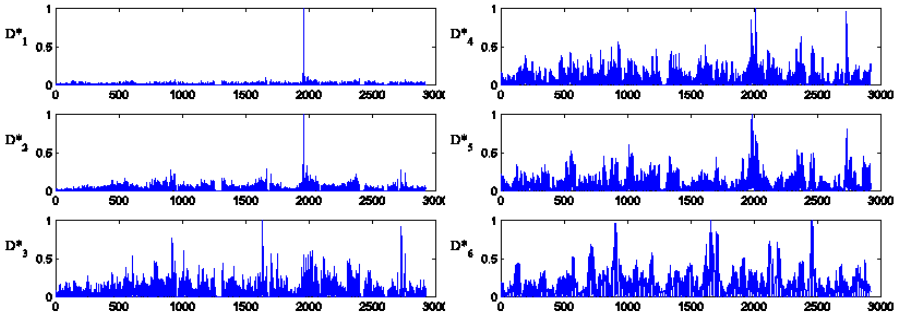

FIGURE 3.26. Absolute value of normalized coefficients of Figure 3.22.

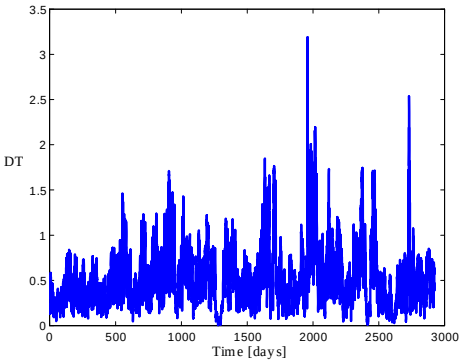

FIGURE 3.27. Signal obtained by summing the coefficients of temperature.

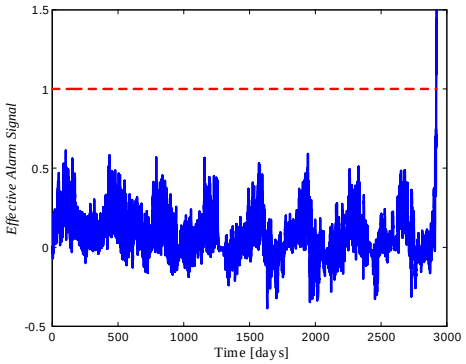

FIGURE 3.28. *Effective Alarm Signal.* The threshold is exceeded only in the case of structural problem.

In order to check if this procedure is able to distinguish between cases of structural problems and cases of instrumental ones, the same analysis has been performed once again by referring now on the couple temperature-displacement of figure 3.17 in which spikes are present in both signals.

The wavelet coefficients of the relative thermoelastic power and temperature have already been determined (see respectively figure 3.21 and figure 3.23). After the normalization, they are combined always according to equation 3.4 and equation 3.5 respectively.

Now the contemporary presence of a spike on the last datum in both the derived signals (figure 3.31 and figure 3.32) determines an *Effective Alarm Signal* that does not exceed the fixed threshold as shown in figure 3.33: so the *Effective Alarm Signal* is not sensitive to transient problems in the acquisition system.

First remark that can be done is the necessity to pass through the thermoelastic analysis i.e. is it possible to obtain an alarm signal by considering directly wavelet transform of displacement and of temperature, or is it really necessary to take into account of thermoelastic analysis? Why it is necessary to calculate the thermoelastic power?

One may think to consider displacement and temperature time-histories, to evaluate their wavelet transform, to combine the coefficients (for example always in such a way to reduce the contribution

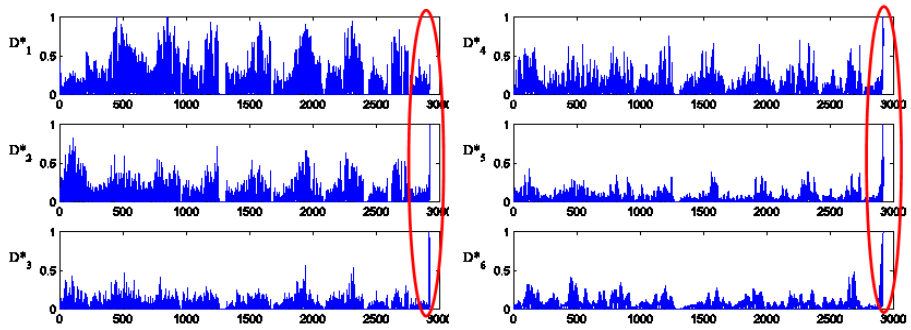

FIGURE 3.29. Absolute value of normalized coefficients of figure 3.21.

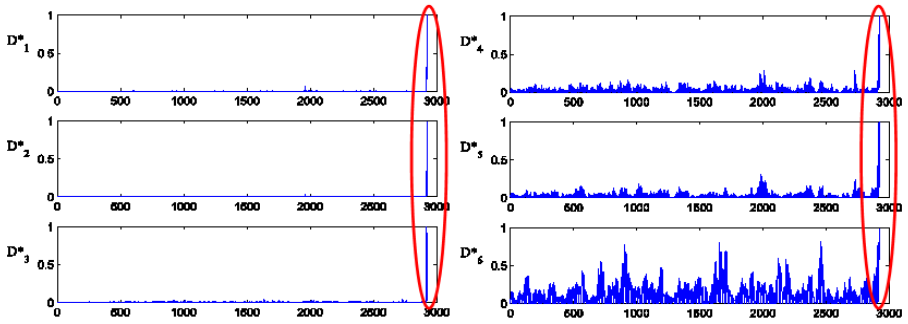

FIGURE 3.30. Absolute value of normalized coefficients of figure 3.23.

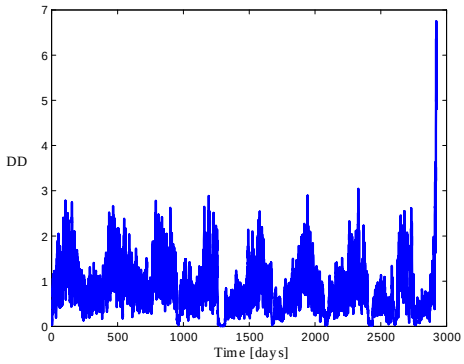

FIGURE 3.31. Signal obtained by combining the coefficients of figure 3.29.

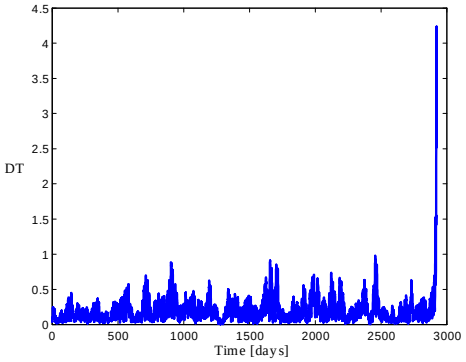

FIGURE 3.32. Signal obtained by summing the coefficients of figure 3.30.

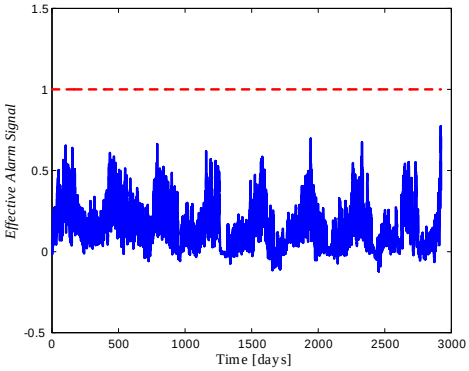

FIGURE 3.33. *Effective Alarm Signal.* The threshold is not exceeded in the case of an acquisition problem.

of the most noisy levels) and finally to obtain an alarm signal, still able to distinguish between instrumental and structural problems.

In reality, analyses performed in this way (by considering displacement and temperature signals) are not able to give an *Effective Alarm Signal.* Figure 3.34 and figure 3.35 show the results obtained by following this procedure in case of structural problem and instrumental problem respectively.

The obtained signals in both cases give not an effective alarm; in fact several times the threshold is exceeded, but not when necessary i.e. at the beginning of a structural problem. This is due to the fact that all local maxima of displacement time-history are here considered, not allowing to give prominence to the only one to which is associated biggest thermoelastic power which corresponds to the case of a structural problem.

Therefore the methodology proposed before, by accounting at the same time of thermoelastic analysis and of wavelet capabilities, gives a reliable tool to perform *in real-time* a selection between real structural problems and instrumental one when they occur. Thermoelastic analysis is of fundamental importance since structural problems produces biggest isolated singularity on thermoelastic power while all the small singularities that could be present on displacement signal but not representative of structural problems do not produce high values of thermoelastic power and thus are neglected.

3.2.3 Additional remarks

The study presented here is an application, on real experimental data, of a general procedure for a real-time monitoring. The aim of this work is in fact to detect singularities presented in the last datum of the displacement signal associated with possible structural problems.

However this methodology can be applied also in case in which spikes are on central data of the time-histories, allowing to a distinction between cases of instrumental errors and cases of possible structural problems. This study could be useful for *a posteriori* analysis of data logged by instruments or also when frequency acquisition is high that past data refer to an instant just passed (therefore the analysis is close to be in real-time).

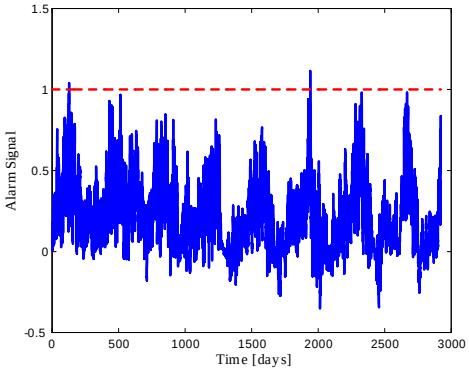

FIGURE 3.34. *Signal* obtained by wavelet coefficients of displacement and temperature (case of a structural problem). The threshold is overcame several times but not on the last datum where displacement signal originally presented an *anomalous* value.

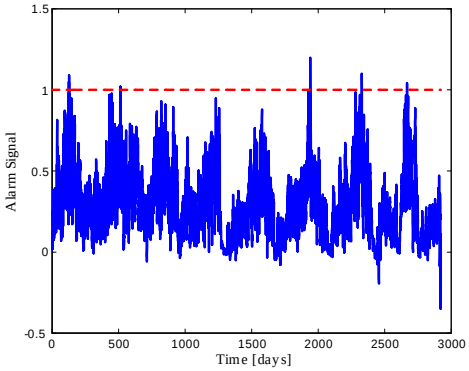

FIGURE 3.35. *Signal* obtained by wavelet coefficients of displacement and temperature in case of a problem on the acquisition system. The threshold is overcame several time while any structural problem has occurred.

In this case only a wavelet analysis of the thermoelastic potentials is here necessary.

In order to illustrate briefly also these situations, consider displacement and temperature signals presented in figure 3.36. The first two graphics refer to a real structural problem: in the displacement signal a spike occurs around time $t = 1550$ and it is followed by a rigid translation of the whole signal (original signal is in dotted line), while in the temperature signal no spike is present. In the second case instead an isolated spike is present at the same time in both displacement and temperature histories (figure 3.36 B)) indicating a malfunction of acquisition system.

By performing the wavelet analysis on the thermoelastic power associated, and again by combining the normalized coefficients in such a way to amplify the contribute of lower frequencies, the signal obtained directly by thermoelastic power is already an *Effective Alarm Signal* (figure 3.37): it overcomes the threshold in correspondence of the jump in the displacement signal.

The same analysis performed in case of instrumental error gives a signal that does not exceed the threshold (figures 3.38). Even if the momentary malfunction is only of a deformometer or only of a thermometer (spike only in a signal) no overcome of the threshold is produced (figure 3.39 and figure 3.40).

The analysis of singularities present in central data results therefore easier since it is directly perform on thermoelastic power, without requiring the wavelet analysis of temperature. This is due to the fact that, by knowing data that follow the initial spike present on the displacement, one have a disposal also informations about the low frequency components of the signal. By comparing in fact displacement signal of figure 3.36, one can argue that the jump that follows the spike in case on a structural problem determines a change on low frequencies and therefore on wavelet coefficients associated to them. The isolated spike of an instrumental error determines instead changes only on the high frequency components. The combination of wavelet coefficients of thermoelastic power (that we remind was performed by amplifying low frequencies) determines therefore different signals in case of structural problems and instrumental ones.

When instead the analysis is performed in real-time, data that follow the spike are unknown; low frequencies levels of wavelet analysis can not give sufficient informations to distinguish between instru-

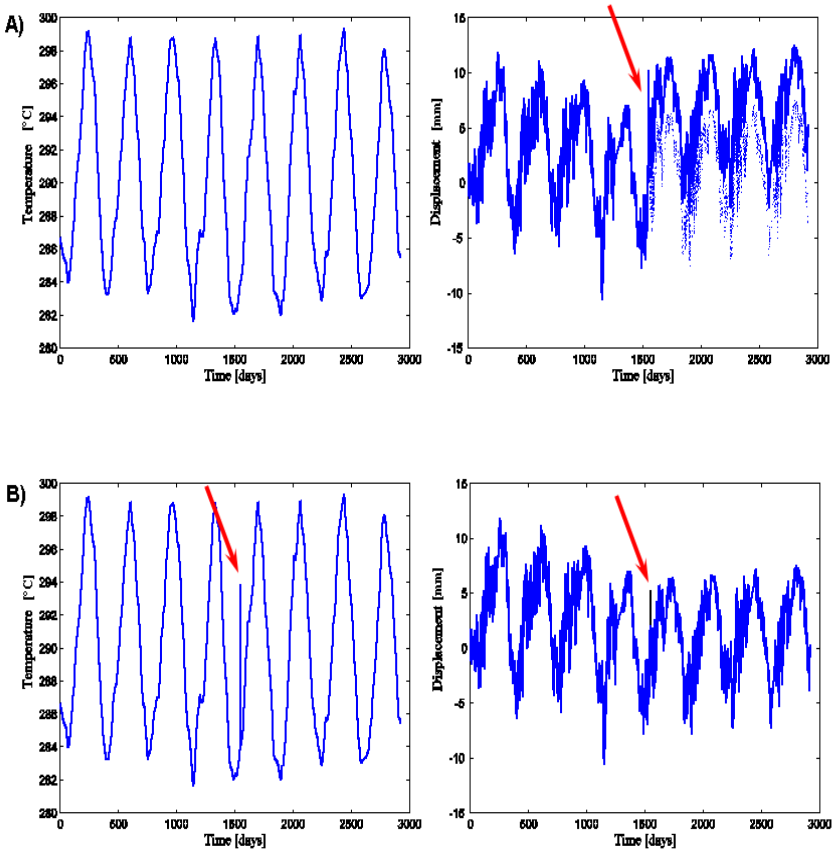

FIGURE 3.36. A) Temperature and displacement signals associated to a structural problem that occurs around time $t = 1550$: original displacement signal in dotted line, displacement signal simulating the structural problem in continuous line. B) Temperature and displacement signals associated to an acquisition error occuring always at time $t = 1550$: a spike appears at the same time in displacement and temperature time-histories.

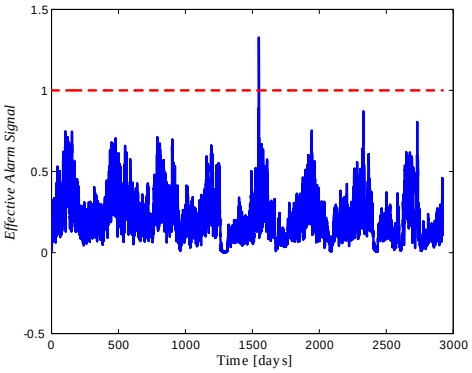

FIGURE 3.37. *Effective Alarm signal*. The threshold is exceeded just in correspondence with the possible structural problem.

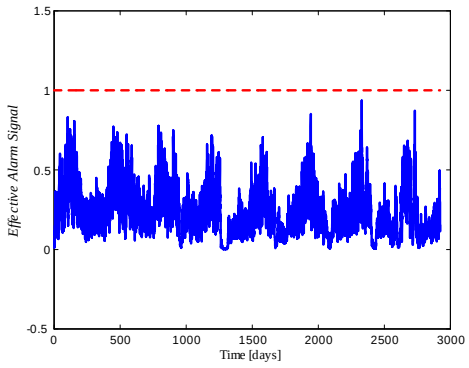

FIGURE 3.38. *Effective Alarm Signal* when displacement and temperature signals have a spike. The threshold is not exceeded.

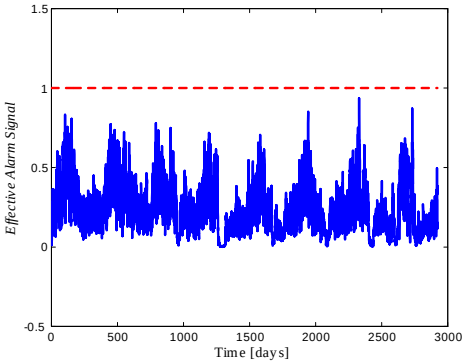

FIGURE 3.39. *Effective Alarm Signal* associated with the case of a momentary malfunction only of the deformometer. The threshold is not exceeded.

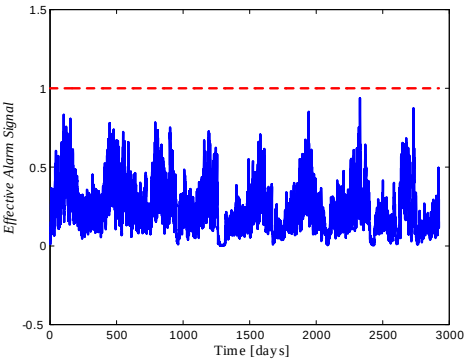

FIGURE 3.40. *Effective Alarm Signal* associated with the case of a momentary malfunction only of the thermometer. The threshold is not exceeded.

mental or possible structural problems and therefore also temperature must be considered.

3.2.4 The procedure in brief

The methodology presented for an early warning monitoring system can be summarized in the following steps:

- Evaluate the thermoelastic power associated with deformation and temperature signals logged by sensors.
- Choose an appropriate wavelet filter (in this step it is important to remember that wavelet coefficients give the degree of resemblance of the signal to the wavelet selected: more significant results can be obtained by choosing a wavelet similar to the discontinuity that one wants to detect). The shapes of discontinuities that can be identified by the shorter wavelets are simpler than those that can be identified by the longest wavelets. Let us remind also that in wavelet analysis '*what it is gained in frequency resolution is lost in time resolution*' i.e. by referring to Heisenberg box presented previously, if one chooses a filter too short (that therefore gives an extreme precise frequency resolution), one will loose information on time and real-time identification of singularity could result difficult; on the other hand the use of long filters could not lead to an identification of some singularities. Tentative must be done in order to determine the most appropriate filter referring to the signal under analysis.
- Perform wavelet analysis on both the signals (thermoelastic power and temperature).
- Normalize the wavelet coefficients and take their absolute value D_j^*.
- Combine the wavelet coefficients derived from the thermoelastic power history according to the equation

$$DD := c_1 D_1^* + c_2 D_2^* + c_3\ D_3^* + c_4\ D_4^* + c_5\ D_5^* + c_6\ D_6^*;$$

  the choice of the weight coefficients c_i has to be done with respect to the noise level of the signal.

- Combine the wavelet coefficients derived by the temperature history
$$DT = D_1^* + D_2^* + D_3^* + D_4^* + D_5^* + D_{6.}^*$$
- Evaluate the *Effective Alarm Signal* and compare with a threshold fixed at 1
$$E.A.S. = DD - DT.$$

The study presented here is a special application on experimental data coming from the monitoring system installed on the Brunelleschi dome. The methodology could however be applied also to other structures under thermoelastic regime, by setting up appropriately the parameters involved (the weight c_i, for example).

The procedure is proven relevant with respective to several monitoring conditions.

Since the numerical effort required is very small and the calculation is very fast (some seconds in a standard laptop computer), an application for a warning monitoring of a real structure is therefore possible.

A simplified methodology for detecting *anomalous events* happened in the past of logged time-histories is also briefly presented: the analysis allows to control data already logged and to identify those singular events not always clearly evident only by a visual inspection of time-histories.

4
Study of crack stability

The early-warning methodology previously presented is a useful tool to detect in real-time anomalous events that could occur on the structures. As discussed, these events can represent a sudden and dangerous increase of structural damage.

Unfortunately, the proposed methodology could not give any information on the causes and, above all, on the consequences of these events. In order to have a complete knowledge of structural behavior and in particular of structural safety, a mechanical study of the structure is necessary.

With this aim, it would be interesting to reproduce, even with a basic numerical finite element model (f.e.m.), the main features of the structure. Once the model exists, it is then possible to investigate if loads that the structure undergone, could lead to an instable growing of the main cracks by determining an irreversible damaging process.

This procedure has been followed in order to complete the analysis on Brunelleschi dome: the structure has been reproduced by means of a finite element model; this model has been loaded with the static loads of the structure itself and the real temperature variations logged by sensors.

Actually, only temperature on the exterior layers of the dome are available; thus, first, it has been necessary to determine temperature

distribution inside the masonry by integration of Fourier's law, and then the determined distribution has been applied on the structure.

The structural response obtained by the finite element simulation has been compared with the real data of displacements; the achieved agreement between data allows to use the finite element model for a study of the stability of the fracture. Using fracture mechanics theory, in fact, by knowing displacement field and stress distribution induced by external loads on the proximity of crack tip, it is possible to evaluate crack stability i.e. if the material is still able to undergo external loads without increasing, in an irreversible way, crack opening or if at the contrary, limit values of displacements (or stress) have already been overcame and the fracture could now growth without meeting any material resistance.

It is important to remark that the values of displacement measured on the dome are available only punctually where sensors (in this case one sensor) are placed (and not always they are very close to crack tip). Instead, in order to correctly estimate fracture stability, it is necessary to know all the displacement (or stress) distribution on the proximity of crack tip: a basic f.e.m., able to reproduce structural behavior in this zone and that can give all the distribution of stresses around the tip is thus necessary.

In what follows attention is first focused on the set up of the finite element model, on the evaluation of temperature distribution inside the masonry and on the numerical results obtained (also compared with logged data).

After a short introduction on fracture mechanics, the analysis of fracture stability on Brunelleschi dome and the obtained results are finally given.

4.1 The numerical analysis

4.1.1 The numerical model

S.Maria del Fiore cathedral is a complex structure and a complete model that considers all the structural elements is difficult to set up for the uncertainties on the material, on the real constrains, on the links between the structural elements, etc. However, a basic model able to reproduce the main features of the structure is possible. In fact, in order to study the behavior of the dome and in particular

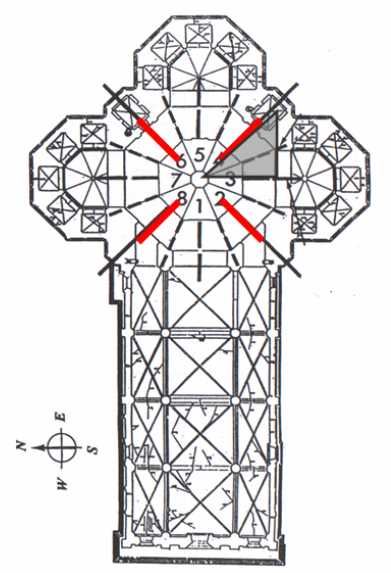

FIGURE 4.1. Sketch of S.Maria del Fiore cathedral: in red the main fractures; the shadowed area is the one modeled in the numerical simulation.

the tendency of the cracks to grow, it is not necessary to consider the overall structure: a basic model, able to reproduce local features of the structure on the crack zone is useful as well.

Here only the dome and in particular the internal shell has been considered. In addition, due to the symmetric disposition of the cracks it was possible to model only a part of the dome it-self, as shown in figure 4.1 and figure 4.2. We know in fact that, after the opening of the main cracks, the structure now behaves like four drifting half-arches, linked just below the upper clerestory (see section 3.1.3). Thus, only an eighth of the structure has been reproduced: a half of web 3 and a half of web 4 (just till the crack), allowing only deformations consistent with the symmetry of the problem. At the base, restraints have been placed to account for pillars elasticity and allowing small deformations.

Concerning with the material characterization, elastic homogeneous isotropic behavior has been assumed: mechanical and thermal parameters are those determined by the experimental tests made when the monitoring system has been installed [16] i.e.

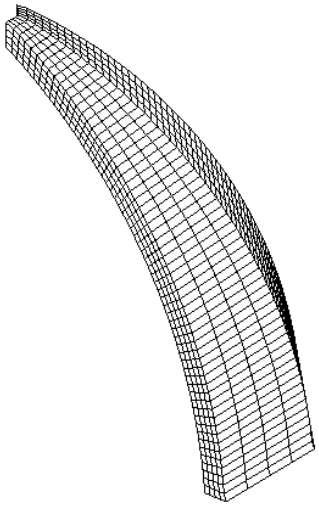

FIGURE 4.2. Model of a 1/8 of the dome. Brunelleschi dome is constituted by two shells linked by joining elements (see figure 3.1 and figure 3.3). The here proposed model reproduces only the inner dome.

Young modulus	$E = 500000 N/cm^2$
Poisson's ratio	$\upsilon = 0,1$
coefficient of thermal dilatation	$\alpha = 0,8\ 10^{-5}\ ^\circ C$
thermal conductivity	$K = 0,5\ W/m\ ^\circ C.$

Thermal conductivity indicated in literature [47] has been considered since any value has been reported from in-situ tests.

Solver CASTEM 2006 [13]; in the mesh cubic finite elements have been used, in particular hexahedral elements at 8 nodes, each of which with a degree of freedom, with linear base functions.

4.1.2 Loading conditions

The structure is loaded only by its own weight and by temperature variations. As a preliminary analysis we have neglected the temperature and evaluated the crack opening determined by the own weight. Afterwards time-histories of temperature variations of a four years period, combined with own weight load have been applied.

On the temperature distribution, analyses of logged data (see section 3.1.3) gave that it can be considered uniform along the parallels

and the meridians of the dome; a gradient is instead present in the radial direction. Variations of the temperature inside the masonry are available only in the half of the thickness of the dome due to the presence of a thermometer place there. No information about all the distribution of the temperature inside the thickness of the dome are however given.

Thus to evaluate the effects that temperature variations induce on the structure, first temperature gradient inside the masonry has been determined.

Since the thermal variations occur very slowly, it was possible to solve preliminarily the thermic problem and then to use the obtained temperature distribution, in order to evaluate the effects combined with the ones induced by the own weight.

According to heat conduction law, also know as Fourier's law, when temperature time-histories are known at the boundaries, the temperature distribution in space is given by

$$\frac{\partial^2 T}{\partial x^2} = \frac{1}{C}\frac{\partial T}{\partial t}, \tag{4.1}$$

where $C = \frac{K}{\rho c} = 3,7e^{-7} m^2/s$ is the thermal diffusibility, where $K = 0,5\ W/m\ ^\circ C$, thermal conductivity, $c = 800\ J/kg/^\circ C$ specific heat, $\rho = 1700\ kg/m^3$ the density of the material. Specific heat too is the one indicated in literature, while material density is the experimental value obtained in-situ.

Boundary conditions of temperatures in this case are the values logged by the sensors on the external and on the internal layer of the dome.

Equation 4.1 has been integrated by means of a numerical method: the convergence and the stability of the calculation have been achieved by using implicit method that does not require excessive time and space steps reduction.

Data of the sensor placed in the thickness of the dome has instead been used for correlation: comparing the calculated temperature with the logged one (see figure 4.3), numerical integration is shown able to reproduce the real thermal distribution.

Since the calculated time-history in this point reproduces quite exactly the real one logged, all the temperature distribution calculated on the thickness is supposed to be close to the real one.

Looking now at the temperature distribution inside the masonry (figure 4.4), one can remark that even if the tendency is to a linear

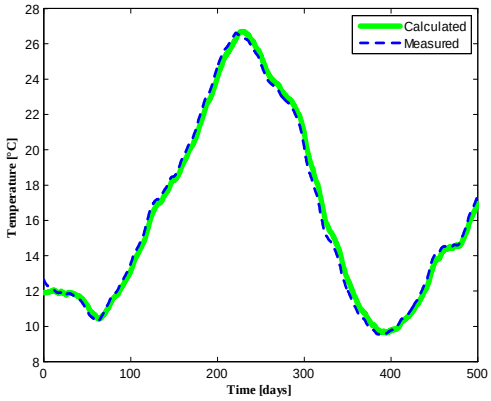

FIGURE 4.3. Temperature time-history in the semi-thickness of the dome: logged values (in blue), calculated (in green) ones.

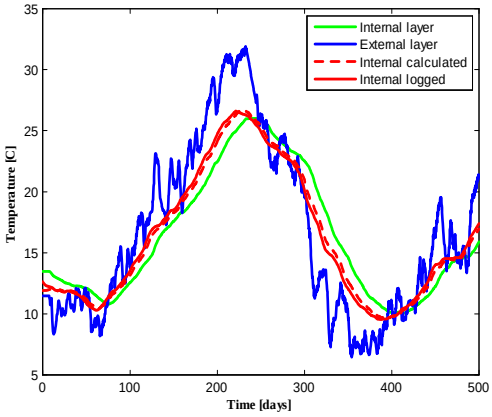

FIGURE 4.4. Temperature distribution in the dome.

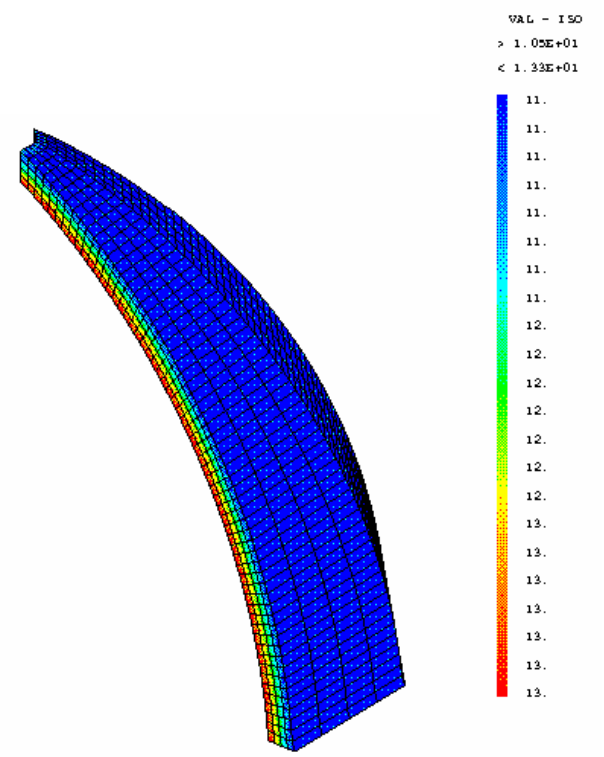

FIGURE 4.5. Temperature distribution on the modeled dome at a time t of the calculation: the distribution of the temperature in uniform along the meridians and the parallels while the gradient obtained by solving Fourier's law is applied on the thickness.

gradient, due to thermal inertia, not always the internal layers follow exactly the temperature variations induced by the atmospheric elements on the external part of the dome, determining a distribution different from the linear.

By knowing the temperature distribution inside the masonry, the thermo-mechanic calculation has been performed by evaluating the effects of temperature and own weight on the structure. Therefore:

- temperature logged by estrados sensors is applied to all the external nodes of the f.e.m of the structure;
- temperature logged by intrados sensors is applied to all the internal nodes of the f.e.m of the structure;

- temperature distribution as previously determined by Fourier's law has been applied along the thickness of the structure.

A picture of temperature distribution on the structure is shown in figure 4.5.

4.1.3 Results of the numerical calculation

In order to compare computed and measured data, the exact positions of the deformometers on the structure is considered: this leads to properly associate local displacements.

Several observations follow:

- first, the maximum crack opening induced by the combined effect of temperature and own weight is around 1 mm while the corresponding value obtained without thermal effects is less than $0,4$ mm. Therefore we can say that, without temperature effects once the fracture has formed, a displacement on the tangential direction of less than an half of millimeter would be in any case present due to the weight of the structure. This deformation is increased or decreased depending on the temperature action that determines more than the 60% of the overall value.

- Figure 4.6 and 4.7 present a comparison between logged displacements and numerical ones: even if the calculated displacements are similar to the real ones, they are not able to reproduce them exactly. In particular here we refer to the *first corridor level* and we compare measured and computed values of displacements at the intrados and the estrados respectively. Analogous results (see figure 4.8 and figure 4.9) are obtained for the *second corridor level*[1].

- A relative displacement between the internal and the external layer of the dome, i.e. the rotation of the edge of the fracture, can better reproduce local features since it is more independent on the deformations and on the global influence of the whole structure. Absolute displacements, on the contrary, are influenced above all by pillar deformations and tambour real connection.

[1] For the location of the '*first corridor* and *'second corridor'* refer to figure 3.1.

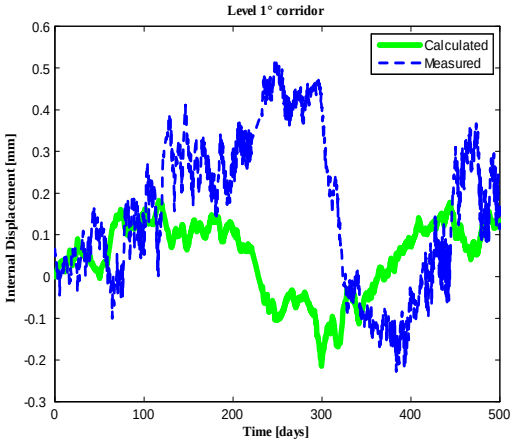

FIGURE 4.6. Comparison between the numerical and the measured displacements on the intrados of the dome at the *first corridor level*.

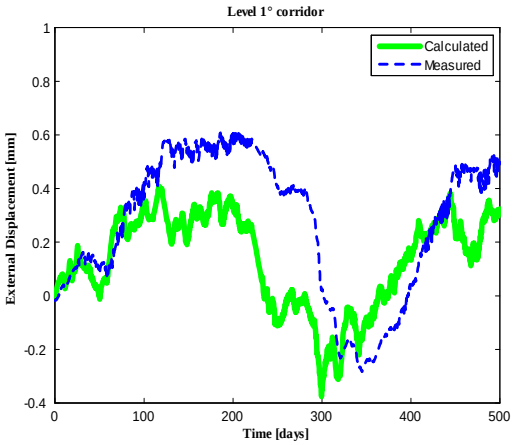

FIGURE 4.7. Comparison between the numerical and the measured displacements on the extrados of the dome at the *first corridor level*.

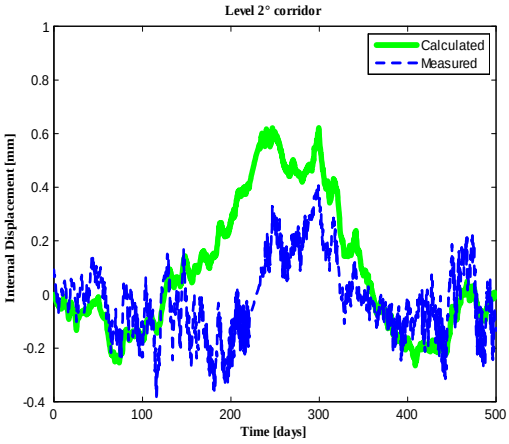

FIGURE 4.8. Comparison between the numerical and the measured displacements on the intrados of the dome at the *second corridor level*.

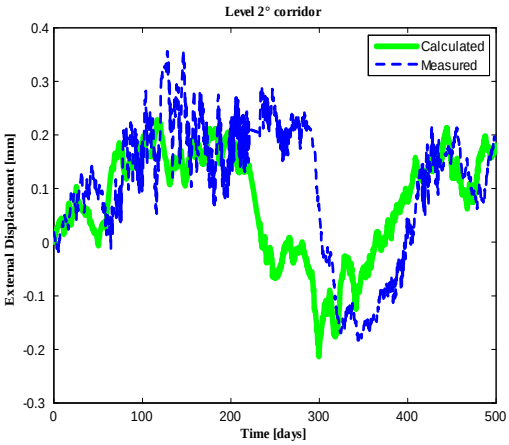

FIGURE 4.9. Comparison between the numerical and the measured displacements on the extrados of the dome at the *second corridor level*.

In this comparison between real and simulated rotations a quite perfect agreement is reached at the *first corridor level* (figure 4.10) as at the *second corridor level* (figure 4.11).

A perfect reproduction of real data by the numerical simulation was not possible due the simplicity of the assumed model compared to the complexity of the real structure and also in reason of all the uncertainties that arise when dealing with historical structures made by masonry[2]. In any case, even with these uncertainties, the basic model used here is able to reproduce some of the main local features of the structural behavior, in particular those close to the crack. Rotations are reproduced with a good approximation; for the displacements, the model is not able to follow exactly the real data; it is however possible to observe that the range of the values reached by both numerical and logged data is quite the same.

A better agreement could be achieved by a more complex model that, on the other hand, would require a higher number of assumptions (on structural connections and interactions for example), by increasing in this way the level of uncertainties; obtained results could however not be able to reproduce better (than the one here reported) real displacements.

Therefore, since the final aim in modelling the dome is not only to determine temperature distribution inside the masonry and try to reproduce exactly structural behavior via a basic scheme, but above all to understand crack behavior, in reason of all the uncertainties of the problems, the level of approximation achieved by means of this basic structural model has been accepted. The model itself has thus used to study the fracture stability.

The stability of cracks is evaluated by standard Fracture Mechanics: displacement field (or stress field) induced by the external loads can be compared with the maximum one that the material (in function of its own properties) can undergone still giving a resistance against a crack instable growth.

In order to evaluate the safety of the structure, here it has been chosen a basic approach.

[2] Even if experimental tests have been performed in the past, one can not state for sure the uniformity of materials on all the dome or know the real interaction between different structural elements (just to make examples).

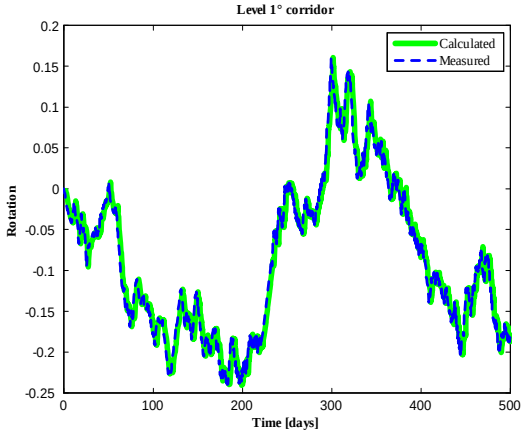

FIGURE 4.10. Comparison between rotaton on the real structure and the one obtained by the numerical simulation at the *first corridor level.*

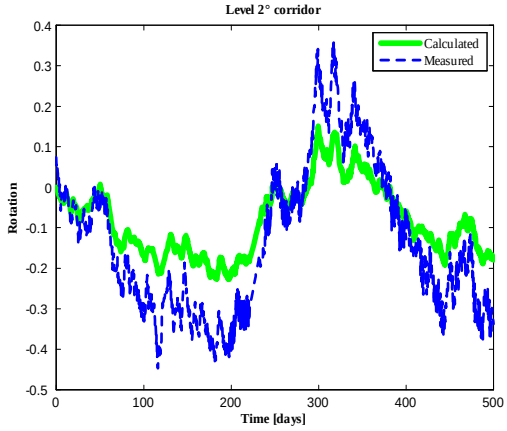

FIGURE 4.11. Comparison between rotaton on the real structure and the one obtained by the numerical simulation at the *second corridor level.*

Before to present the application on the dome, a brief introduction of fracture mechanics and on the theory that allows to evaluate fracture stability by knowing displacement or stress distributions around the crack tip, is given in the following.

4.2 Analysis of crack stability

The study of the fracture mechanics was started by an aeronautical engineer A.A. Griffith to explain the failure of brittle materials. He was faced with the problem that theoretical calculations showed that the stress at the tip of a sharp crack approaches infinity. Accordingly, any cracked structure should fail, independently to the size of the crack and the load applied. To solve this dilemma he approached the problem by an energetic viewpoint by computing the energy required to open a crack and see when this process becomes favorable.

Griffith's work was ignored for over twenty years until a group leaded by G.R. Irwin used it to developed a modified form of Griffith's approach, by reformulating it in terms of stress rather than energy. Their work leads to a definition of a new materials property, the *toughness* K_c, now universally used to define properties of materials as regard as fracture mechanics.

In the following, after a small introduction on fracture vocabulary, the formulation in terms of stress will be presented in linear elastic setting (for a complete review on fracture mechanics, see [24], [29], [11]). This formulation is the one used in our application referring to Brunelleschi dome.

4.2.1 Basis of fracture mechanics

Fracture represents an irreversible process characterized by the separation in two parts with respect of a geometric surface S of a continuous body. This separation determines a discontinuity for the displacement field

$$[u_i] = u_i^+ - u_i^-$$

where u_i^+ and u_i^- are the displacements on the two parts created by the fracture i. The normal component $[u_n]$ is the crack opening, it is definite positive; conversely the tangential component represents the sliding between the two sides and can be positive or negative, or can not be present at all.

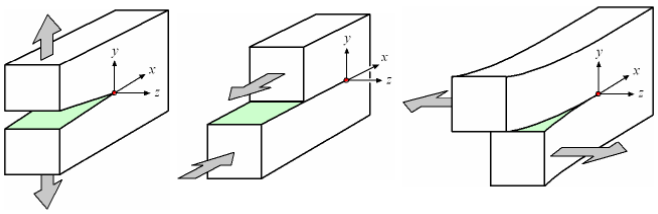

FIGURE 4.12. Fracture modes: mode I corresponds to a tensile stress condition, mode II to a shear stress, mode III to a tearing one.

In a cinematic classification one can define three different fractures modes: mode I corresponds only to a crack opening without sliding component; mode II and mode III correspond to a sliding, respectively normal and parallel to the front of the fracture itself (see figure 4.12). A generic fracture is obtained by a combination of the three modes.

In mathematical terms, a crack is a boundary condition for the elastic strain field, with in general the additional complication that the precise shape of the crack is unknown, depending in the stress field acting on it. By prescribing the crack geometry or by knowing it, one can then compute the stress field.

In the simple case of an elliptic crack under tensile stress, in an infinite two dimensional medium, the solution of the elastic equation of equilibrium yields the stress concentration at the edge of the ellipse

$$K = \frac{\sigma_{\max}}{\sigma} = 1 + \frac{2a}{b}, \tag{4.2}$$

with σ the nominal applied stress and $\sigma_{\max}$ the maximum one. In reality cracks typically are not elliptic but they present a sharp tip. In rewriting equation 4.2 in terms of the curvature radius $\rho = b^2/a$, one can see that K diverges as $1/\sqrt{\rho}$ as $\rho \to 0$.

K is called *stress intensity factor* and correlates stress field around the crack tip with the geometry as

$$\sigma_{ij} = \frac{K}{\sqrt{2\pi r}} f_{ij}(\theta)$$

where f_{ij} is a crack-tip function that, as K, depends on the particular loading conditions.

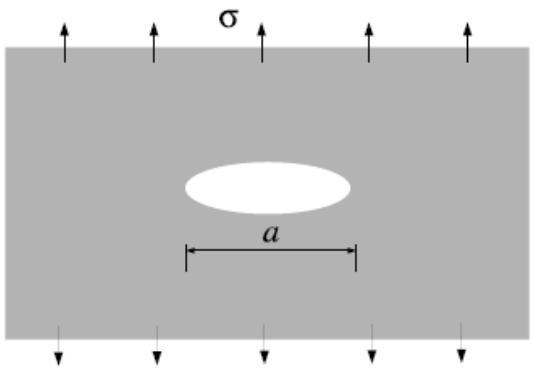

FIGURE 4.13. An elliptic crack in a two dimensional medium.

Analysis of stresses and displacements distributions around the crack is based on Linear Elastic Fracture Mechanics (LEFM). Linear Elastic Fracture Mechanics first assumes that the material is isotropic and linear elastic. With this assumption, the stress field near the crack tip is calculated using the theory of elasticity. Based on the linear theory, as we have seen, the stresses at the crack tip are infinity but in reality there is always a plastic zone at the crack tip that limits the stresses to finite values. It is very difficult to model and calculate the actual stresses in the plastic zone and compare them to the maximum allowable stresses of the material to determine whether a crack is going to grow or not.

An engineering approach is to perform a series of experiments and reach at a critical stress intensity factor K_c for each material, called the *fracture toughness* of the material. The critical stress corresponds to the development of the fracture process in an irreversible way. By knowing the value of K_c and K (K_c is an intrinsic property of the material, K depends on loading conditions), then one can verify if the fracture tends to propagate or not, i.e. if the fracture is stable. The fracture will be stable if $K < K_c$.

Values of stresses and displacements can been determined (see for a complete explanation [11], [7]) in terms of stress intensity factors. In an linear elastic material, let us consider a point $P\ (r, \theta)$, in a system of polar coordinates with the origin on the crack tip and $\theta = 0$ corresponding to the tangential direction as in figure 4.14.

In plane deformations, for P close to the tip (i.e. $r \ll l$), stress field has the following asymptotic expressions:

$$\begin{aligned}
\sigma_{rr} &= \frac{K_I}{4\sqrt{2\pi r}}\left[5\cos\left(\frac{\theta}{2}\right) - \cos\left(3\frac{\theta}{2}\right)\right] + \\
&\quad + \frac{K_{II}}{4\sqrt{2\pi r}}\left[-5\sin\left(\frac{\theta}{2}\right) + 3\sin\left(3\frac{\theta}{2}\right)\right] + O(1) \\
\sigma_{\theta\theta} &= \frac{K_I}{4\sqrt{2\pi r}}\left[3\cos\left(\frac{\theta}{2}\right) + \cos\left(3\frac{\theta}{2}\right)\right] + \\
&\quad + \frac{K_{II}}{4\sqrt{2\pi r}}\left[-3\sin\left(\frac{\theta}{2}\right) - 3\sin\left(3\frac{\theta}{2}\right)\right] + O(1) \\
\sigma_{r\theta} &= \frac{K_I}{4\sqrt{2\pi r}}\left[\sin\left(\frac{\theta}{2}\right) + \sin\left(3\frac{\theta}{2}\right)\right] + \\
&\quad + \frac{K_{II}}{4\sqrt{2\pi r}}\left[\cos\left(\frac{\theta}{2}\right) + 3\cos\left(3\frac{\theta}{2}\right)\right] + O(1). \qquad (4.3)
\end{aligned}$$

(Therefore stresses admit a singularity at fracture tip as $1/\sqrt{r}$).

Stress intensity factors K_I, K_{II}, K_{III}, that appear on the expressions 4.3, depend on the geometry of both the domain and the fracture and on the type and the intensity of the applied loads.

Also vectorial discontinuity of displacements across the fracture, in proximity of crack tip, can be expressed in function of the stress intensity factors as follows

$$[u] = \frac{4}{\mu}\sqrt{\frac{r}{2\pi}}\{(1-\nu)[K_I\bar{\imath} + K_I\bar{j}] + K_{III}\bar{k}\} + O(r). \qquad (4.4)$$

In the previous expressions the terms $O(r^\alpha)$ indicate generic terms of order r^α for r small; K_I, K_{II} and K_{III} are the stress intensity factors corresponding to mode I, II and III; $[u]$ represents the vectorial discontinuity on displacements due to the fracture.

Expression 4.4 gives the *cinematic interpretation* of the stress intensity factors i.e., since they are directly proportional to $[u]$, they can be considered as a factor of vectorial discontinuity of displacement on crack edges. This implies that K_I must always be not negative. In fact, in the simple case of a fracture only in mode I, a vectorial discontinuity of displacement not positive would mean a permeation of fracture edges.

Fracture toughness is a material characteristic that can be measured by laboratory tests on some samples. The validity of the concept of material toughness (validity that is problematic on a theoretic

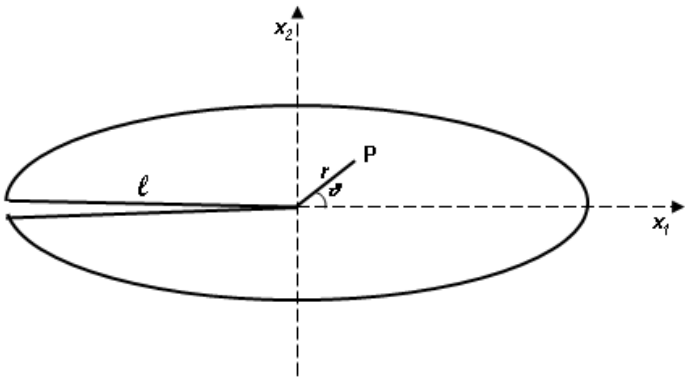

FIGURE 4.14. Local geometry in the proximity of crack tip.

point of view since in elastic field it implies the presence of a plastic zone around the crack tip), it is instead well demonstrated in the experimental setting.

Irwin [29], in 1975, proposed as a criterion to evaluate the fracture stability, to compare fracture toughness of the material with the actual stress intensity factor induced by the load conditions, i.e.

$$\begin{cases} K_I < K_{IC}, & \text{the fracture is stable,} \\ K_I \geq K_{IC}, & \text{the fracture is instable.} \end{cases}$$

4.2.2 Fracture stability in the Brunelleschi dome

The evaluation of crack stability is usually based on the comparison between the value of K determined by the geometry configuration and loads with the material characteristic K_C. This comparison is usually performed in a repetitive way in order to simulate the possible propagation of the fissure due to load time-history.

This methodology needs a precise evaluation of the stress intensity factor associated to the real configuration (of loads and geometry). Analytic solutions (or semi-analytic) have been determined (see for example [29]) for fissured solids with simple geometry[3].

[3] As a trivial exemple for an uniform load applied at an infinite distance from fracture edges, analytic expression gives

$$\begin{aligned} K_I &= \sigma\sqrt{\pi a} \\ K_{II} &= \tau\sqrt{\pi a} \end{aligned}$$

Unfortunately, these solutions, applied on real complex structures (with a more complex geometry etc. as in the Brunelleschi dome) would lead approximate solutions, not useful for a correct evaluation of structure safety.

More precise solutions can be achieved only via numeric methods; most of them, as the one here used, are based on finite elements model of the crack configuration.

This remark was necessary since, at a first glance, one could think to apply directly expression 4.4 (or some more specific expression that can better represent load and geometry conditions under analysis) to the values of displacements logged by the sensor on the fracture in order to evaluate its stability. In reality, as discussed, obtained results would be not precise. The finite element model of the dome and in particular a finite element model able to reproduce with a good approximation local values of deformation around the crack, is thus necessary.

Model of a fissured solid requires nevertheless some specific considerations here summarized. First, in linear fracture mechanics fissure is represented by a discontinuity of displacements throughout the edges that are reproduced by a line. The finite element model must therefore account of this condition: base function used on the proposed f.e.m. are for construction continuous on the domain and since therefore fracture can not cross some elements, it has been placed on the frontier of the elements. In particular, if all the dome would have been modeled, it was necessary to reproduce the fracture by using double nodes to reproduce fracture edges. In the proposed model instead, due to symmetric disposition of cracks, it has been possible to consider only an half of the fracture by allowing possible (on the considered edge) the deformations compatible with crack configuration.[4]

Convergence to the exact solution is achieved by the use of a fine mesh (for a complete investigation see [7]); therefore on the initial set up of the model a quite fine mesh has been chosen.

---

with a fracture length and σ, τ applied stresses.

[4] Another possible approach (not considered here) to the analysis of fracture stability is the use of *eXtended Finite Element Method* i.e. a method that uses, in addition to the classicial base functions associated to not fissured solid, some complementary functions that account of the discontinuity of displacements througth the fissure.

Evaluation of the stress intensity factor has finally been performed by the so called *extrapolation method*. This method consists on considering the obtained displacements on the nodes of the fracture edge more close to tip. By using the expression 4.4, these values are used to evaluate the stress intensity factors as follows

$$K_I \approx \frac{E}{8(1-\upsilon^2)}\sqrt{\frac{2\pi}{d}}[u_t(B)], \qquad K_{II} \approx \frac{E}{8(1-\upsilon^2)}\sqrt{\frac{2\pi}{d}}[u_n(B)],$$

where $[u_t(B)]$ and $[u_n(B)]$ are respectively tangential and normal components of the jump of displacements of the nodes at a distance d from a point B close to the crack tip.

This calculation must be repeated in an iterative way for all the time-history of displacements associated to external loads evolution (in the Brunelleschi dome temperature evolution).

In reality, due to the direct proportion between stress intensity factor and $[u]$, maximum value of K (the one that must be compared with K_C) is reached in correspondence of maximum displacement. Therefore, the calculation has been performed only on this limit condition.

In the analysis of the Brunelleschi dome it has been possible to neglect the effect of mode II since displacements are quite completely in the tangential direction (the normal contribute can be considered null). Thus the fracture undergoes only a tensile stress and only the corresponding stress intensity factor has been determined.

The analysis has thus been performed as previously explained. In the most severe condition, a maximum value of $5,37\ N/mm^{3/2}$ has been obtained.

This value, associated to maximum displacement undergone by fracture edges, must be compared with the value of the *toughness* of the masonry under analysis. Unfortunately, not direct data of *toughness* of the brick of Brunelleschi dome are available, thus it has been possible only to refer to the general literature [38] that gives a masonry *toughness* of about $10,6\ N/mm^{3/2}$.

Unfortunately, this value does not refer to historical masonry as the one under analysis and more adequate value have not been found on the literature.

Nevertheless, factor 2 between maximum obtained K_I and given K_{IC} can be however considered as a safe factor that allows to state

that the structure is still on a stable condition and material can still give a resistance against an irreversible growth of the fracture.

A deep investigation on real material properties would be in any case desirable for a more precise evaluation of fracture stability and a final evaluation. In fact, with time passing, material could have undergone a degrading process and thus reduced its mechanical properties and in particular its *toughness*. Stress intensity factor induced by external loads could thus not be so far from effective masonry *toughness.*

A continuous monitoring of displacements is however useful since a sudden increase of crack opening due to some external causes could lead to a definitively warring stress intensity factor value.

5
Concluding remarks

The present work has addressed the risk of collapse of monumental buildings under static conditions. This risk is often underestimated, while the collected examples of catastrophic collapses happened in the past, show that this event can occur by determining enormous losses, both tangible (human, economical) and intangible (cultural, social and historical) ones.

To deal with this risk is not a trivial task since one has to tackle in the main time uncertainties characteristic of monumental buildings and uncertainties referred to the hazard. Monumental buildings, in fact, can not be treated as all the other structures: in reason of their uniqueness (uniqueness on the history, on the typology, on the materials, on the phases and modalities of construction, etc.) they can not be analyzed in statistical terms. These features (history, typology, materials, phases and modalities of construction, etc.) represent in the same time unknowns, since to have complete informations about them is rarely possible.

Moreover also the hazard is difficult to define: in fact the collapse is induced by an intrinsic weakness of the structure itself, thus it is not possible to define classes of intensity level.

Therefore these structures present, in the same time, high vulnerability and high possible tangible and intangible losses.

Here the proposed risk management process begins with an analysis of the hazard. In this step, structural health monitoring has recently emerged as a reliable and efficient approach to control the system performance, to detect damage and to assess the structural serviceability. Monitoring aim is to identify anomalies in the structure if there are, anomalies that can represent a damage and thus determine a source of harm for the structural stability. These anomalies can be seen as singularities: an innovative way to detect these singularities is the first tool presented in this work. Its potentials application on detecting crack in a region of the structure embedded by sensors and its potentials use on identifying anomalous data in a time-history has been presented in the chapter 2.

Once the damage (that is the possible cause of the collapse itself) has been identified, it is necessary to avoid that its increase would provoke the final structural collapse, by determining casualties and losses.

In addressing to monumental buildings, all the uncertainties previously exposed, seldom allow to set up a numerical finite element model able to reproduce the structural behavior. This is possible only in a qualitative way that does not help in preventing the collapse or in reducing the risk. In some cases, instead, even if it is possible to set up the finite element model, it requires however a certain time after the crack pattern has been identified. In order to assure the structural safety in the meantime, an early warning monitoring system is the useful tool that can forecast the dangerous event (the risk of collapse), giving alarm and thus avoiding the collapse or at least reducing the final losses.

The early warning monitoring system proposed in this work, even if referred to the data of S. Maria del Fiore cathedral, is applicable to any structure that undergoes a thermoelastic behavior as well. Early warning systems usually employed in the prevention of natural disasters use a statistical study of past events in order to forecast future ones, (e.g. statistical analyses of past time-histories in order to foresee the future data). In our case, statistical properties of data logged by sensors in the Brunelleschi dome, makes difficult the use of this kind of analysis: in fact these data present a non Gaussian, non stationary distribution. In addition, one may note that, in order to set up a warning system that could be applicable to any structures,

it is desirable to have a tool independent on the statistical properties of the past time-history.

The early-warning system here proposed instead, is able to identify anomalous data present in the time history of displacement, by means of a wavelet analysis on thermo-mechanic energy associated to the crack opening. The method could be tested also in other structures that undergo a temperature dependent crack opening, just modifying some parameters related to noise level of the acquired signals. The *Effective Alarm Signal* generated indicates the presence of an anomalous displacement and the risk of the imminent collapse in real-time.

The *Effective Alarm Signal* is also a reliable tool since it is able to neglect all the cases in which the anomalous data are due to instrumental errors. Instrumental errors that can occur for example during thunderstorms.

As said, the study presented here is a special application on experimental data coming from the monitoring system installed on the Brunelleschi dome. The methodology could however be applied also to other structures under thermoelastic regime.

Since the numerical effort required is very small and the calculation is very fast (some seconds in a standard laptop computer), an application for a warning monitoring of a real structure is possible.

Once the early warning system has been set up it has been found interesting to understand how far can be consider the fracture of the S. Maria del Fiore dome from an instable growing i.e. if it has the tendency in the immediate future to grow in an instable way. With this aim, a study of the mechanics of the fracture has been done. A basic but effective model has been set up: it is, in fact, able to reproduce local main features of the dome, in particular around the crack.

The followed study of the stability of the crack in mechanical terms, reveals that fracture in Brunelleschi dome is still stable; in any case the uncertainties on the effective material proprieties suggest that a continuos monitoring of the structure is necessary, in order to verify in real-time that no anomalous events could occur. The early-warning monitoring proposed is therefore useful in this aim.

References

[1] Augusti G., Ciampoli M., Giovenale P. (2001). Seismic Vulnerability of Monumental Buildings, *Structural Safety*, 23:253-274.

[2] Augusti G., Ciampoli M. (2000). Heritage Buildings ans Seismic Reliability, *Prog. Struct. Engng. Mater.*, 2:225-237.

[3] Bartoli G., Chiarugi A., Gusella V. (1996). Monitoring Systems on Historic Buildings: the Brunelleschi Dome, *Journal of Structural Engineering*, 122(6):663-673.

[4] Bartoli. G., Blasi C., Gusella V. (1993). Monitoring of the Brunelleschi Dome, *IABSE Symposium*, Roma.

[5] Bavetta F. (1994). Problemi di Cupole di Grosso Spessore con Particolare Riferimento alla Cupola di Santa Maria del Fiore di Firenze, *Master Thesis, University of Florence*, Firenze.

[6] Binda L., Saisi A. State of the Art of Research on Historic Structures in Italy

[7] Bonnet M., Frangi A. (2006). Analyse des solides déformables par la méthode des éléments finis, *Les éditions de l'école polytechnique,* Palaiseau Cedex.

[8] Bosi A. (2007). A wavelet-based methodology for monitoring thermoelastic structures, *Meccanica*, 42:477-485.

[9] Bosi A., Mariano P. M., Salvatori L. (2007). Gross Scale Effects of Atomic Rearrangements in Quasicrystals: Numerical Simulations and Wavelet Analysis, *AIMETA 2007*, Brescia.

[10] Boley B. A., Weiner, J. H. (1960). Theory of thermal stresses, *John Wiley & Sons*, New York.

[11] Bui H. D. (1978). Mécanique de la rupture fragile, *Masson*, Paris.

[12] Carlson D. E. (1992). Linear thermoelasticity, in *Handbuch der physik*, (ed. Truesdell C.), vol.VIa/2:297-345.

[13] http://www-cast3m.cea.fr

[14] Castoldi A., Anesa F., Imperato F., Gamba F. (1989). Cattedrale di S. Maria del Fiore, Firenze: Sistema di Monitoraggio Strutturale delle Cupola e del Suo Basamento, *I quaderni dell'ISMES n.262*, Bergamo.

[15] Chiarugi A. (1990). Sui Sistemi di Monitoraggio Strutturale degli Edifici Monumentali, *Costruire in Laterizio*, n.16/90.

[16] Chiarugi A., Bartoli G., Bavetta F. (1990). Raccolta monografica: elaborazione ed interpretazione di dati sperimentali provenienti dal sistema di monitoraggio della Cattedrale di Santa Maria del Fiore a Firenze, *DIC, Struct. Sect. 13/90 (Internal Rep.)*, Civ. Eng. Dept., University of Florence.

[17] Daubechies I. (1992). Ten Lectures on Wavelets, *SIAM*, Philadelphia, PA.

[18] Doebling S. W., Farrar C. R., Prime M. B. (1998). A summery review of vibration-based damage identification methods, *The Shock and Vibration Digest*, 30(2):91-105.

[19] Doglioni F., Moretti A., Petrini V. (1994). Le Chiese e il Terremoto, *Edizioni LLINT*, Trieste.

[20] Dipartimento di Ingegneria Civile (1993). Elaborazione dei Dati Provenienti dal Sistema di Monitoraggio della Cupola del Brunelleschi. Dati Rilevati Fino al 31 Dicembre 1002. *Università degli Studi di Firenze, Dipartimento di Ingegneria Civile*, Firenze.

[21] Gabbanini F., Vanucci M., Bartoli G., Moro A. (2004). Wavelet Packet Methods for the Analysis of Variance of Time Series with Application to Cracks Widths of the Brunelleschi Dome, *J. Comp. Graph. Stat.*, 13:639-653.

[22] Gabor D. (1946). Theory of communication, *J. IEE,* 93:429-457.

[23] Giaquinta M., Modica G. (2005). Note di Metodi Matematici per Ingegneria Informatica, *Pitagora Editrice Bologna.*

[24] Griffith A. A. (1921). Phil. Trans. Roy. Soc., Ser. A, London.

[25] Guasti C. (1857). La Cupola di S. Maria del Fiore, *Barbera ed., Bianchi e Comp.*, Firenze.

[26] Hera A., Hou Z. (2004). Application of Wavelet Approach for ASCE structural health monitoring benchmark studies, *Journal of Engineering Mechanics*, 130:1(96).

[27] Heyman J. (1995). The Stone Skeleton: structural engineering of masonry architecture, *Cambridge University Press*, Cambridge.

[28] Hu C., Wang R., Ding D-H. (2000). Symmetry Groups, Physical Property Tensors, Elasticity and Dislocations in Quasicrystals, *Reports on Progress Physics*, 63:1-39.

[29] Irwin G.R. (1958). Fracture, *Handbuch der physik*, vol.VI, *Springer,* Berlin.

[30] Jeong H.-C., Steinhardt P. J. (1993). Finite-temperature Elasticity Phase Transition in Decagonal Quasicrystals, *Phys. Rev. B,* 48:9394-9403.

[31] Lagomarsino S. (1998). Seismic Damage Survey of the Churches in Umbria, *Proc. Workshop on Seismic Performance of Monuments MONUMENT'98*, Lisbon.

[32] Lubarda V. A. (2004). On thermodynamic potentials in linear thermoelasticity, *Int. J. Solids Structures*, 41:7377-7398.

[33] Mallat S. (1998). A Wavelet Tour on Signal Processing, *Academic Press*, New York.

[34] Mariano P. M. (2006). Mechanics of Quasi-periodic Alloys, *J. Nonlinear Science,* 16:45-77.

[35] Mariano P. M., Stazi F. L., Gioffré M. (2006). Stochastic Clustering and Self-organization of Gross Deformation and Phason Activity in Quasicrystals: Modeling and Simulations, *J. Comp. Theor. Nanoscience*, 3:479-486.

[36] Ministero Beni Culturali e Ambientali (1985). Rapporto sulla Situazione del Complesso Strutturale Cupola-basamento della Cattedrale di Santa Maria del Fiore in Firenze, *Soprintendenza per i Beni Ambientali e Architettonici per le provincie di Firenze e Pistoia*, Firenze.

[37] Newland D. E., (2005) An Introduction to Random Vibrations, Spectral & Wavelet Analysis, *Dover*, New York.

[38] Olivito R.S., Stumpo P. (2001). Fracture Mechanics in the Characterisation of Brick Masonry Structures, *Material and structures*, 34:217-223.

[39] Opera Di Santa Maria Del Fiore (1939). Rilievi e Studi sulla Cupola del Brunelleschi Eseguiti dalla Commissione Nominata il 12 Gennaio 1934, *Tipografia Ettore Rinaldi*, Firenze.

[40] Plate E. J. (1999). Early Warning Systems for River Floods and Other Types of Natural Disasters, *ICSU General Assembly*, Cairo.

[41] Quek S.T., Wang Q., Zhang L., Ang K.K. (2001). Sensitivity analysis of crack detection in beams by wavelet technique, *International Journal of Mechanical Sciences*, 43:2899-2910.

[42] Rapetti F., Vittorini S. (1988). Le Variazioni del Clima di Firenze dal 1822 al 1986, *Bollettino della Società Geografica Italiana n.1.3.1988*, Roma.

[43] Reda Taha M. M., Noureldin A., Lucero J. L., Baca T. J. (2006). Wavelet Transform for Structural Health Monitoring: a Compendium of Uses and Features, *Structural Health Monitoring*, 5(3):0267-29.

[44] Schmicker D., Van Smaalen S. (1996). Dynamical Behavior of Aperiodic Intergrowth Crystals, *Int. J. Mod. Phys. B*, 10:2049-2080.

[45] Shechtman D., Blech I., Gratias D., Cahn J. W. (1984). Metallic Phase with Long-range Orientational Order and no Translation Symmetry, *Phys. Rev. Lett.,* 53:1951-1954.

[46] Sneddon I. N. (1974). The linear theory of thermoelasticity, *Springer-Verlag*, Wien, CISM Udine.

[47] UNI 10355:1994. Murature e solai. Valori della resistenza termica e metodo di calcolo.

[48] Urban M. (2006). Earthquake Risk Assessment of Historical Structures, *PhD thesis*, *Doctoral Course on Risk Management on Build Environment*, Firenze and Braunschweig.

[49] Vannucci M. (2005). Lecture in: Wavelet-based Statistical Modeling and Applications, *Intensive course on wavelets, 18-22 July, Dip. Statistica "G. Parenti",* Firenze.

[50] Vasari G. (1550). Le vite dé più eccelenti architetti, pittori et scultori italiani, da Cimabue insino a' tempi nostri, *Edizione Giuntina e Torrentiniana.*

[51] Wang Q., Deng X., (1999). Damage Detection with Spatial Wavelets, *International Journal of Solids and Structures*, 36:3442-3468.

[52] Ximenes L. (1757). Del Vecchio e Nuovo Gnomone Fiorentino e delle Osservazioni Fisiche ed Architettoniche, *Stamperia Imperiale*, Firenze.

Appendix A

An introduction on the mechanics of quasicrystals

From the crystallographic definition *crystals* are three dimensional period arrangements of atoms with translation symmetry along its three principal axes. In 1984 Shechtman and co-workers [45] discovered the existence of some metallic alloys in which atoms were clustered with symmetry not compatible with the periodicity in space of some crystalline cell (icosahedral symmetry in space and pentagonal one in plane). As a consequence such alloys presented an *intrinsically quasiperiodic* atomic structures and were called *quasicrystals.* The break of the translational symmetry was not a consequence of the presence of defects, but it was due to the presence of atomic clusters with symmetry different from the prevailing one. These topological alterations were called *worms* and ensure the existence of lattices with a prevailing icosahedral symmetry[1]. The essential point is that worms may be created and destroyed everywhere in the lattice as a consequence of atomic rearrangements which have a prominent influence on the gross mechanical behavior. So quasicrystals are prominent examples of complex bodies.

[1] As an example let us think of a planar space ambient and try to construct over it a lattice with pentagonal symmetry covering the whole plane. From elementary geometry we know that it is not possible to fill the whole plane only by using pentagons; structures with a symmetry different from the prevaling one must be introduced. These structures represent a topological alteration that alters the prevaling periodicity.

A complex body is a body in which changes in the material substructure have prominent macroscopic effects due to the interactions generated by substructural changes. Their mechanical behavior is naturally described by multifield theories; here we refer to [34].

A.1 Summary of the mechanics of quasicrystals

We consider a quasicrystalline body in a regular region $\mathcal{B}_0$ of $\mathbb{R}^3$, a region that we take as reference. A deformation of $\mathcal{B}_0$ is a sufficiently smooth orientation-preserving one-to-one mapping $x \longmapsto y \in \mathbb{R}^3$, with $x \in \mathcal{B}_0$, that 'displaces' generic material element from its reference place x to its actual one $y = y(x)$. The actual place of the body is then $\mathcal{B} = y(\mathcal{B}_0)$. The standard displacement vector $u = y - x$ collects the degrees of freedom of each material element in the ambient space (the so-called *phonon degrees of freedom* because they are associated with the common deformation governing the standard acoustic regime).

In quasicrystals, in addition to the crowding and the sharing of material elements, local rearrangements of the crystalline structures occur. These atomic rearrangements (the so-called *phason activity*) have a significant influence on the gross mechanical behavior and are described by a vector w attached at each generic material element. w collects internal degrees of freedom, the so-called *phason degrees of freedom*. Roughly speaking, w is a morphological descriptor that describes the local shift of atoms within the crystalline structure, (see, e.g., [34], [30], [44]).

Motions are described by the time-parameterized vector fields $u = \tilde{u}(x,t), w = \tilde{w}(x,t)$, where t is the time, as usual and with

$$\begin{aligned} \mathcal{B}_0 \times [0,t] \quad &\ni \quad (x,t) \to y := y(x,t) \in \mathbb{R}^3, \\ \mathcal{B}_0 \times [0,t] \quad &\ni \quad (x,t) \to w := w(x,t) \in \mathbb{V}_w, \end{aligned}$$

where $\mathbb{V}_w$ is the space in which w exists and can be identified with $\mathbb{R}^3$.

The analysis of diffraction patterns obtained by x-ray experiments indicate that the phason activity has no peculiar kinetic energy. Moreover, internal dissipation is associated with the atomic changes [44].

Referring to [34] we indicate with $\mathfrak{b}$ any part of $\mathcal{B}_0$ (any subset of $\mathcal{B}_0$ with nonnull volume measure and the same regularity properties of $\mathcal{B}_0$). $\mathfrak{b}$ is assumed to interact with the rest of the body and the external environment by means of interactions of bulk and contact nature (these ones through the boundary $\partial\mathfrak{b}$). The external power $\mathcal{P}^{ext}_{\mathfrak{b}}(\dot{x}, w)$ of all external actions over $\mathfrak{b}$, is given by

$$\mathcal{P}^{ext}_{\mathfrak{b}}(\dot{x}, \dot{w}) = \int_{\mathfrak{b}} (b \cdot \dot{x})\, dV + \int_{\partial\mathfrak{b}} (Pn \cdot \dot{x} + \mathcal{S}n \cdot \dot{w})\, \mathrm{d}\mathfrak{H}^2,$$

where b represents standard bulk forces (that collects inertial and non inertial actions); P and $\mathcal{S}$ are respectively the first Piola-Kirchhoff stress and phason stress. Pn represents the traction-developping power in the relative change of place of neighboring material elements at the boundary $\partial\mathfrak{b}$, by imaging the phason activity frozen. $\mathcal{S}n$ pictures interactions developed across the boundary $\partial\mathfrak{b}$ between neighboring material elements which do not change place but display different phason activity [34].

Now the *invariance* of $\mathcal{P}^{ext}_{\mathfrak{b}}(\dot{x}, w)$ with respect to (classical) changes in observers governed by rigid body motions (ruled by $S(O)$), is required. For such change, if $\dot{x}^*$ is the value of the velocity $\dot{x}$ after the change in the observer, we get

$$\dot{x}^* = c(t) + \dot{q}(t) \times (x - x_0) + \dot{x},$$

where $c(t)$ is the translational velocity, constant in space, x_0 a point chosen arbitrarily and $\dot{q}\times \in \mathfrak{so}\ (3)$ at each time t. Moreover by indicating with $\dot{w}^*$ the rate $\dot{w}$ measured after the change in observer, one gets

$$\dot{w}^* = \dot{w} + \dot{q}(t) \times w,$$

(translation is not defined in the space $\mathbb{V}_w$).

Now we require the invariance $\mathcal{P}^{ext}_{\mathfrak{b}}(\dot{x}^*, \dot{w}^*) = \mathcal{P}^{ext}_{\mathfrak{b}}(\dot{x}, \dot{w})$, for any choice of translational c and rotational $\dot{q}$ velocities and for any part $\mathfrak{b}$. Therefore from the arbitrariness of c, $\dot{q}$, and $\mathfrak{b}$, one gets the pointwise balance equations, i.e. first the standard balance of forces

$$b + DivP = 0.$$

For the balance of phason interactions, there exists a pure dissipative self-action $z^{\upsilon} = Div\mathcal{S}$ (with $z^{\upsilon} \cdot \dot{w} \geq 0$) such that

$$skwPF^* = skw(w \otimes z^{\upsilon} + (\nabla x)^* \mathcal{S}).$$

This equation tells us that the Cauchy stress is not symmetric *a priori*; the lack of symmetry is due to phason interaction.

The body force b, the microstress $\mathcal{S}$, the self-force z^{υ}, and the Piola-Kirchhoff stress P have counterparts defined over $\mathcal{B}$, namely f, $\mathcal{S}_a$, z^{υ}_a and Cauchy stress σ. They are linked with one other by Piola transform $f = (\det F)^{-1} b F^T$, $\mathcal{S}_a = (\det F)^{-1}\mathcal{S}F^T$, $z^{\upsilon}_a = (\det F)^{-1} z^{\upsilon} F^T$ and $\sigma = (\det F)^{-1} P F^T$. From now on we will consider infinitesimal deformation regime, where $b \simeq f$, $S \simeq s$, $z^{\upsilon}_a \simeq z^{\upsilon}$ and $P \simeq \sigma$. Also, we 'confuse' $\mathcal{B}$ with $\mathcal{B}_0$, and the actual and referential differentials operator.

Now, since the elastic energy is a quadratic form in small deformation regime, one gets

$$\begin{aligned} \sigma &= \mathbb{C}\nabla u + \mathbb{K}'\nabla w, \\ \mathcal{S}_a &= \mathbb{K}'^{\mathrm{T}}\nabla u + \mathbb{K}\nabla w, \end{aligned}$$

where $\mathbb{C}$, $\mathbb{H}$, and $\mathbb{K}$ are fourth order tensors. In the case of planar quasicrystals with fivefold symmetry [30], one has

$$\begin{aligned} \mathbb{C}_{ijhk} &= \lambda\delta_{ij}\delta_{hk} + \mu\left(\delta_{ih}\delta_{jk} + \delta_{ik}\delta_{jh}\right), \\ \mathbb{K}'_{ijhk} &= k_1\delta_{ih}\delta_{jk} + k_2\left(\delta_{ij}\delta_{hk} - \delta_{ik}\delta_{jh}\right), \\ \mathbb{K}_{ijhk} &= k_3\left(\delta_{i1} - \delta_{i2}\right)\left(\delta_{ij}\delta_{hk} - \delta_{ih}\delta_{jk} + \delta_{ik}\delta_{jh}\right), \end{aligned}$$

where $i, j, h, k = 1, 2$, δ_{ij} is Kronecker symbol, λ and μ are Lamé constants, k_1 and k_2 are constants characterizing the pure phason behavior, and k_3 is the phonon-phason interaction constant: only in the last expression, no summation is assumed over repeated indices.

As a sample case we consider the $Al_{30.3}Pd_{21.5}Mn_{8.2}$ alloy. For it, typical values of elastic constants and mass density are $\lambda = 0.75 \times 10^{11} N/m^2$, $\mu = 0.65 \times 10^{11} N/m^2$, $k_1 = 0.81 \times 10^{11} N/m^2$, $k_2 = -0.42 \times 10^{11} N/m^2$, and $\rho = 5100 kg/m^3$, (see [28]). The experimental determination of k_3 is uncertain. A stochastic approach considering such uncertainties is presented in [35]. Here the experimental mean value $k_3/k_1 = 0.1$ is assumed in the numerical simulations.

A.2 The performed numerical simulation

By using appropriate test functions $x \longmapsto \delta u := \delta u(x) \in \mathbb{R}^3$ and $x \longmapsto \delta w := \delta w(x) \in \mathbb{R}^3$, the weak form of balance equations reads

$$\int_{\mathcal{B}_0} \nabla\delta u \cdot P \, \mathrm{d}X + \int_{\mathcal{B}_0} \nabla\delta w \cdot \mathcal{S} \, \mathrm{d}X - \int_{\mathcal{B}_0} \delta w \cdot z \, \mathrm{d}X = \int_{\mathcal{B}_0} \delta u \cdot \rho\ddot{u} \, \mathrm{d}X + \int_{\mathcal{B}_0} \delta u \cdot b \, \mathrm{d}X + \int_{\partial\mathcal{B}_0} \delta u \cdot \mathfrak{t} \, \mathrm{d}\mathfrak{H}, \tag{A.1}$$

where the vector density $\mathfrak{t} = Pn$ represents standard external tractions, being n the unit normal to the boundary $\partial\mathfrak{b}_0$ of $\mathfrak{b}_0$. Since we do not know any loading device able to prescribe a phason traction $\mathcal{S}n$ at the external boundary $\partial\mathcal{B}_0$, we presume that it vanishes there. To obtain a finite element scheme, the domain $\mathcal{B}_0$ is partitioned into finite elements $\mathfrak{b}_0^e$ $(e = 1, \ldots, N)$. In each $\mathfrak{b}_0^e$, some points (finite in number) represent the integration nodes. The nodal displacements and the phason degrees of freedom of the e-th finite element are collected in the vectors $\mathbf{U}^e$ and $\mathbf{W}^e$ respectively. Over each finite element, the interpolations $u(x,t) = \mathbf{\Phi}_u^e(x)\,\mathbf{U}^e(t)$, $w(x,t) = \mathbf{\Phi}_w^e(x)\,\mathbf{W}^e(t)$ are considered, with $\mathbf{\Phi}_u^e$ and $\mathbf{\Phi}_w^e$ the matrices of the shape functions. In the numerical simulations presented below, triangular finite elements are considered. The test fields are chosen to be of the form $\delta u = \mathbf{\Phi}_u^e \delta\mathbf{U}^e, \delta w = \mathbf{\Phi}_w^e \delta\mathbf{W}^e$, where $\delta\mathbf{U}^e$ and $\delta\mathbf{W}^e$ are arbitrary variations of nodal displacements and phason degrees of freedom vectors. By substituting into (A.1), and taking into account that equation (A.1) must hold for any choice of the variations $\delta\mathbf{U}^e$ and $\delta\mathbf{W}^e$, one obtains

$$\begin{bmatrix} \mathbf{M}_{uu}^e & \mathbf{0} \\ \mathbf{0} & \mathbf{0} \end{bmatrix} \begin{bmatrix} \ddot{\mathbf{U}}^e \\ \ddot{\mathbf{W}}^e \end{bmatrix} + \begin{bmatrix} \mathbf{0} & \mathbf{0} \\ \mathbf{0} & \mathbf{D}_{ww}^e \end{bmatrix} \begin{bmatrix} \dot{\mathbf{U}}^e \\ \dot{\mathbf{W}}^e \end{bmatrix} + \begin{bmatrix} \mathbf{K}_{uu}^e & \mathbf{K}_{uw}^e \\ (\mathbf{K}_{uw}^e)^{\mathrm{T}} & \mathbf{K}_{ww}^e \end{bmatrix} \begin{bmatrix} \mathbf{U}^e \\ \mathbf{W}^e \end{bmatrix} = \begin{bmatrix} \mathbf{F}_u^e(t) \\ 0 \end{bmatrix}, \tag{A.2}$$

where $\mathbf{M}_{uu}^e, \mathbf{K}^e$'s, $\mathbf{D}_{ww}^e$ are mass, stiffness and viscosity matrices obtained by integrating the matrices of shape function and the constitutive coefficients as usual.

Equation (A.2) is a system of ordinary differential equations and represents the discrete (in space) form of the equations of motion for the e-th element. The contribution of each finite element can

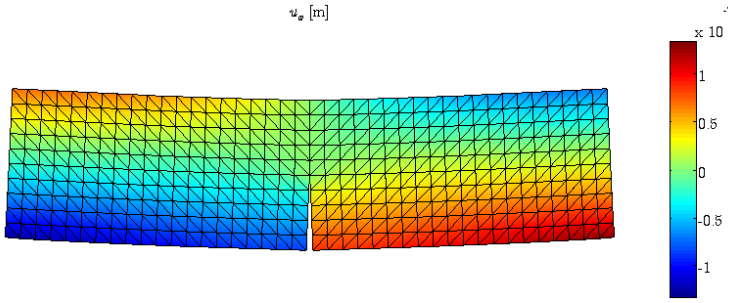

FIGURE A.1. Standard displcements in the static setting: no peculiar differences with the displacement field associated to a simple body undergoing the same load conditions are remarkable

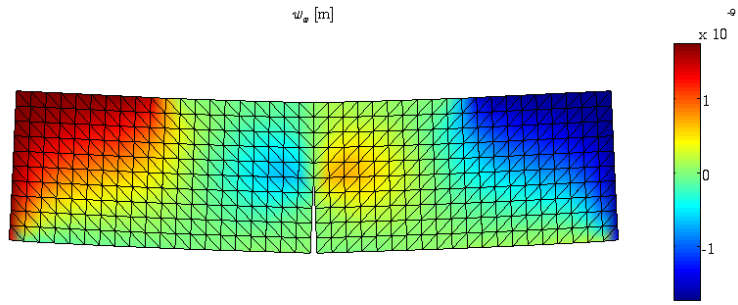

FIGURE A.2. Phason activity in static setting: a localization of the phason activity is evidenced in the vicinity of the macro-crack tip.

be assembled in a standard way by considering nodal compatibility and balance. Then, nodal restrains (discretized Dirichlet boundary conditions) can be prescribed.

Results of the analysis of the static setting are presented in figure A.1 and figure A.2: here the static displacements resulting from the analysis (magnification factor 5×10^5) are plotted, referring first to the standard displacements and then to the phason activity. A localization of the phason activity is evidenced in the vicinity of the macro-crack tip. Macro-displacements on the other hand appear qualitatively similar to those of a standard Cauchy body.

In order to perform numerical analysis in the dynamical setting, it has been necessary first to discretize also in time Eq. (A.2). The solution of the equations of motion can be obtained by standard time-

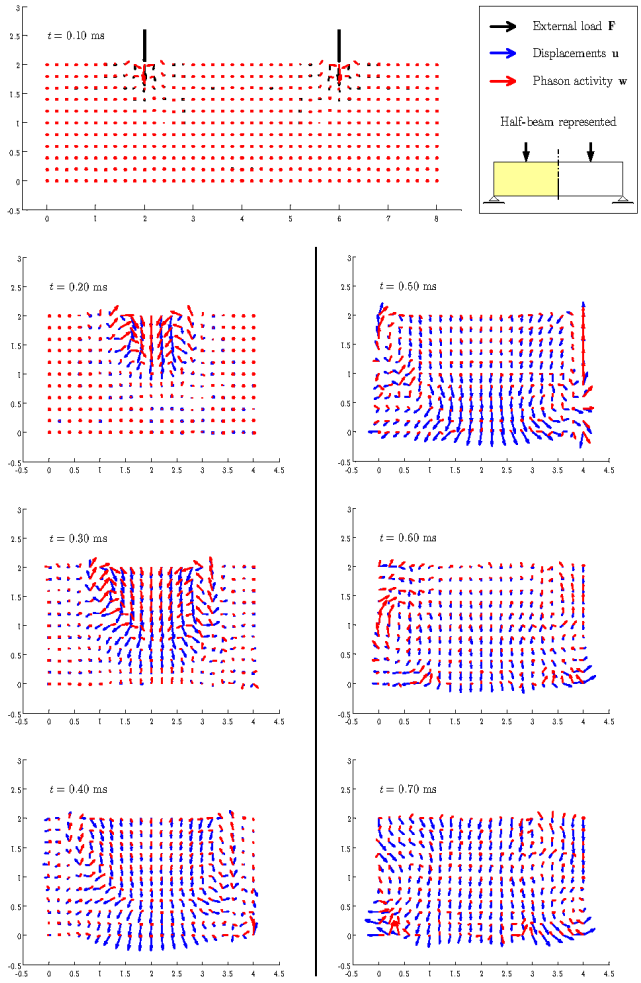

FIGURE A.3. Snapshots of the response time-histories referred to standard displacements and phason activity

integration algorithms. Here a Newmark scheme with trapezoidal rule is adopted. The time step is chosen to be $\Delta t = 2.0 \times 10^{-6} s$. Snapshots of the response time-histories referred to standard displacements and phason activity are presented in figure A.3. A clear characterization of the gross behavior and of the phason activity is not possible only by means of this analysis, giving therefore reason to the performed use of wavelets.